Response to reviewer #1

We really appreciate your constructive comments and suggestions on our manuscript. We have considered every comment carefully, and responded on a point to point and marked every change in red in the revised version.

## General comments

This paper presents TROPOMI formaldehyde retrievals over China. The main difference with respect the operational HCHO retrievals distributed by ESA is the use of specific a-priori information during the air mass factor (AMF) calculation to much better the current knowledge of HCHO distributions over China.

Overall, the results presented here are interesting but the paper lacks details essential to understand the value and implications of the new retrieval. The specific comments section suggests may aspects where the manuscript could improve by including further details.

Definitely providing information about TROPOMI level 1 radiances and irradiances is absolutely necessary since they are the base for the retrievals described in section 3.

**Responses:** Thank you very much for this suggestion. Information about TROPOMI level 1 radiances and irradiances and the S5P cloud operational product are added in Section 2.1. TROPOMI has four spectrometers for medium wave ultraviolet (UV), long wave ultraviolet combined with visual (UVIS), near infrared (NIR), and short wave infrared (SWIR), covering non-overlapping and non-contiguous wavelengths from 270 to 2385 nm which are divided into eight spectral bands. The Band 3 with wavelength from 320 to 405 nm is used for HCHO retrieval. Radiance in Band 3 is measured by UVIS spectrometer. The detector for UVIS spectrometer is a two-dimensional charge-coupled device (CCDs) with one dimension for wavelengths and the other dimension for across track spatial coverage (450 rows). Earth radiance is collected along the dayside of the earth, while solar irradiance measurements are performed near the North Pole every 15 orbits, approximately once a day. In the UVIS channel, the spectral resolution and spectral sampling is about 0.5 nm and 0.2 nm, respectively. Individual ground pixels size of radiance measurement is approximately 3.5 km in the across-track and 7 km (5.5 km since August 2019), with integration time of 1.08 s (0.84 s since August 2019). The Level 1B radiance and solar irradiance are available at the Copernicus Open Access Hub (https://scihub.copernicus.eu/, last access: 22 May 2019).

**Changes in manuscript:** L66-76, P3-4 in the revised version.

Likewise, for the S5P cloud operational product whose uncertainties will become of paramount importance while assessing the uncertainties of the HCHO retrieval presented here.

**Responses:** Thank you very much for this suggestion. Information about the S5P cloud operational product are added in Section 2.3.

**Changes in manuscript:** L100-105, P5 in the revised version.

The description of the retrieval process also lacks many details. To start with, Figure 1 is included but never referenced in the text.

**Responses:** Thank you very much for this suggestion. Figure 1 is cited at L123, P6 in Section 2.5

Figure 2 shows two HCHO signals superimposed with the spectral fit residual. It will be more informative to include a similar figure showing the contributions from each one of the parameters included in Table 2.

**Responses:** Thank you very much for this suggestion. We plotted the spectral fitting residuals with considering different cross sections (shown in Figure. A1) on 6 August 2018 over China (orbit 4211). For HCHO polluted case, considering $O_3$ cross sections at 228K and 295K reduces residual significantly while considering $NO_2$, BrO and $O_4$ cross sections affects residual little (Figure. A1 (a)). Moreover, Ring effect and $O_3$ cross sections affect SCD largely and help reduce random error. For HCHO clean case, considering $NO_2$, BrO and $O_4$ cross sections reduces residual largely (Figure. A1 (b)). Moreover, the uncertainties of selection of fitting window, polynomial and TROPOMI slit function are discussed in Section 4.1.

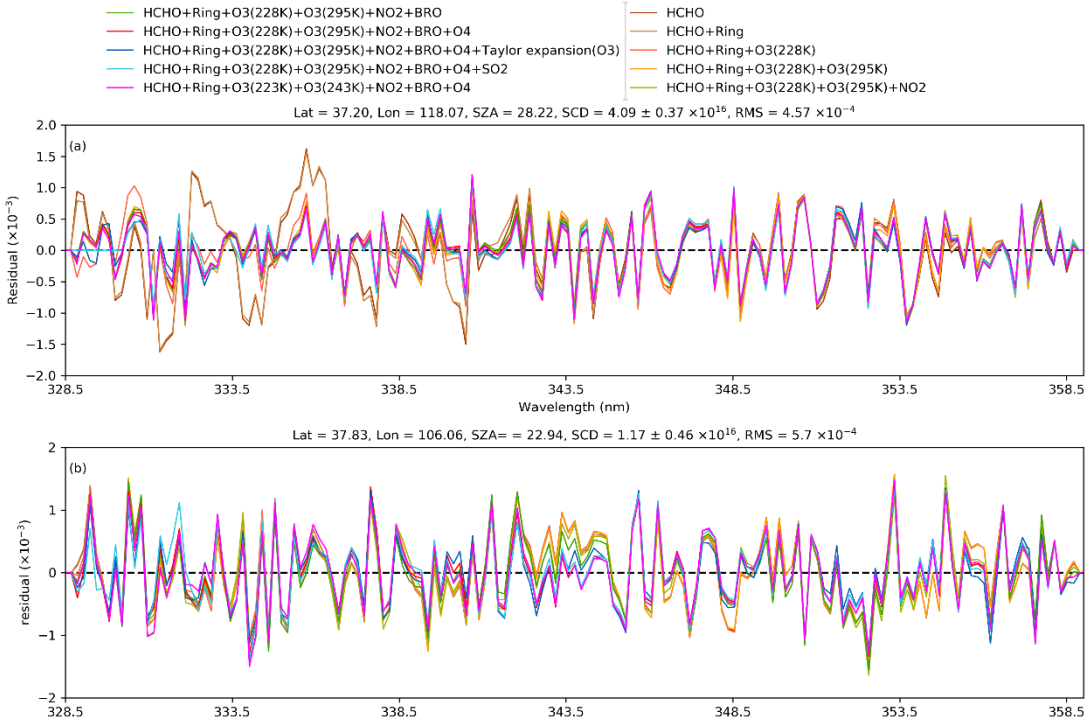


Figure. A1 Fitting residuals with considering different cross sections on 6 August 2018 over China for (a) polluted case and (b) clean case. The legend "HCHO" represents only considering HCHO cross section in spectral fitting and the legend "HCHO+Ring+O3(228K)+ O3(295K)+NO2+BRO+O4+Talor expansion(O3)" represents considering all cross sections listed in Table 1 and taking into account the first order Taylor series expansion for $O_3$ SCD at two temperatures in spectral fitting.

**Changes in manuscript:** L183-185, P8 in the revised version and L25-45, P3 and Figure S3 in supplement file.

Table A1. The spectral fitting results with considering different cross sections. The unit of DSCD and random error of DSCD is $10^{16}$ molec $cm^{-2}$ and the RMS is expressed in $10^{-4}$. The fitting results which cross sections are considered in our DSCD retrieval are marked in red.

| | Polluted case | | | Clean case | | |
|---|---|---|---|---|---|---|
| | DSCD | Random error of DSCD | RMS | DSCD | Random error of DSCD | RMS |
| HCHO | 4.51 | 0.43 | 6.3 | 0.59 | 0.42 | 6.3 |
| HCHO+Ring | 4.32 | 0.44 | 6.3 | 0.57 | 0.44 | 6.3 |
| HCHO+Ring+$O_3$(228K) | 4.27 | 0.34 | 4.9 | 0.57 | 0.44 | 6.3 |
| HCHO+Ring+$O_3$(228K)+$O_3$(295K) | 3.99 | 0.35 | 4.7 | 0.68 | 0.46 | 6.3 |
| HCHO+Ring+$O_3$(228K)+$O_3$(295K)+$NO_2$ | 3.96 | 0.34 | 4.6 | 0.64 | 0.45 | 6.1 |
| HCHO+Ring+$O_3$(228K)+$O_3$(295K)+BrO | 4.09 | 0.37 | 4.6 | 1.15 | 0.48 | 6.0 |
| HCHO+Ring+$O_3$(228K)+$O_3$(295K)+BrO+$O_4$ | 4.09 | 0.37 | 4.6 | 1.17 | 0.46 | 5.7 |
| HCHO+Ring+$O_3$(228K)+$O_3$(295K)+BrO+$O_4$ +Taylor expansion ($O_3$) | 4.38 | 0.42 | 4.6 | 1.10 | 0.49 | 5.6 |
| HCHO+Ring+$O_3$(228K)+$O_3$(295K)+BrO+$O_4$ +$SO_2$ | 4.40 | 0.40 | 4.5 | 1.73 | 0.51 | 5.6 |
| HCHO+Ring+$O_3$(223K)+$O_3$(243K)+BrO+$O_4$ | 4.12 | 0.37 | 4.6 | 1.19 | 0.46 | 5.8 |

It is very difficult to estimate the quality of this new retrieval without seen the results for one full orbit at least (where issues such as stripes and noise are easier to appreciate). While current figure 3 does this in part, the color scale employed masks may of the possible issues (leaving out negative values) and providing little sensitivity to the region between 0.5 and 1.5 x 1016 molecules $cm^{-2}$ most relevant for HCHO retrievals. It will also be very helpful to have plots showing the WRF-Chem simulations used to extract a priories as well as the GEOS-Chem simulation used for background corrections. Finally and of outmost importance, a discussion of the retrieval uncertainties is completely missing. While section 4 provides some bias estimates, the retrieval section should include a description of the random and systematic uncertainties linked to spectral fit and AMF calculation. Because there is no description of the operational HCHO TROPOMI retrieval in detail, it is impossible to assess the weight and validity of the conclusions derived from the comparison exercise between both products (the one presented here and the operational one). The authors focus on the impact due to the ΔSCD retrieval and the AMF calculation but do not devout any time evaluating the impact of using different earthshine radiances. It is also necessary to include a discussion of the MAX-DOAS errors.

Responses: These comments are also referred in Specific comments. We responded on a point to point in Specific comments.

Figure 5 shows some vertical profiles. What are they? Seasonal averages, daily averages,… Are they representative of similar periods of time and time of day? This results should be place into context with literature recently published (https://www.atmos-meas-tech-discuss.net/amt-2020-30/).

**Responses:** Thank you very much for this suggestion. The Figure 5 in the old version is Figure 7 in the revised version. Figure

7 shows seasonal averages of vertical HCHO profiles from MAX-DOAS, WRF-Chem and TM5-MP model at CAMS site. In AMF calculations, both WRF-Chem and TM5-MP simulations are interpolated to TROPOMI spatial resolution. Interpolated WRF-Chem and TM5-MP simulations within 20 km of the MAX-DOAS site are spatially averaged to compare with MAX-DOAS profiles. MAX-DOAS profiles are temporally averaged in the period 13:30-14:30 (Local Time) within ±1 h around the TROPOMI overpass time. And the error bars in Figure 7 represent 1σ standard deviation of seasonal variation.

**Changes in manuscript:** L366-370, P16 in the revised version.

Given the statistical uncertainties and the methodology used, an affirmation such as "These results suggest that our retrieval is better than the operational product both in urban and suburban in China" is probably over confident. First the MAX-DOAS measurements are representative of a small region in China dominated by large urban development. Second, small differences in the SCDs and the use of a higher spatial resolution model in the new retrieval indicates that both perform similarly. If the authors could provide some details about the appearance and differences of box-AMFs between both retrievals it will be possible to get a better idea of the impact of the a priori profiles.

**Responses:** Thank you very much for this suggestion. Due to limitation of MAX-DOAS data sets, we validate TROPOMI HCHO observations at three MAX-DOAS sites in Beijing including one urban site (CAMS site) and two suburban sites (NC and UCAS sites) (shown in Figure A3). The distances of three MAX-DOAS sites from central Beijing are 8, 27 and 61 km of CAMS, NC, and UCAS sites. The three MAX-DOAS sites are representative of urban and suburban region.

We using a different spectral retrieval technique (BOAS method) of HCHO slant columns. Moreover, the background correction has also been improved. Although DOAS and BOAS HCHO DSCDs show a similar spatial pattern. The spatial distribution of BOAS HCHO SCD is expected to be smooth, less noisy. Besides, operational product using different SCD retrieval methods is compared with MAX-DOAS HCHO measurements. Using the BOAS HCHO SCDs reduced the underestimation in summer and overestimation in winter of the operational product. In summer, using different SCD retrieval methods results a difference of 7.00% (± 1.71%, ± Error) from the TROPOMI operational HCHO VCD. The result shows that using the BOAS HCHO SCDs reduced the underestimation in summer and overestimation in winter of the operational product. Fig. A2 (a) and (c) show daily averaged a priori HCHO profiles from WRF-Chem and TRM5-MP simulations and MAX-DOAS measured profiles. Besides higher horizontal resolution, WRF-Chem simulation also has a higher vertical spatial resolution compared to TM5-MP data set. Although the difference in vertical resolution only shows negligible effect on box AMF under clear sky condition (Fig. A2 (b)), lower vertical resolution profiles would cause significant impact for cloudy cases due to the interpolation of coarse grid (Fig. A2 (d)).

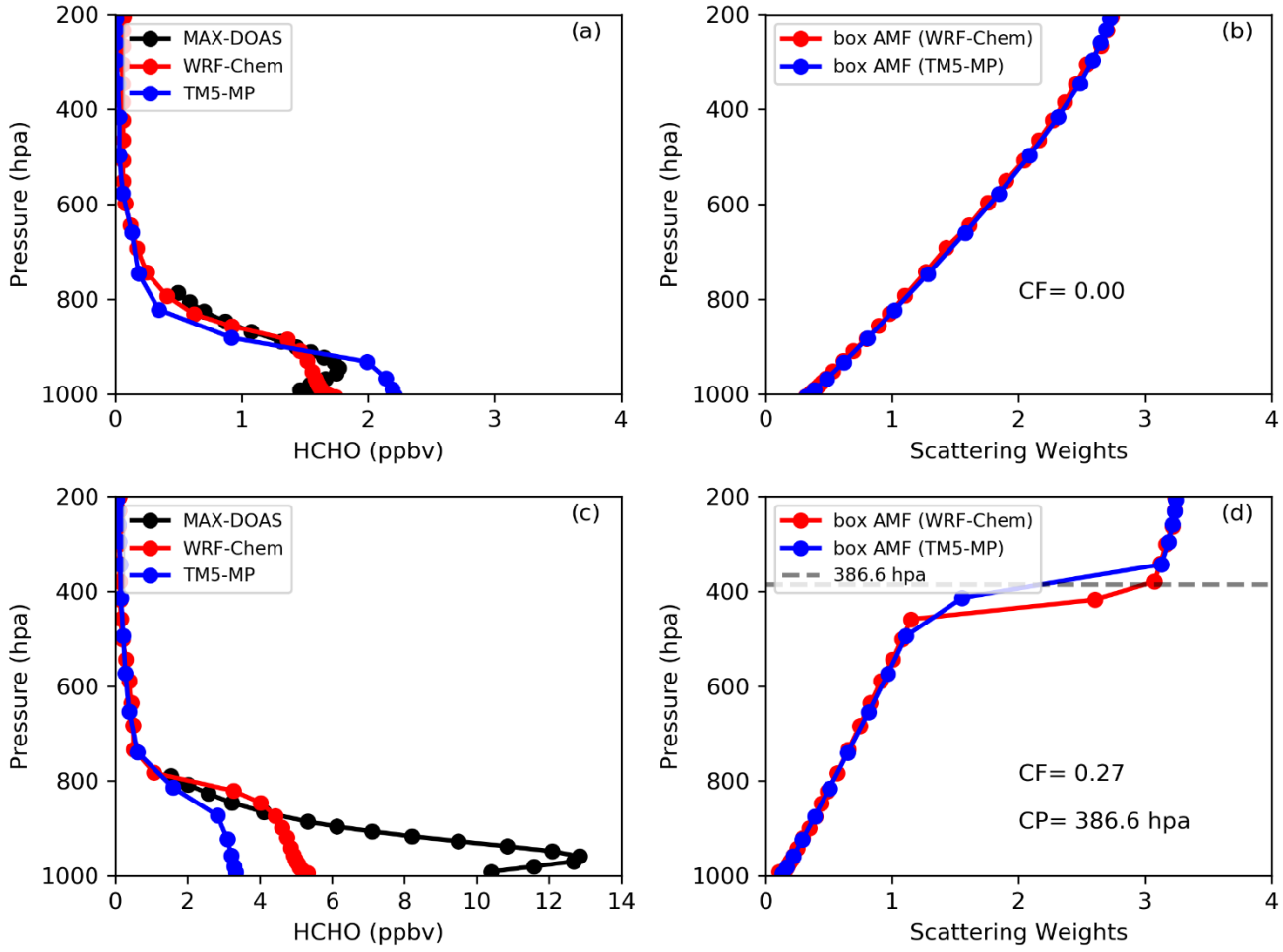


Figure A2. Daily averaged vertical HCHO profiles obtained from MAX-DOAS, WRF-Chem and TM5-MP model in clean case on 03 March 2019 (a) and in polluted case on 26 June 2019. Comparisons of box AMF using WRF-Chem and TM5-MP simulations in clean case with clear sky on 03 March 2019 (b) and in polluted case with cloudy sky on 26 June 2019 (c). The locations of two pixels are within 20 km of the CAMS site.

**Changes in manuscript:** L126-128, P6 and L370-374, P16-17 in the revised version.

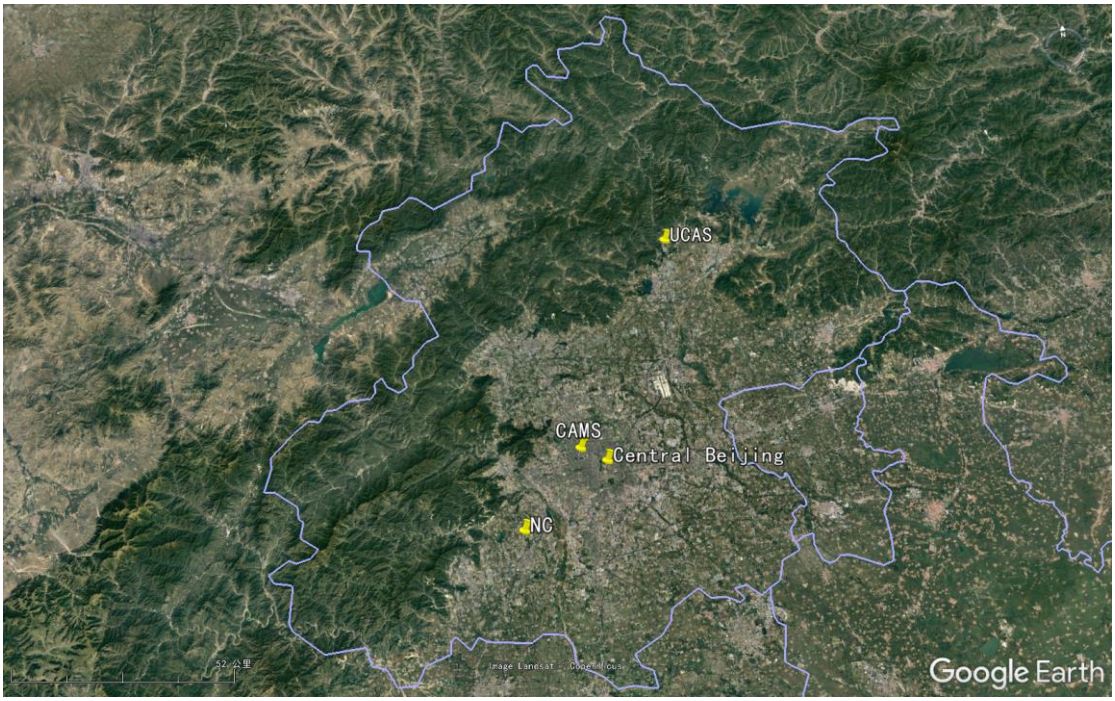


Figure A3. Locations of three MAX-DOAS sites in Beijing

The organization of the paper is clear (despite missing important aspects). However, while the use of English in the paper is good enough to be understandable it could benefit from further proofreading and grammar correction. Some language specific suggestions provided in the technical corrections section represent few of the possible improvements. While this reviewer will love to provide detailed language corrections it is time consuming and out of the scope of the reviewer duties.

For the reasons mentioned above the paper needs several major revisions and needs to expand to include essential details. The results shown are promising but in its current form, it will be difficult for anyone outside the authors to use the presented retrievals for a scientific study.

## Specific comments

### Abstract

A reference to the paper describing the operational TROPOMI HCHO retrieval by De Smedt et al., should be added here.

Recently Vigouroux et al., have published an excellent operational TROPOMI HCHO retrieval validation paper (https://www.atmos-meas-tech-discuss.net/amt-2020-30/). To cite in the introduction will provide a nice platform to place the results from this study into context later on.

**Responses:** Thank you very much for this suggestion. We have cited De Smedt et al. and Vigouroux et al. in the introduction.

**Changes in manuscript:** L50, P1 and L54-57, P3 in the revised version.

### Data sets

The retrieval of slant column densities requires the use of calibrated TROPOMI radiances. This is maybe, the most important

dataset that necessary to obtain the results presented in this work. Its description and how the authors obtained it should be a section in data sets.

**Responses:** Thank you very much for this suggestion. We have added the introduction of TROPOMI radiance in Sect. 2.1.

**Changes in manuscript:** L66-76, P3-4 in the revised version.

1. The original spatial resolution of TROPOPMI observations at NADIR was 3.5 km x 7 km but it improved to 3.5 km x 5.5 km in August 2019.

**Responses:** Thank you very much for this suggestion. We have modified it.

**Changes in manuscript:** L74-75, P4 in the revised version.

2. Fitting parameters considered in the spectral fitting of the operational product?

**Responses:** Thank you very much for this suggestion. The fitting parameters considered in the spectral fitting of the operational product are added in Table 1.

**Changes in manuscript:** L81-82, P4 and Table 1 in the revised version.

3. How is the reference sector correction applied in the operational product?

**Responses:** Thank you very much for this suggestion. The reference sector correction in the operational product is described in Sec. 2.2.

**Changes in manuscript:** L90-99, P4-5 in the revised version.

4. Procedures used to generate earthshine radiance over the remote Pacific in the operational HCHO retrieval.

**Responses:** Thank you very much for this suggestion. Daily detector row averaged radiance over the equatorial Pacific (latitude from 5°S to 5°N and longitude from 180°W to 140°W) is used as reference spectra. Due to residual HCHO signals in reference, the differential SCD (DSCD) is retrieved in spectra fitting.

**Changes in manuscript:** L85-87, P4 in the revised version.

5. Besides a-priori profiles and observation geometry, information about clouds, aerosols and surface reflectance play important roles in AMFs calculations. How is the operational product accounting for them?

**Responses:** Thank you very much for this suggestion. Information about data sets used in AMF calculation was added in Table 1.

**Changes in manuscript:** L222, P10 and Table 1 in the revised version.

6. Does the model simulation include information about pyrogenic sources?

**Responses:** Thank you very much for this suggestion. The open burning emission is obtained from the Fire INventory from NCAR (FINN) model (Wiedinmyer et al., 2010).

**Changes in manuscript:** L118-119, P5 in the revised version.

7. What was the spin off period of the simulations?

**Responses:** Thank you very much for this suggestion. Maybe the referee has a doubt about the spin-up period of the WRF-Chem simulations. WRF-Chem simulation is carried out from July 2019 to July 2019 with five days spun up prior to the simulation.

**Changes in manuscript:** L119-120, P5 in the revised version.

8. It will be interesting to have a reference for the MEIC inventory.

**Responses:** Thank you very much for this suggestion. The paper of (Li et al., 2017) was cited in the revised version.

**Changes in manuscript:** L116, P5 in the revised version.

9. What are the uncertainties associated with TROPOMI HCHO retrievals and MAX-DOAS observations. Table 1 could be expanded with information about the estimated uncertainties for each site as well as the dates and amount of available data.

**Responses:** Thank you very much for this suggestion. Error analysis of TROPOMI HCHO retrieval is added in Section 4. Available days and averaged relative error of MAX-DOAS measurements within ±1 h around the TROPOMI overpass time are added in Table 2.

**Changes in manuscript:** L241-292, P11-13 and Table 2 in the revised version.

**HCHO SCD retrieval: wavelength calibration**

One has to assume that S represents the preflight instrument slit function. It will be very beneficial to discuss the behavior of the preflight slit function. Are they available to the public? How stable the instrument slit function has been after launch?

**Responses:** Thank you very much for this suggestion. The Full-Width at Half-Maximum (FWHM) and asymmetric factor of the instrument slit function are obtained by fitting the daily irradiance to the high resolution solar spectra using the Gauss-Newton Nonlinear Least Squares (NLLS) method assuming the asymmetric Gaussian shape of slit function. The time series of the fitted TROPOMI slit function parameter from August 2018 to July 2019 in Fig. A4 shows that the TROPOMI slit function is stable after lunch. Therefore, the preflight TROPOMI slit function is used in wavelength calibration procedure. The preflight slit function is obtained from the TROPOMI Calibration Key Data (CKD) (available at http://www.tropomi.eu/data-products/isrf-dataset, last access: 22 May 2019) which is derived from TROPOMI calibration measurements performed in March 2015 at CSL in Liege. Comparing the spectral fit residual of using different versions of preflight slit function in the spectral fitting, we found that using version v3.0.0 results in lowest residual (Fig. S3). The preflight instrument slit function version v3.0.0 is used in our retrieval, while the operational product uses version v1.0.0 preflight slit function.

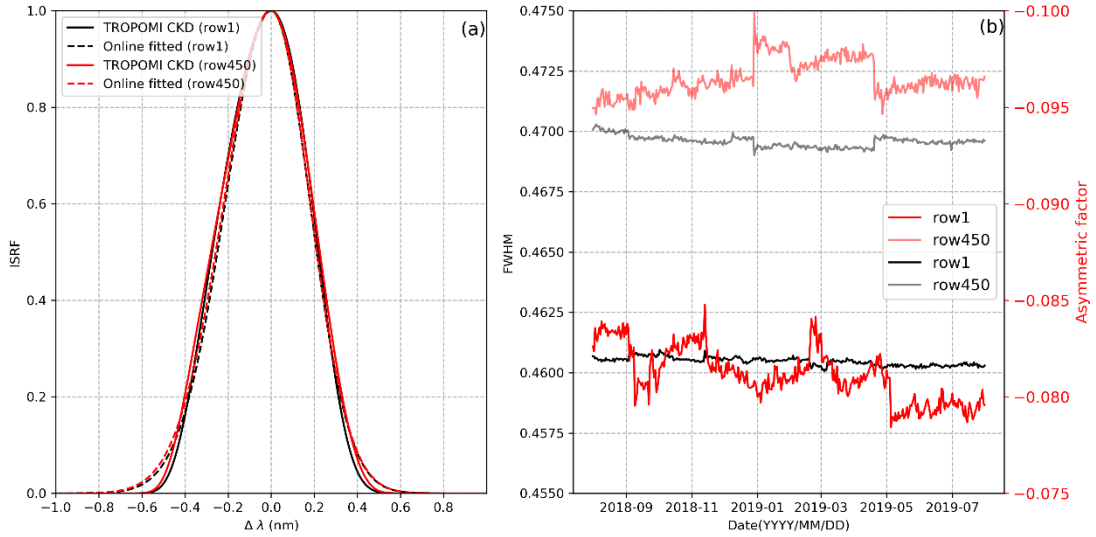


Figure A4. (a) The slit function from TROPOMI CKD at 340nm and online fitted for row 1 and row 450 on 01 August 2018. (b) Time series of FWHM and asymmetric factor of online fitted slit function from August 2018 to July 2019.

**Changes in manuscript:** L159-169, P7-8 in the revised version.

### HCHO SCD retrieval: Radiance fitting

As mentioned above, there is lack of detail in the description of the methodology employed. Please explain the following questions:

(1) Methodology employed to calculate the daily average earthshine radiance over the Pacific.

**Responses:** Thank you very much for this suggestion. Radiances measured 1 day before the processing day over the Pacific with latitudes ranging from 30°S to 30°N and longitude ranging from 180°W to 140°W are averaged and used as reference in the spectral fit.

**Changes in manuscript:** L179-180, P8 in the revised version.

(2) Any I0 corrected cross sections in the spectral fit.

**Responses:** Thank you very much for this suggestion. $O_3$ cross sections at two temperatures are $I_0$ corrected in the spectral fitting.

**Changes in manuscript:** Table 1 in the revised version.

(3) What is the impact of not including $SO_2$ when if $SO_2$ optical thickness becomes relevant.

**Responses:** Thank you very much for this suggestion. We plotted the spectral fitting residual with (red lines) and without (wathet lines) considering $SO_2$ cross section for HCHO polluted (a) and clean (b) cases in $SO_2$ polluted region (Fig. A1). Considering $SO_2$ cross section has no contribution on reducing residual and increases residual at some wavelengths on the contrary.

(4) What is the impact of not including water vapor?

**Responses:** Thank you very much for this suggestion. Laboratory measurements of water vapor absorption lines only extend to 25,470 $cm^{-1}$ (393 nm) (Dupre et al., 2005). (Lampel et al., 2016) indicated that water vapor can potentially have an impact on the spectral retrievals of tropospheric HCHO while the absorption at 335 nm could not be unambiguously identified in measurements so far.

(5) Which method is employed to estimate Raman spectra?

**Responses:** Thank you very much for this suggestion. The high resolution solar spectrum (Chance and Kurucz, 2010) is convolved with the rotational Raman spectra of $O_2$ and $N_2$ to produce the Raman spectrum (Chance and Spurr, 1997). The paper (Chance and Spurr, 1997) is cited in the revised version.

**Changes in manuscript:** L181, P8 and Table 1 in the revised version.

(5) How was the fitting window selected? HCHO retrievals show big dependencies with fitting windows.

**Responses:** Thank you very much for this suggestion. We use the same fitting window with operational product in DSCD retrieval. The uncertainty of fitting window selection is discussed in Section 4.1.

(6) New O3 cross sections have become available in recent years (for example Serdyuchenko et al., 2014 (https://www.atmos-meas-tech.net/7/609/2014/)). (7) Have the authors taken into account the effect of ozone in the fitted slant columns as described by Pukite et al., 2008 (https://www.atmos-meas-tech.net/3/631/2010/amt-3-631-2010.pdf).

**Responses:** Thank you very much for this suggestion. In our retrieval, we didn't take into account the first order Taylor series expansion for $O_3$ SCD. The uncertainty without considering Taylor expression for $O_3$ SCD is discussed in Section 4.1. We did the sensitivity tests about effect from difference of $O_3$ cross sections and Taylor series approach for HCHO polluted and clean cases. The spectral fitting residuals are plotted in Figure. A1 and fitting SCDs, random errors and RMS are presented in Table A1. For HCHO polluted case, using newly published $O_3$ cross sections changes SCD by 0.7% with random error and RMS unchanged. For HCHO clean case, using newly published $O_3$ cross sections changes SCD by 1.7% with random error unchanged and RMS increasing 0.1. The effect of using Taylor series of $O_3$ cross section in the spectral retrieval is evaluated through sensitivity analysis (Table 3). After reference sector correction, systematic difference regarding to Taylor series of $O_3$ cross section is estimated to be 3.49%. The uncertainties from $O_3$ cross section and without using Taylor series approach are discussed in Section 4.1.

## AMF calculation

Details missing in the AMF calculation include: (1) Terrain height and surface pressure corrections.

**Responses:** Thank you very much for this suggestion. The surface pressure and terrain height we used are obtained from the operational HCHO product which are corrected.

(2) Origin of cloud information.

**Responses:** Thank you very much for this suggestion. Cloud parameters used in AMF calculation in our retrieval are from the operational TROPOMI cloud product. Cloud fraction is retrieved using the Optical Cloud Recognition Algorithm (OCRA) and cloud top height (pressure) and optical thickness (albedo) are retrieved using Neural Networks (ROCINN) algorithm using the "Clouds-as-Reflecting-Boundaries" (CRB) model, treating clouds as simple Lambertian surfaces (Loyola et al., 2018). The operational TROPOMI cloud product is also available at the Copernicus Open Access Hub (https://scihub.copernicus.eu/, last access: 22 May 2019).

**Changes in manuscript:** L100-105, P5 in the revised version.

(3) Descriptions of the nodes of the box AMF look up table.

**Responses:** Thank you very much for this suggestion. The grid points of parameters in creating the LUT are same with De Smedt et al (2018).

**Changes in manuscript:** L208, P9 in the revised version.

(4) VLIDORT set up.

**Responses:** Thank you very much for this suggestion. The paper (Spurr, 2008) is cited introducing VLIDORT 2.6

**Changes in manuscript:** L207, P9 in the revised version.

(4) Impact of aerosols.

**Responses:** Thank you very much for this suggestion. Aerosol extinction profiles are also retrieved by the MAX-DOAS. Aerosol optical properties, such as single-scattering albedo (SSA) and Ångström exponent obtained from the Aerosol Robotic Network (AERONET) station in Beijing (https://aeronet.gsfc.nasa.gov/, last access: 22 May 2019) are used as input parameters for the MAX-DOAS aerosol profile retrieval. As the aerosol profiles from MAX-DOAS are retrieved at 360nm, we further converted the profile to 340nm using Ångström exponent obtained from the AERONET measurements. To estimate aerosol effect on TROPOMI HCHO retrieval, we calculate the AMFs using MAX-DOAS measured aerosol extinction profiles using VLIDORT (version 2.6) (Spurr, 2008). The AMFs are applied on the operational product and our retrieval. The TROPOMI HCHO VCDs with and without considering aerosols are compared to MAX-DOAS HCHO VCDs. The comparison results are shown in Figure 10. The results show that considering aerosol in the AMF calculations does not improve the agreement with ground based measurements. Considering aerosol effect in TROPOMI retrieval reduces HCHO VCDs by 11.46% ( $\pm$ 1.48%) for the operational product and 17.61% ( $\pm$ 1.92%) for our retrieval in winter. The reduction over urban site is more significant than suburban sites, mainly due to higher aerosol load. Operational product using both HCHO and aerosol extinction profiles from MAX-DOAS shows underestimation of 8.36 % ($\pm$ 4.63 %). Our retrieval using MAX-DOAS HCHO and aerosol extinction profiles for AMF calculation underestimates HCHO VCD by 18.53% ( $\pm$ 4.04 %).

**Changes in manuscript:** L452-466, P20 in the revised version.

(5) Error analysis.

**Responses:** Thank you very much for this suggestion. Error analysis in TROPOMI HCHO retrieval is discussed in Section 4.2.

**Changes in manuscript:** L241-292, P11-13 in the revised version.

### Reference sector correction of SCDs

Add description of the GEOS-Chem configuration employed in the reference sector correction. Which longitudes define remote Pacific? Is the correction applied only to -30 degrees to 30 degrees? That region is used to calculate the earthshine radiance. Any contributions outside -30 to 30 degrees will not be correcting for the residual HCHO column but for biases of different origin.

**Responses:** Thank you very much for this suggestion. Radiances measured 1 day before the processing day over the Pacific with latitudes ranging from 30°S to 30°N and longitude ranging from 180°W to 140°W are averaged and used as reference in the spectral fit. The first step of reference sector correction is retrieving the DSCDs using average earthshine radiance reference, calculating the corresponding AMFs and storing them as a separate database. The HCHO VCD over remote Pacific Ocean is simulated by GEOS-Chem assuming HCHO over this region is mainly from the oxidation of $CH_4$. The simulated HCHO SCD is calculated by multiplying the VCD ($VCD_G$) taken from GEOS-Chem with the corresponding AMF ($M_0$). Assuming HCHO in the reference sector correction is well simulated by GEOS-Chem, the difference between the simulated and retrieved DSCD ($DSCD_0$) is recognized as the SCD bias caused by residual HCHO signal in reference spectrum. TROPOMI measurements over the Pacific (latitude from 90°S to 90°N and longitude from 160°W to 140°W) are first binned according to their latitude to 500 bins with a resolution of 0.36°. The median value of each bin is then used for the calculation of the SCD background correction (González Abad et al., 2015; González Abad et al., 2016). Assuming the SCD correction is constant in the longitude direction, the SCD correction at 500 gridded latitude points from 90°S to 90°N are linearly interpolated to the latitude of each pixel over China. The interpolated SCD correction is then applied on the retrieved DSCDs to calculate SCDs. Therefore, DSCDs outside -30 to 30 degrees are also corrected. We have clarified in the revised version.

**Changes in manuscript:** L179-180, P8 and L231-240, P11 in the revised version.

### Comparison of operational and improved HCHO product

What are the coincidence criteria to match TROPOMI and MAX-DOAS measurements? To use daily averages in the case of MAX-DOAS seems inappropriate considering the diurnal variations of HCHO columns.

**Responses:** MAX-DOAS measurements are temporally averaged within $\pm$1 h around the TROPOMI overpass time, while TROPOMI pixels within 20 km of the MAX-DOAS site are spatially averaged for comparison. TROPOMI pixels in our retrieval and operational product are both filtered for intensity-weighted cloud fraction smaller than 0.3, root mean square of spectral fit residual (RMS) smaller than $10^{-3}$, AMF larger than 0.1 and SZA smaller than 70°, quality assurance value (QA value) larger than 0.55 and successful SCD retrieval. The histograms showing the distributions of RMS of spectral fit of the operational product and our retrieval on 06 August 2018 over China are shown in Figure. S5. About 15% and 17% of measurements in the operational product and our retrieval show RMS larger than $10^{-3}$.

**Changes in manuscript:** L307-313, P14 in the revised version.

### Comparisons of SCD retrievals

This discussion applies to SCDs or ΔSCDs? The result of the spectral fit is in both cases the differential slant column but the

title of the section indicates the comparison of slant columns. In that case, differences are not only due to the spectral fit but also to the reference sector correction. What is the impact of using different earthshine radiances?

**Responses:** Thank you very much for this suggestion. In section 5.1.1, we compare DSCDs and SCDs after applying reference sector correction between operational product and the new retrieval. The biases between DSCDs and RMS in operational product and our retrieval are mainly related to the difference of retrieval method, retrieval settings and selection of reference. To investigate the impact of selection of earthshine radiance reference, we retrieved HCHO DSCDs using daily detector row averaged radiance over the equatorial Pacific (latitude from 5°S to 5°N and longitude from 180°W to 120°W) as reference using BOAS method. Comparisons of HCHO DSCDs and HCHO SCDs after applying reference sector correction using different earthshine radiance reference are presented in Figure. A5. The retrieved DSCDs using different earthshine radiance reference correlated well (R=0.99, Slope=0.99) and with a difference of 30% ($0.11 \pm 0.08 \times 10^{16}$ molec cm$^{-2}$). The bias is compensated (1.9%) by the reference sector correction (Figure. A5 (b)).

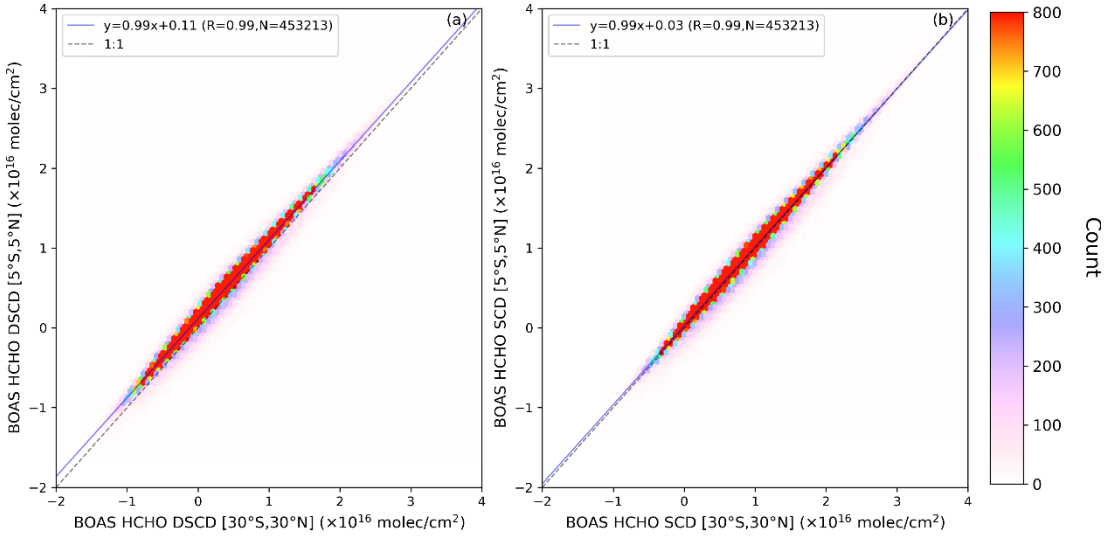


Figure A5. Pixel to pixel comparisons of BOAS HCHO DSCDs (a) and BOAS HCHO SCDs (b) using different earthshine radiance reference on 06 August 2018 in the region between 73° E and 130° E, and 18° N and 54° N. The labels with [30°S, 30°N] represent that average of radiances of the equatorial Pacific (latitude from 30°S to 30°N and longitude from 180°W to 140°W) is used as reference spectra. The labels with [5°S, 5°N] represent that average of radiances of the equatorial Pacific (latitude from 5°S to 5°N and longitude from 180°W to 120°W) is used as reference spectra.

**Changes in manuscript:** L339-345, P15 in the revised version and Figure. S6 in the supplement file.

What are the reasons to filter out retrievals with RMS higher than $10^{-3}$. What is the percentage of retrievals with RMS above the threshold? What is the definition of outliers? Showing a histogram of the distributions of both datasets will help to understand the outlier definition.

**Responses:** Thank you very much for this suggestion. The histograms of the distributions of RMS in operational product retrieval and our retrieval are shown in Figure. A6. About 15% and 17% of measurements in the operational product and our

retrieval show RMS larger than $10^{-3}$.

**Changes in manuscript:** L312-313, P14 in the revised version and Figure. S5 in the supplement file.

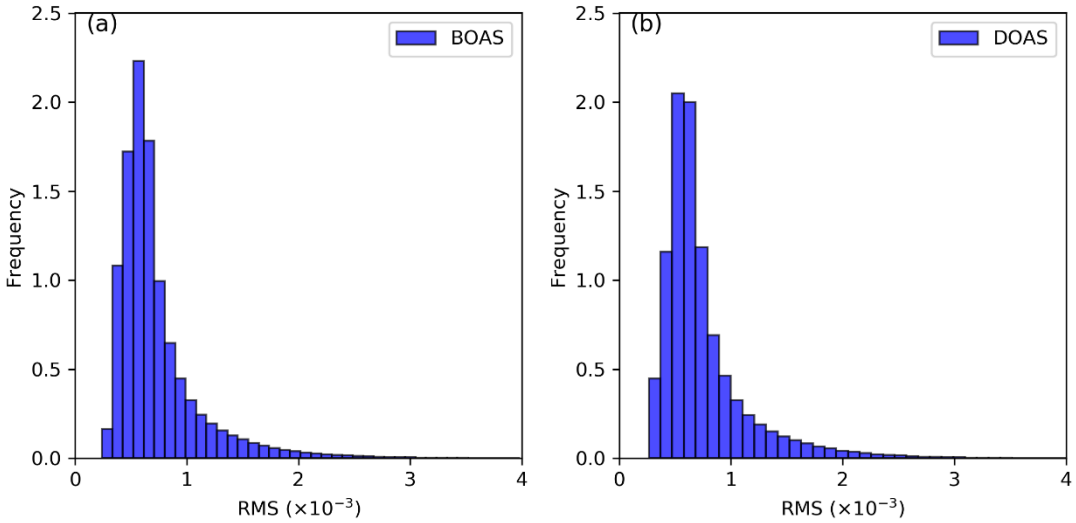


Figure A6. The histograms of the distributions of RMS in operational product retrieval (a) and our retrieval (b).

The authors make a distinction between non-corrected and corrected SCDs. It is not clear in the text what corrected implies. One has to assume we are talking about reference sector corrected and non-corrected SCDs. If that is the case, one could argue that part of the differences observed between SCDs in the non-corrected case are due to the different selection (or calculation) of earthshine radiance reference. To make a real comparison of the performance of booth fitting algorithms they should be using consistent earthshine radiances. The results seem to indicate that part of the biases are due to using different earthshine radiances since the correlation for the non-corrected and corrected SCDs columns is similar for both products but the bias between them is significantly reduced after applying the correction.

**Responses:** Thank you very much for this suggestion. Due to residual HCHO signals in reference, the differential SCD (DSCD) is retrieved in spectra fitting. Therefore, reference sector correction has to be applied on the retrieved DSCDs to calculate SCDs. The reference sector correction is described on Sec. 3.3. We have cleared it in the revised version. To investigate the impact of selection of earthshine radiance reference, we retrieved HCHO DSCDs using daily detector row averaged radiance over the equatorial Pacific (latitude from 5°S to 5°N and longitude from 180°W to 120°W) as reference using BOAS method. Comparisons of HCHO DSCDs and HCHO SCDs after applying reference sector correction using different earthshine radiance reference are presented in Figure. A5. The retrieved DSCDs using different earthshine radiance reference correlated well (R=0.99, Slope=0.99) and with a difference of 30% ($0.11 \pm 0.08 \times 10^{16}$ molec $cm^{-2}$). The bias is compensated (1.9%) by the reference sector correction (Figure. A5 (b)). To investigate the impact from retrieval method, BOAS HCHO DSCDs using same retrieval settings with operational DSCD retrieval are compared with DOAS HCHO DSCDs (Figure. A7). Using same retrieval settings, difference between DOAS HCHO DSCDs and BOAS HCHO DSCDs (27.33%) is significantly reduced and the remaining difference is due to retrieval algorithm. Besides, smaller difference (4.41%) in HCHO SCDs indicates that

reference sector correction reduces the effect from retrieval method (Figure. A7 (b)).

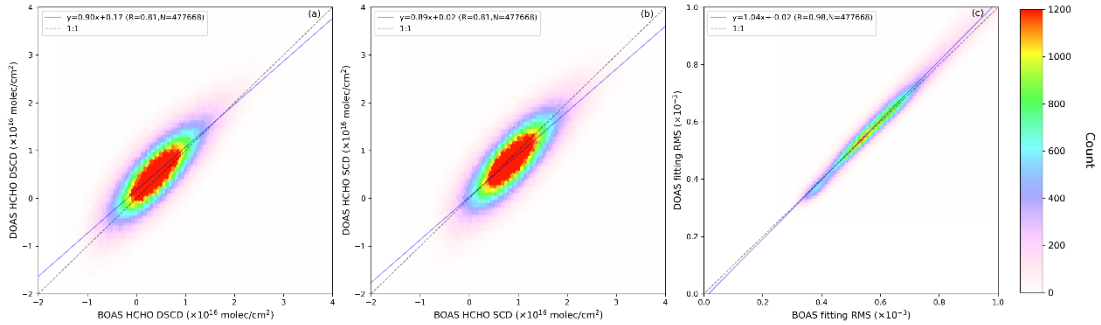


Figure A7. (a) Pixel to pixel comparisons of DOAS and BOAS HCHO DSCDs, (b) DOAS and BOAS HCHO SCDs and (c) DOAS and BOAS fitting RMS on 06 August 2018 in the region between 73° E and 130° E, and 18° N and 54° N. Same retrieval settings are used in DOAS and BOAS retrieval.

**Changes in manuscript:** L340-349, P15-16 in the revised version and Figure. S7 in the supplement file.

### Comparisons of retrievals after AMF calculations

One question that raises this section and always permeates the use of high-resolution models is how much information is folded back from the model in the retrieval. To better understand this question it will be very useful to know more about the WRF-Chem simulations and how they were used. The operational product employs daily forecast interpolated in time and space. This procedure should be added to the methodology. How do the box-AMFs of the different retrievals compare?

**Responses:** Thank you very much for this suggestion. Information about more WRF-Chem is added in the Sect. 2.4. A priori HCHO profile for TROPOMI AMF calculations are calculated by interpolating WRF-Chem simulation spatio-temporally to the measurement time and location. This information is added in Sect. 3.2. The information that the operational product employs daily forecast interpolated in time and space is also added in Sect. 2.2.

Besides higher horizontal resolution, WRF-Chem simulation also has a higher vertical spatial resolution compared to TM5-MP data set. Although the difference in vertical resolution only shows negligible effect on box AMF under clear sky condition (Fig. 6 (b)), lower vertical resolution profiles would cause significant impact for cloudy cases due to the interpolation of coarse grid (Fig. 6 (d)).

**Changes in manuscript:** L89, P4**,** L200-201, P9 and L371-374, P17 in the revised version.

### Comparison between HCHO VCDs observed by MAX-DOAS and TROPOMI

Blue lines in figure 7 right panels, more than speaking of the retrieval, speak about the difference between the a priori profiles for both models and the retrieved MAX-DOAS profiles. Slopes and correlation coefficients are similar (within error estimates) for both retrievals when using model a priori. It is easier to imagine how the comparison of the operational retrieval with MAX-DOAS observations will also suffer a dramatic improvement if MAX-DOAS a priori were to be used in the AMF calculations.

**Responses:** Thank you very much for this suggestion. We have recalculated HCHO VCD for the operational product by using MAX-DOAS HCHO profiles as a priori profiles. The Pearson correlation coefficient (R) between the recalculated operational

product and MAX-DOAS HCHO VCD decreases by 0.02 to 0.79. The slope of the regression line increases by 0.19 to 0.84 with offset reduces by $0.24 \times 10^{16}$ molec $cm^{-2}$ to $0.15 \times 10^{16}$ molec $cm^{-2}$. Although the recalculated TROPOMI operational product shows improved correlation with MAX-DOAS observations, our retrieval using MAX-DOAS measurements as a priori profile still shows a better agreement with MAX-DOAS HCHO VCDs. It also indicates that the BOAS spectral retrieval of SCDs agree better to the ground based observations over China.

**Changes in manuscript:** L406-412, P18 in the revised version.

### Technical corrections

Line 18 (grammatical suggestion (GS)): Since what is improved is the HCHO retrieval a more correct grammatical structure will be "We present an improved retrieval of formaldehyde (HCHO) over China from the TROPO…"

**Responses:** Thank you very much for this suggestion. Changed.

Line 23 (GS): remove "the" from "agreement with the ground based…" since it is possible there are more than MAXDOAS measurement than those used in this study.

**Responses:** Thank you very much for this suggestion. Changed.

Line 25 (GS): add "s" to "profile" "…higher resolution a priori profiles".

**Responses:** Thank you very much for this suggestion. Changed.

Line 26: The percentage of what is reported by 61.11% and 0.15%? With the current text it is impossible to know if it refers to the change in the mean VCD, or the percentage of the bias correction attributed to each step. Please specify.

**Responses:** Thank you very much for this suggestion. We added the error bar in Table 3 and find the conclusion that changing SCD retrieval method only shows a tiny effect of 0.15% is less rigorous. The sentence is changed into "The improvements are mainly related to the AMF calculation with more precise a priori profiles in winter. Using more precise a priori profiles in general reduces HCHO VCDs by 52.37 % ($\pm$ 27.09 %) in winter.

**Changes in manuscript:** L24-25, P1 in the revised version.

Line 29 (GS): Change "indicating" to "indicate".

**Responses:** Thank you very much for this suggestion. Changed.

Line 45 (GS): Add "to" after compared "Compared to its predecessor"

**Responses:** Thank you very much for this suggestion. Changed.

Line 53 (GS): Add "s" to "profile" and "a" after "from". Which regional model is employed?

**Responses:** Thank you very much for this suggestion. The AMF calculation is improved by using higher resolution a priori profiles from the regional Weather Research and Forecasting model (WRF-Chem). Changed. A priori HCHO profile for TROPOMI AMF calculations are calculated by interpolating WRF-Chem simulation spatio-temporally to the measurement

time and location.

Line 64 (GS): Change “is” to “are” “.., which are devided in …”.

**Responses:** Thank you very much for this suggestion. Changed.

Line 91 (GS): Add “the” in “… is located in the Chinese…”

**Responses:** Thank you very much for this suggestion. Changed.

Line 105: The first step of the methodology explained in this paper is the calculation of ΔSCD, not SCD.

**Responses:** Thank you very much for this suggestion. Changed.

Line 111: There can be other causes for wavelength miss-alignment can be Doppler shift, non-uniform illumination of the slit due to presence of clouds or other high reflectance surface in the pixel.

**Responses:** Thank you very much for this suggestion. Added.

**Changes in manuscript:** L147-148, P7 in the revised version.

Line 115: What is the benefit of having two closure polynomials during wavelength calibration considering that it is done using TOA irradiances and there for are not affected by the presence of clouds or aerosols that may introduce low-frequency structures?

**Responses:** Thank you very much for this suggestion. We compared fitting residuals with and without considering the third baseline and scaling polynomials during wavelength calibration. Considering the third scaling and baseline polynomials decreases the residual largely.

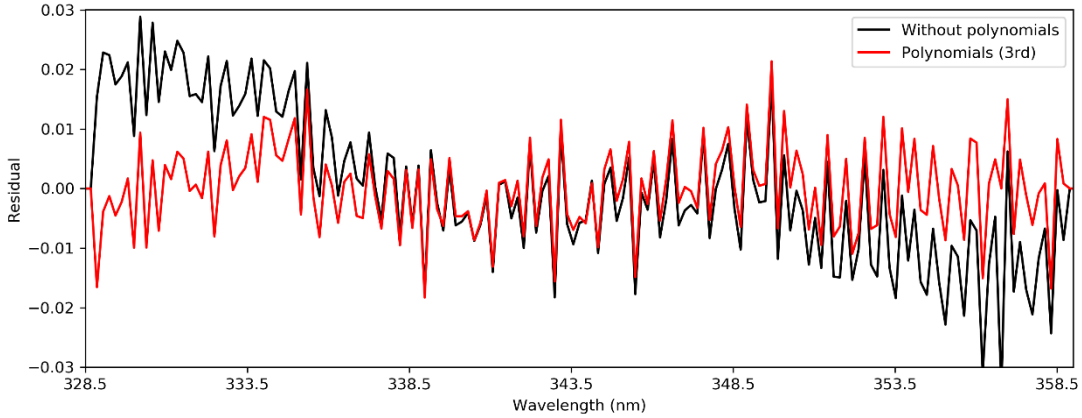


Figure A8. Comparison of fitting residuals with and without considering the third baseline and scaling polynomials during wavelength calibration.

**Changes in manuscript:** L68-171, P8 in the revised version.

Line 142 (GS): Add “presence of” to “… atmosphere (presence of clouds, vertical HCHO distribution…”

**Responses:** Thank you very much for this suggestion. Changed.

Line 143: What is a comprehensive radiative transfer model?

**Responses:** Thank you very much for this suggestion. The sentence seems superfluous because the following content has a detailed introduction about AMF calculation. The sentence is deleted.

Line 150 (GS): Add “on” as “The box AMF depends on wavelength, …”

**Responses:** Thank you very much for this suggestion. Changed.

Line 173 (GS): Add “be” to “… is known to be caused by …”

**Responses:** Thank you very much for this suggestion. The sentence is changed into “Using earthshine radiance over remote Pacific Ocean as reference significantly reduces the influence from unresolved spectral structures which could significantly improve the spectral retrieval of weak absorber, i.e., HCHO.”

Line 173: Could the authors provide a reference for the known cause of stripping?

**Responses:** Thank you very much for this suggestion. The sentence is changed into “Using earthshine radiance over remote Pacific Ocean as reference significantly reduces the influence from unresolved spectral structures which could significantly improve the spectral retrieval of weak absorber, i.e., HCHO.”

Line 175: AMFs are not retrieved; they are calculated and are independent of a remote Pacific earthshine radiance.

**Responses:** Thank you very much for this suggestion. Changed. The first step of reference sector correction is retrieving the DSCDs using average earthshine radiance reference, calculating the corresponding AMFs and storing them as a separate database.

Line 204 & 209 (GS): Change “outliners” to “outliers”.

**Responses:** Thank you very much for this suggestion. Changed.

Line 216 & 217: What is the error associated to the average SCDs? Standard deviations?

**Responses:** Thank you very much for this suggestion. Standard deviations are shown in the brackets associated to the average DSCDs. Changed.

Line 222: How is the 32.32% lower calculated? A difference of 0.02 x $10^{16}$ molecules $cm^{-2}$ looks rather small.

**Responses:** Thank you very much for this suggestion. The sentence is changed to “Averaged SCD taken from the operational product on 06 August 2018 over China ($0.85 \pm 0.69 \times 10^{16}$ molec $cm^{-2}$) is on average 4.49 % lower than our retrieval ($0.89 \pm 0.61 \times 10^{16}$ molec $cm^{-2}$).”

Line 223-226 (GS): Please rewrite sentence.

**Responses:** Thank you very much for this suggestion. The sentences are changed into "We use SCDs in our retrieval and AMFs in operational product to calculated the updated HCHO VCD. The NMB of the two data sets are shown in Table 5. The bias between the updated HCHO VCD and operational HCHO VCD is caused by difference in SCD retrieval. The updated and operational product is also compared to the MAX-DOAS observations."

Line 228: How does BOAS compute mean random errors? Does this calculation use the operation product random error definition? Without describing both is impossible to interpret BOAS random errors lower than DOAS by 22%.

**Responses:** Thank you very much for this suggestion. The random uncertainty in DSCDs retrieval is described in Sect. 4.1.

Figure 1: What is figure 1 trying to illustrate. It is not mention in the text.

**Responses:** Thank you very much for this suggestion. Figure 1 shows the location and HCHO concentration of three MAX-DOAS sites. It is cited in L123, P6 in Section 2.5.

Table 1: What is the definition of viewing azimuth angle? Probably clock wise with respect to North.

**Responses:** Thank you very much for this suggestion. The original Table 1 is Table 2 in the revised version. Viewing azimuth angle of the north is taken as zero degree. It is added in the caption of Table 2.

Table 2: What is the methodology employed to calculate the Raman spectra? What is the definition of Pacific (remote)? Will it be possible to provide a reference for the pre-flight instrument slit function?

**Responses:** Thank you very much for this suggestion. The original Table 2 is Table 1 in the revised version. The high resolution solar spectrum (Chance and Kurucz, 2010) is convolved with the rotational Raman spectra of $O_2$ and $N_2$ to produce the Raman spectrum (Chance and Spurr, 1997). The paper (Chance and Spurr, 1997) is cited in the revised version.

Radiances measured 1 day before the processing day over the Pacific with latitudes ranging from 30°S to 30°N and longitude ranging from 180°W to 140°W are averaged and used as reference in the spectral fit.

The preflight TROPOMI slit function is obtained from the TROPOMI Calibration Key Data (CKD) (available at http://www.tropomi.eu/data-products/isrf-dataset) which is derived from TROPOMI calibration measurements performed in March 2015 at CSL in Liege.

The information is added in the revised version.

**Changes in manuscript:** Table 2, L163-165, P7 and L179-180, P8, in the revised version.

Figure 2: What the figure shows is the ΔSCD not SCD. Please correct. The size of the residuals in plot (b) seem to be large considering an RMS of $2.78 \times 10^{-4}$.

**Responses:** Thank you very much for this suggestion. Figure 2 shows the spectral retrieval of HCHO DSCDs and Figure 2 is updated. The values are updated.

Figure 3: A different color map, extending to negative values, will provide a better picture of the BOAS retrieval performance since there is a significant number of pixels with negative columns. Which orbits contribute to these plots?

**Responses:** Thank you very much for this suggestion. The color bar range in Figure 4 is changed into from -2 x $10^{16}$ to 2 x $10^{16}$. And the Figure 3 is updated. The orbits from 04210 to 04213 contribute to these plots.

Figure 4: Does plot (a) show ΔSCDs and plot (b) SCDs? Please clarify. Does this regression consider an independent variable? Probably is better to consider the errors of both variables in the linear fit.

**Responses:** Thank you very much for this suggestion. Figure 5 (a) shows the DSCDs comparison and (b) shows SCDs comparison. It is clarified in the revised version. We don't consider an independent variables in the linear fit. The linear fit in our study is more direct to show the difference between the two data sets.

Table 3: It is very difficult to interpret. How can be the NMBs between satellite and MAX-DOAS be 0% for the operational product? The caption needs to be re-written to provide a proper description of what the table is showing.

**Responses:** Thank you very much for this suggestion. $NMB_{S1,S2}$ is NMBs between TROPOMI HCHO VCDs with different retrieval settings, and $NMB_{S1,M}$ is NMBs between TROPOMI and MAX-DOAS observations. The caption is changed into "NMBs between TROPOMI HCHO VCDs with different retrieval settings ($NMB_{S1,S2}$) and NMBs between TROPOMI and MAX-DOAS observations ($NMB_{S1,M}$). TROPOMI HCHO VCDs are calculated with four different settings, (1) operational retrieval setting (2) replacing DOAS SCDs using BOAS SCDs in the operational product, (3) changing the a priori profiles from TM5 to regional WRF-Chem simulations in the operational product and (4) both (2) and (3) changes in the operational product. The error bars ( $\pm$ 2 SE) are also presented. All values are in %."

Figure 5: What is the methodology used to calculate the vertical profiles? Time averaging, filtering of MAX-DOAS observations… Co-registration of models and models with in-situ measurements.

**Responses:** Thank you very much for this suggestion. In AMF calculations, both WRF-Chem and TM5-MP simulations are interpolated to TROPOMI spatial resolution. Interpolated WRF-Chem and TM5-MP simulations within 20 km of the MAX-DOAS site are spatially averaged to compare with MAX-DOAS profiles. MAX-DOAS profiles are temporally averaged in the period 13:30-14:30 (Local Time) within ±1 h around the TROPOMI overpass time.

**Changes in manuscript:** L366-370, P16 in the revised version.

Figure 6: Using a divergent color map scale in plot © will help to appreciate the positive and negative differences. What is the effect of clouds and aerosols? Some of the big differences resemble cloud structures. What is the correlation between both AMF calculations?

**Responses:** Thank you very much for this suggestion. The original Figure 6 is Figure 7 in the revised version. The color bar of Figure. 7(c) is updated to appreciate the positive and negative differences easily. We added the spatial distribution of cloud fraction (d) of orbit 04211 on 06 August 2018 in Figure. 7(d). The results show a similar spatial pattern. However, WRF-Chem AMF is mostly higher than the one calculated with TM5-MP HCHO profiles. The big differences of two AMFs are mainly

occurred in pixels with large cloud fraction.

**Changes in manuscript:** L383-384, P17 in the revised version.

Figure 8: Do these plots show improve HCHO data? It seems to show gridded data. What is the spatial sampling of the grid? Which methodology was used to calculate the gridded fields?

**Responses:** Thank you very much for this suggestion. Figure 8 shows the averaged HCHO VCDs in four seasons. Before averaging, TROPOMI HCHO VCDs in our retrieval are gridded into same grids (0.1°×0.1°). The grid methodology follows the method in (Zhu et al., 2017). The weights are calculated using relative error (Re) and intensity-weighted cloud fraction (cf):

$$\overline{N_V}(i) = \frac{\sum_{p=1}^{p=n(i)} \frac{N_v(p)}{\left(Re(p) * (1 + 3 * cf(p))\right)^2}}{\sum_{p=1}^{p=n(i)} \frac{1}{\left(Re(p) * (1 + 3 * cf(p))\right)^2}}$$

Where $\overline{N_V}(i)$ is gidded HCHO VCDs of grid cell. n(i) is number of satellite pixels falling in the grid cell i.


Boersma, K., Eskes, H., Dirksen, R., Veefkind, J., Stammes, P., Huijnen, V., Kleipool, Q., Sneep, M., Claas, J., and Leitão, J.: An improved tropospheric NO 2 column retrieval algorithm for the Ozone Monitoring Instrument, Atmos. Meas. Tech., 4, 1905-1928, https://doi.org/10.5194/amt-4-1905-2011, 2011a.

Boersma, K. F., Eskes, H., Dirksen, R., Veefkind, J. P., Stammes, P., Huijnen, V., Kleipool, Q., Sneep, M., Claas, J., and Leitao, J.: An improved tropospheric NO2 column retrieval algorithm for the ozone monitoring instrument, Atmos. Meas. Tech., 4, 1905-1928, https://doi.org/10.5194/amt-4-1905-2011, 2011b.

Chance, K., and Kurucz, R. L.: An improved high-resolution solar reference spectrum for earth's atmosphere measurements in the ultraviolet, visible, and near infrared, Journal of quantitative spectroscopy and radiative transfer, 111, 1289-1295, https://doi.org/10.1016/j.jqsrt.2010.01.036, 2010.

Chance, K. V., and Spurr, R. J.: Ring effect studies: Rayleigh scattering, including molecular parameters for rotational Raman scattering, and the Fraunhofer spectrum, Appl Optics, 36, 5224-5230, https://doi.org/10.1364/AO.36.005224, 1997.

De Smedt, I., Theys, N., Yu, H., Danckaert, T., Lerot, C., Compernolle, S., Van Roozendael, M., Richter, A., Hilboll, A., and Peters, E.: Algorithm theoretical baseline for formaldehyde retrievals from S5P TROPOMI and from the QA4ECV project, https://doi.org/10.5194/amt-11-2395-2018, 2018.

Dupre, P., Gherman, T., Zobov, N. F., Tolchenov, R. N., and Tennyson, J.: Continuous-wave cavity ringdown spectroscopy of the 8ν polyad of water in the 25195−25340cm−1 range, J. Chem. Phys., 123, 154307, 2005.

González Abad, G., Liu, X., Chance, K., Wang, H., Kurosu, T. P., and Suleiman, R.: Updated Smithsonian Astrophysical Observatory Ozone Monitoring Instrument (SAO OMI) formaldehyde retrieval, Atmos. Meas. Tech., 8, 19-32, https://doi.org/10.5194/amt-8-19-2015, 2015.

González Abad, G., Vasilkov, A., Seftor, C., Liu, X., and Chance, K.: Smithsonian Astrophysical Observatory Ozone Mapping and Profiler Suite (SAO OMPS) formaldehyde retrieval, Atmos. Meas. Tech., 9, 2797-2812, https://doi.org/10.5194/amt-9-2797-2016, 2016.

Lampel, J., Pohler, D., Polyansky, O. L., Kyuberis, A. A., Zobov, N. F., Tennyson, J., Lodi, L., Fries, U., Wang, Y., and Beirle,

S.: Detection of water vapour absorption around 363 nm in measured atmospheric absorption spectra and its effect on DOAS evaluations, Atmos. Chem. Phys., 17, 1271-1295, 2016.

Li, M., Zhang, Q., Kurokawa, J., Woo, J., He, K., Lu, Z., Ohara, T., Song, Y., Streets, D. G., and Carmichael, G. R.: MIX: a mosaic Asian anthropogenic emission inventory under the international collaboration framework of the MICS-Asia and HTAP, Atmos. Chem. Phys., 17, 935-963, https://doi.org/10.5194/acp-17-935-2017, 2017.

Spurr, R.: LIDORT and VLIDORT: Linearized pseudo-spherical scalar and vector discrete ordinate radiative transfer models for use in remote sensing retrieval problems, in: Light Scattering Reviews 3: Light Scattering and Reflection, edited by: Kokhanovsky, A. A., Springer Berlin Heidelberg, Berlin, Heidelberg, 229-275, 2008.

Wiedinmyer, C., Akagi, S. K., Yokelson, R. J., Emmons, L. K., Alsaadi, J. A., Orlando, J. J., and Soja, A. J.: The Fire INventory from NCAR (FINN): a high resolution global model to estimate the emissions from open burning, Geosci Model Dev, 4, 625-641, https://doi.org/10.5194/gmd-4-625-2011, 2010.

Zhou, Y., Brunner, D., Boersma, K. F., Dirksen, R., and Wang, P.: An improved tropospheric NO2 retrieval for OMI observations in the vicinity of mountainous terrain, Atmos. Meas. Tech., 2, 401-416, https://doi.org/10.5194/amt-2-401-2009, 2009.

Zhu, L., Jacob, D. J., Keutsch, F. N., Mickley, L. J., Scheffe, R., Strum, M., Gonzalez Abad, G., Chance, K., Yang, K., Rappengluck, B., Millet, D. B., Baasandorj, M., Jaegle, L., and Shah, V.: Formaldehyde (HCHO) As a Hazardous Air Pollutant: Mapping Surface Air Concentrations from Satellite and Inferring Cancer Risks in the United States, Environ Sci Technol, 51, 5650-5657, https://doi.org/10.1021/acs.est.7b01356, 2017.

Response to reviewer #2

We really appreciate your constructive comments and suggestions on our manuscript. We have considered every comment carefully, responded on a point to point and marked every change in red in the revised version.

## General comments

The paper aims to present an improved TROPOMI HCHO retrieval over China. Compared to the ESA operational product, two major differences are highlighted: (1) the use of BOAS instead of DOAS for the of fit the slant columns, (2) the use of a priori profiles from a regional model in order to recalculate the AMF, with a finer spatial resolution, and optimized emissions over China.

Overall, the paper fails in showing an improvement of the slant columns, the differences between the two products being negligible.

**Responses:** Thank you very much for this suggestion. We using a different spectral retrieval technique (BOAS method) of HCHO slant columns. Moreover, the background correction has also been improved. Although DOAS and BOAS HCHO DSCDs show a similar spatial pattern. The spatial distribution of BOAS HCHO SCD is expected to be smooth, less noisy. Besides, operational product using different SCD retrieval methods is compared with MAX-DOAS HCHO measurements. Using the BOAS HCHO SCDs reduced the underestimation in summer and overestimation in winter of the operational product. In summer, using different SCD retrieval methods results a difference of 7.00% (± 1.71%, ± Error) from the TROPOMI operational HCHO VCD. The result shows that using the BOAS HCHO SCDs reduced the underestimation in summer and overestimation in winter of the operational product.

The scientific interest of the paper lies in the second improvement. The authors should focus more on this aspect, and go further into a detailed analysis of the spatio-temporal effects of using more precise profiles for satellite HCHO observations. However, it is not demonstrated how the finer spatial resolution of the model improves the validation. Here it could help to show that the improvement is more important over the urban site compared to the sub-urban sites. Or is it more an effect of the different model chemistry/emissions, and not a spatial resolution effect?

**Response:** Thank you very much for this suggestion. We followed the reviewer's comment. We also compared simulated a priori HCHO profiles and MAX-DOAS HCHO profiles at suburban site (UCAS) in the revised version. The improvement of WRF-Chem simulations at urban site is more significant than suburban site, which is mainly related to the finer spatial resolution and more up to date emission inventory over China used in the simulations. The bias between simulated and measured HCHO profiles at urban site is larger than that at suburban site, which is mainly due to smaller spatial gradient over suburban areas.

Moreover, TROPOMI HCHO VCDs are compared with MAX-DOAS measurements. The results show that the improvements of our VCD retrieval in winter time is more significant than summer and the improvement at urban site is also more significant than suburban sites in winter. The results indicates better anthropogenic emission inventory and the finer spatial resolution over China in WRF-Chem simulations.

Distributions of operational HCHO VCD in four seasons are compared with distributions of the improved HCHO VCD in Section 5.4. Operational product shows similar spatio-temporal distribution with our retrieval over China while the absolute

values are (slight) smaller than our retrieval (Figure 12). In summer, hotspots can be observed over BTH, YRD, PRD, Shandong province, Henan province, Wuhan (Hubei's provincial capital), SCB and cities along Fen nutrient-laden valley in Shaanxi and Shanxi provinces in our retrieval. These hotspot patterns are strongly correlated to the population density and industrial emission pattern indicating a significant anthropogenic contribution. These hotspots are less obvious in the operational product in summer.

In a conclusion, both enhanced emission inventory and resolution of WRF-Chem simulations contribute to improving TROPOMI HCHO retrieval.

Along the paper, the numbers are often used in a quite subjective way. (0.15% difference being called an improvement for exemple). I recommend writing quantitative comparisons with a more rigorous analysis to strengthen the message of the paper.

**Responses:** Thank you very much for this suggestion. In the revised version, we added the error bar in calculating the NMBs (Table 3). The error bars of NMBs are two times standard error (SE) and is calculated following:

$$\text{Error} = 2 \times \sqrt{\frac{1}{n(n-1)} \frac{\sum_{i=1}^{i=n} \left(V_T(i) - V_M(i) - \overline{V_T(i) - V_M(i)}\right)^2}{\left(\sum_{i=1}^{i=n} V_M(i)/n\right)^2}} \times 100\% \qquad \text{(A1)}$$

The error shows 95% confidence interval (Streiner, 1996) and The NMBs larger than error are statistically significant. The 0.15% difference is statistically insignificant. The sentence "while the SCD retrieval only shows a minor effect of 0.15 %" is deleted.

**Changes in manuscript:** L302-306, P14-15 in the revised version.

The paper needs major revisions before being published in AMT.

## Specific comments

The title does not fairly reflect the contents of the paper. Unless the results are significantly extended, the title of the paper should focus more on the "improved AMF calculation over China".

**Responses:** Thank you very much for this suggestion. In addition to the improvement of AMF calculation, we are also using a different spectral retrieval technique of HCHO slant columns. Moreover, the background correction has also been improved. We think the title suggested by the reviewer neglected these points, and therefore, would like to keep the title of the manuscript as is.

The section called "Improved HCHO retrieval algorithm" presents the retrieval algorithm developed for this study. As described in this section, it is actually very similar to the ESA operational product. The similarities and the differences need to be clearly explained. For example, the wavelength calibration. The description is the same as for the operational product. Why a specific section dedicated to this aspect? It would be interesting to see a comparison of the calibration results between the 2 products.

**Responses:** Thank you very much for this suggestion. The theory of wavelength calibration in our retrieval is same with operational product. While the parameters used in the wavelength calibration including the TROPOMI slit function and polynomial orders are different from operational product. The preflight slit function is obtained from the TROPOMI

Calibration Key Data (CKD) (available at http://www.tropomi.eu/data-products/isrf-dataset, last access: 22 May 2019) which is derived from TROPOMI calibration measurements performed in March 2015 at CSL in Liege. Comparing the spectral fit residual of using different versions of preflight slit function in the spectral fitting, we found that using version v3.0.0 results in lowest residual (Fig. A1). The preflight instrument slit function version v3.0.0 is used in our retrieval, while the operational product uses version v1.0.0 preflight slit function. In the operational algorithm, polynomials are not considered in wavelength calibration. In our retrieval, the third order polynomials are selected through sensitivity analysis (Fig. A1). The result shows that using the third order polynomials contributes to reducing residual in wavelength calibration.

**Changes in manuscript:** L163-171, P7-8 in the revised version.

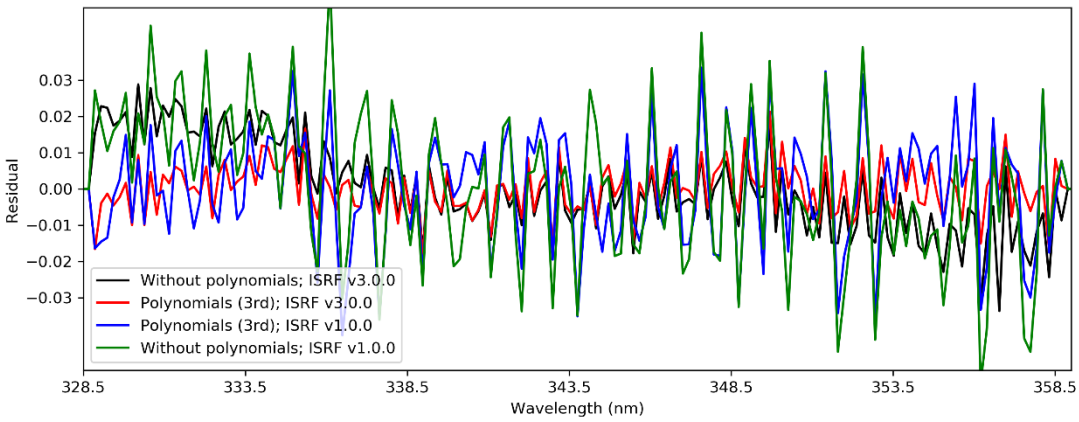


Figure A1. Comparisons of spectral fit residuals using different version of preflight slit function and using different polynomials during wavelength calibration.

The same holds for the AMF calculation part. It is very similar to the Tropomi HCHO ATBD and the differences are not clearly explained, except for the a priori profiles. Same for the reference sector correction.

**Responses:** Thank you very much for this suggestion. The AMF calculation is improved by using more precise a priori HCHO profiles in my study. Cloud information, surface albedo and surface pressure used in AMF calculations in our retrieval is same with operational product. The similarities and differences are listed in Table 1.

In Reference sector correction, we improved the reference sector correction by considering the variability of $M_0/M$ ratio.

**Changes in manuscript:** Table 1 and L240, P11 in the revised version.

It is not shown in the paper that the SCDs have been improved. There is a contradiction between the introduction ("BOAS has been reported featured with lower fitting uncertainties to the standard DOAS method") and the result section, where it is stated (page 10) that the RMS are identical. So the "lower fitting uncertainties" of the BOAS technique are not demonstrated. As for Figure 4 with the slant columns, a figure with RMS comparison needs to be added.

**Responses:** Thank you very much for this suggestion. The sentence at Line 341 in page 15 "On the other hand, RMS of both methods is very similar." is not rigorous. We added RMS comparisons in the Figure 5 in the revised version. RMS comparisons shown in Fig. 5(c) indicate that averaged RMS of the DOAS retrieval ($6.1 \pm 1.56\times10^{-4}$) is slightly higher than that of BOAS

retrieval ($5.95 \pm 1.50\times10^{-4}$). The sentence "BOAS has been reported featured with lower fitting uncertainties to the standard DOAS method" is deleted.

**Changes in manuscript:** L336-337, P15 in the revised version.

In section 4.1.2, it is explained that the operational product has been updated using a priori profile from WRF model. Does it mean that operational averaging kernel have been used? Or did the authors used their own radiative transfer calculation? It is important to know in order to understand if other sources of differences, such as the albedo, can play a role in the observed vcd differences.

**Responses:** Thank you very much for this suggestion. The operational averaging kernel (AK) has not been used in AMF calculation. We recalculated AMF using LUT table following Sect 3.2. The parameters used in AMF calculation are same with operational algorithm except for a priori HCHO profiles. Besides higher horizontal resolution, WRF-Chem simulation also has a higher vertical spatial resolution compared to TM5-MP data set. Although the difference in vertical resolution only shows negligible effect on box AMF (below 2%) under clear sky condition (Fig. A2 (b)), lower vertical resolution profiles would cause significant impact for cloudy cases due to the interpolation of coarse grid (Fig. A2 (d)). Therefore, the operational averaging kernel was not used.

**Changes in manuscript:** L371-374, P17 in the revised version.

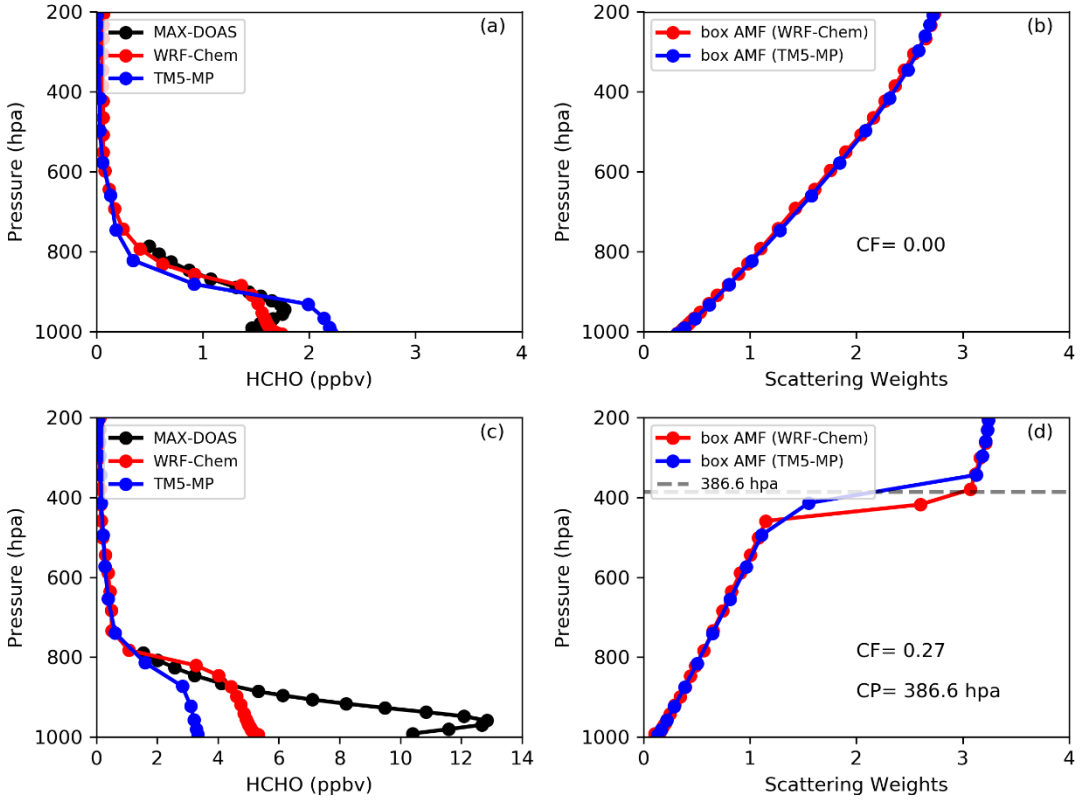

Figure A2. Daily averaged vertical HCHO profiles obtained from MAX-DOAS, WRF-Chem and TM5-MP model in clean case on 03 March 2019 (a) and in polluted case on 26 June 2019 (c). Comparisons of box AMF using WRF-Chem and TM5-MP simulations in clean case with clear sky on 03 March 2019 (b) and in polluted case with cloudy sky on 26 June 2019 (d). The locations of two pixels are within 20 km of the CAMS site.

Improved AMF for China should include some tests about the aerosol effects. They are not even mentioned.

**Responses:** Thank you very much for this suggestion. Aerosol effect on TROPOMI HCHO retrieval is discussed in Section 5.3. To estimate aerosol effect on TROPOMI HCHO retrieval, we calculate the AMFs using MAX-DOAS measured aerosol extinction profiles using VLIDORT (version 2.6) (Spurr, 2008). The AMFs are applied on the operational product and our retrieval. The TROPOMI HCHO VCDs with and without considering aerosols are compared to MAX-DOAS HCHO VCDs. The comparison results are shown in Figure 10. The results show that considering aerosol in the AMF calculations does not improve the agreement with ground based measurements. Considering aerosol effect in TROPOMI retrieval reduces HCHO VCDs by 11.46% (± 1.48%) for the operational product and 17.61% (± 1.92%) for our retrieval in winter. The reduction over urban site is more significant than suburban sites, mainly due to higher aerosol load. Operational product using both HCHO and aerosol extinction profiles from MAX-DOAS shows underestimation of 8.36 % (± 4.63 %). Our retrieval using MAX-DOAS HCHO and aerosol extinction profiles for AMF calculation underestimates HCHO VCD by 18.53% (± 4.04 %).

**Changes in manuscript:** L453-466, P20 in the revised version.

When comparing to the MAX-DOAS data in Beijing, MAX DOAS profiles have been used to re-calculate the amf of the improved Chinese HCHO product (Figure 7). For a fair comparison, the same method needs to be applied to the operational product. All the needed information are provided in the operational L2 files.

**Responses:** Thank you very much for this suggestion. We have recalculated HCHO VCD for the operational product by using MAX-DOAS HCHO profiles as a priori profiles. The Pearson correlation coefficient (R) between the recalculated operational product and MAX-DOAS HCHO VCD decreases by 0.02 to 0.79. The slope of the regression line increases by 0.19 to 0.84 with offset reduces by $0.24 \times 10^{16}$ molec $cm^{-2}$ to $0.15 \times 10^{16}$ molec $cm^{-2}$.

**Changes in manuscript:** L406-409, P18 and Figure 10 in the revised version.

I have some concerns about the way validation results are presented; The operational product, such as most of existing HCHO satellite products, is rather known to be underestimated over emission regions such as Beijing. See for example Jung et al. 2019 (https://doi.org/10.1029/2019EA000702) or Vigouroux et al. 2020 (https://doi.org/10.5194/amt-2020-30) and references therein. Here the authors claim to find an opposite result. The operational product is overestimated, and the improved Chinese product is lower and in better match with the MAX-DOAS. But actually this result holds for winter time only. The results should be discussed more in terms of low column (winter) or high columns (summer). Finally, a link to previous satellite HCHO validation studies should be made, and the reasons for such different conclusions need to be discussed.

**Responses:** Thank you very much for this suggestion. The study of Jung et al. 2019 (https://doi.org/10.1029/2019EA000702) shows that excluding the aerosol effect underestimates HCHO VCDs over East China during 2006-2007. While HCHO VCDs were not compared with ground-based instruments.

At CAMS site, HCHO VCDs are underestimated by TROPOMI observations and the underestimation of our retrieval (5.78 ± 3.49 %) is slightly smaller (29.77 ± 22.83 %) than that of the operational product (8.23 ± 3.09 %). At UCAS site, both our retrieval and operational product overestimate HCHO VCDs and the overestimation of our retrieval (5.22 ±3.49 %) is smaller (51.44 ± 33.70 %) than that of the operational product (10.75 ± 3.09 %). The overestimation of operational product at UCAS site is opposite to previous study that TROPOMI operational product underestimated HCHO VCDs in Xianghe located at ~ 50 km southeast of Beijing compared to FTIR measurements (Vigouroux et al., 2020). In order to investigate the reason of the overestimation, we separated the data by seasons for comparison at three MAX-DOAS sites (Table 5). In summer, high HCHO columns are due to oxidation of VOCs related to enhanced biogenic emissions. Both our retrieval and operational product underestimate HCHO VCD in summer which is consistent with previous studies (Vigouroux et al., 2020; Chan et al., 2020). In wither, lower HCHO columns (< $1\times10^{16}$ molec $cm^{-2}$) are mainly related to anthropogenic emissions including vehicle exhaust and industrial emissions. The vertical HCHO profiles simulated by WRF-Chem model are similar to the one measured by MAX-DOAS in winter, while the TM5-MP profiles show larger difference to the MAX-DOAS measurements. Both our retrieval and operational product overestimate HCHO VCDs in winter. The overestimation of our retrieval (11.23 ± 4.61 %) is 63.18 % (± 22.63 %) smaller than operational product (29.08 ± 5.59 %) and the overestimation in urban area (QKY) is smaller than that in suburban areas (UCAS and NC sites). The improvements of our retrieval in winter time are more significant and the improvement at urban site is also more significant than suburban sites in winter, which are mainly related to better anthropogenic emission inventory and the finer spatial resolution over China in WRF-Chem simulations. In order to eliminate effect from a priori HCHO profile, a priori HCHO profiles from MAX-DOAS measurements are used for AMF calculations for comparison. The overestimations at CAMS and NC sites become less significant. The overestimation at UCAS site of our retrieval reduces to 3.94 % (± 6.87 %), while the overestimation of operational product reduces to 10.60 % ( ± 8.71 %). Our result shows an overestimation of TROPOMI HCHO VCDs during winter at UCAS site. Our result is different from the previous FTIR comparison study (Vigouroux et al., 2020) which shows TROPOMI underestimated HCHO columns in winter. On the one hand, the pollution conditions at three MAX-DOAS sites are different from the FTIR sites used in Vigouroux et al. (2020). On the other hand, HCHO concentrations in the lower troposphere is lower in winter, resulting a relatively larger portion of HCHO above the MAX-DOAS retrieval height of 3km. Therefore, the MAX-DOAS measurements show an underestimation in winter. Our findings are consistence with the previous study that SCIAMACHY HCHO VCDs are in general lower than FTIR measurements while higher than MAX-DOAS observations (Vigouroux et al. 2009). The remaining overestimation is mainly related to a portion of HCHO above 3 km where the MAX-DOAS is not sensitive. In addition, the TROPOMI retrieval assumes aerosol free atmosphere which might also lead to the overestimations.

**Changes in manuscript:** L415-424, P18-19, L427-431, P19 and L434-451, P19-20 in the revised version.

The last paragraph of section 4.2 is the most interesting part of the paper and deserves to be extended. It is found that both algorithms remain underestimated in summer time, when the columns are the largest and mainly related to biogenic emissions. Both models simulate profiles not peaked enough near the surface. However, in winter time, when the columns are the lowest (no biogenic emissions), an improvement is observed compared to the MAX-DOAS observations when using WRF-Chem model as a priori profiles. Can you say something about possible reasons for this? Does the WRF-Chem model perform better than TM5 for anthropogenic emissions? Is it related to the spatial resolution or to the chemistry?

**Responses:** Thank you very much for this suggestion. The anthropogenic emission in WRF-Chem is obtained from The Multi-resolution Emission Inventory for China (MEIC). The MEIC emission inventory has improved the emissions estimation from power plants (Liu et al., 2015), vehicles (Zheng et al., 2014), and residential combustions of non-methane volatile organic compounds (NMVOCs) (Li et al., 2013; Peng et al., 2019).

Comparisons of seasonal averaged a priori HCHO profiles from MAX-DOAS, WRF-Chem and TM5-MP simulations at suburban (UCAS) sites in four seasons are added in the revised version. The improvement of WRF-Chem simulations at urban site is more significant than suburban site, which is mainly related to the finer spatial resolution and more up to date emission inventory over China used in the simulations.

Moreover, TROPOMI HCHO VCDs are compared with MAX-DOAS measurements. The improvements of our VCD retrieval in winter time is more significant than summer and the improvement at urban site is also more significant than suburban sites in winter, which are mainly related to better anthropogenic emission inventory and the finer spatial resolution over China in WRF-Chem simulations.

We think that both enhanced emission inventory and resolution of WRF-Chem simulations contribute to improving TROPOMI HCHO retrieval.

**Changes in manuscript:** L437-439, P19 in the revised version.

The discussion about seasonal variation of the improved Chinese product, and its spatial distribution over China does not bring anything new about current HCHO satellite observations. I advise to either remove this part, either extend with meaningful observations going much more into details. Comparison maps of SCD and AMF are shown. It would be good to do the same for the final VCD.

**Responses:** Thank you very much for this suggestion. The maps of operational HCHO VCDs in four seasons are added in the revised version. Spatial distributions of operational VCD and our retrieval are compared in Section 5.3. Operational product shows similar spatio-temporal distribution with our retrieval over China while the values are smaller than our retrieval (Figure 10). In summer, hotspots can be observed over BTH, YRD, PRD, Shandong province, Henan province, Wuhan (Hubei's provincial capital), SCB and cities along Fen nutrient-laden valley in Shaanxi and Shanxi provinces in our retrieval. These hotspot patterns are strongly correlated to the population density and industrial emission pattern indicating a significant anthropogenic contribution. These hotspots is less obvious in map of the operational HCHO VCDs in summer. The distribution of high HCHO VCDs observed in our retrieval over the Xinjiang Uygur Autonomous Region is related to the unique topography and industrial areas. The total industrial VOCs emission over the Xinjiang Uygur Autonomous Region is higher than Shanxi province (Zheng et al., 2017).

**Changes in manuscript:** L473-474 and L477-480, P21 and Figure 12 in the revised version.

## Technical corrections

### Abstract

L18: We present ~~the~~ an improved retrieval…

**Responses:** Thank you very much for this suggestion. Changed.

L19: The new retrieval optimizes the slant column density retrieval: this is not demonstrated in the paper. Please rephrase.

**Responses:** Thank you very much for this suggestion. We using a different spectral retrieval technique (BOAS method) of HCHO slant columns. Moreover, the background correction has also been improved. Although DOAS and BOAS HCHO DSCDs show a similar spatial pattern. The spatial distribution of BOAS HCHO SCD is expected to be smooth, less noisy. Besides, operational product using different SCD retrieval method is compared with MAX-DOAS HCHO measurements. Using the BOAS HCHO SCDs reduced the underestimation in summer and overestimation in winter of the operational product. In summer, using different SCD retrieval methods results a difference of 7.00% (± 1.71%, ± Error) from the TROPOMI operational HCHO VCD. The result also shows that using the BOAS HCHO SCDs reduced the underestimation in summer and overestimation in winter of the operational product.

L24: MAX-DOAS measurements in ~~China~~ Beijing

**Responses:** Thank you very much for this suggestion.

L26: while the SCD retrieval only shows a minor effect of 0.15%. This is negligible! We can even talk about a perfect agreement between the SCD retrievals.

**Responses:** Thank you very much for this suggestion. The sentence is deleted. Using different SCD retrieval methods results a difference of 7.00% (± 1.71%, ± Error) from the TROPOMI operational HCHO VCD in summer. So we cannot talk about a perfect agreement between the SCD retrievals.

L29-30: The last sentence is not demonstrated in the paper.

**Responses:** Thank you very much for this suggestion.

TROPOMI HCHO VCDs are compared with MAX-DOAS measurements. The improvements of our VCD retrieval in winter time is more significant than summer and the improvement at urban site is also more significant than suburban sites in winter, which are mainly related to better anthropogenic emission inventory and the finer spatial resolution over China in WRF-Chem simulations.

Moreover, the spatio-temporal distribution of the improved and operational HCHO VCDs is compared in Section 5.4 in the revised version. Operational product shows similar spatio-temporal distribution with our retrieval over China while the values are smaller than our retrieval (Figure 10). In summer, hotspots can be observed over BTH, YRD, PRD, Shandong province, Henan province, Wuhan (Hubei's provincial capital), SCB and cities along Fen nutrient-laden valley in Shaanxi and Shanxi provinces in our retrieval. These hotspot patterns are strongly correlated to the population density and industrial emission pattern indicating a significant anthropogenic contribution. These hotspots is less obvious in map of the operational HCHO VCDs in summer. These hotspots are less obvious in the operational product in summer. The distribution of high HCHO VCDs observed in our retrieval over the Xinjiang Uygur Autonomous Region is related to the unique topography and industrial areas. The total industrial VOCs emission over the Xinjiang Uygur Autonomous Region is higher than Shanxi province (Zheng et al., 2017).

These results show that our retrieval is more suitable for the analysis of regional and city scale pollution in China.

**Changes in manuscript:** L473-474 and L477-480, P21 and Figure 12 in the revised version.

**Introduction:**

L48: Again, It is not shown in the paper that the SCDs have been improved. The "lower fitting uncertainties" of the BOAS technique are not demonstrated.

**Responses:** Thank you very much for this suggestion. Thank you very much for this suggestion. We using a different spectral retrieval technique (BOAS method) of HCHO slant columns. Moreover, the background correction has also been improved. Although DOAS and BOAS HCHO DSCDs show a similar spatial pattern. The spatial distribution of BOAS HCHO SCD is expected to be smooth, less noisy. Besides, operational product using different SCD retrieval method is compared with MAX-DOAS HCHO measurements. Using the BOAS HCHO SCDs reduced the underestimation in summer and overestimation in winter of the operational product. In summer, using different SCD retrieval methods results a difference of 7.00% (± 1.71%, ± Error) from the TROPOMI operational HCHO VCD. The result also shows that using the BOAS HCHO SCDs reduced the underestimation in summer and overestimation in winter of the operational product. The sentence "This technique has been reported featured with lower fitting uncertainties compared to the standard differential optical absorption spectroscopy (DOAS) method (Chance and Kurosu, 2003)." is deleted.

L54: the result is expected to be more realistic for the investigation of spatio temporal variation of HCHO over China. ok but this needs to be demonstrated. How the spatio temporal variation of HCHO over China has been improved? In the current version, only a reduction of the bias compared to MAX-DOAS data is shown in winter time.

**Responses:** Thank you very much for this suggestion.

Operational and improved HCHO VCDs are compared with MAX-DOAS measurements. The improvements of our VCD retrieval in winter time is more significant than summer and the improvement at urban site is also more significant than suburban sites in winter, which are mainly related to better anthropogenic emission inventory and the finer spatial resolution over China in WRF-Chem simulations.

Moreover, the spatial distributions of the improved and operational HCHO VCDs in four seasons are compared in Section 5.4 in the revised version. In summer, hotspots can be observed over BTH, YRD, PRD, Shandong province, Henan province, Wuhan (Hubei's provincial capital), SCB and cities along Fen nutrient-laden valley in Shaanxi and Shanxi provinces in our retrieval. These hotspot patterns are strongly correlated to the population density and industrial emission pattern indicating a significant anthropogenic contribution. These hotspots are less obvious in the operational product in summer.

These results show that our retrieval is expected to be more realistic for the investigation of spatio temporal variation of HCHO over China.

**Changes in manuscript:** L473-474 and L477-480, P21 and Figure 12 in the revised version.

Figure 1: The scale could be reduced to better show emission spots.

**Responses:** Thank you very much for this suggestion. The scale is reduced to 1.5.

**WRF-model**

L79: more up to date emission inventory of China: this is really vague and needs to be explained

**Responses:** Thank you very much for this suggestion. The anthropogenic and biogenic emissions are obtained from The Multi-resolution Emission Inventory for China (MEIC) and the Model of Emissions of Gases and Aerosols from Nature (MEGAN) (Guenther et al., 2006; Li et al., 2017), respectively. The MEIC emission inventory has improved the emissions estimation from power plants (Liu et al., 2015), vehicles (Zheng et al., 2014), and residential combustions of non-methane volatile organic compounds (NMVOCs) (Li et al., 2013; Peng et al., 2019).
**Changes in manuscript:** L116-118 in the revised version.

**Improved HCHO retrieval algorithm**

L133: in Table ~~1~~ 2

**Responses:** Thank you very much for this suggestion. Changed

Table 2:

● Why the use of DSCD in the caption?

**Responses:** Thank you very much for this suggestion. Daily detector row averaged radiance over the equatorial Pacific is used as reference spectra. Due to residual HCHO signals in reference, the differential SCD (DSCD) is retrieved in spectra fitting.
**Changes in manuscript:** L86-87, P4 in the revised version.

● Please indicate the differences compared to the operational product.

**Responses:** Thank you very much for this suggestion. The similarities and differences are added in Table 1.
**Changes in manuscript:** Table 1 in the revised version.

● What about the Ring correction?

**Responses:** Thank you very much for this suggestion. The term $\alpha_r X_r(\lambda)$ in Eq. (3) represents Ring effect. $X_r(\lambda)$ is Raman spectrum calculated in Chance and Spurr (1997).
**Changes in manuscript:** Table 1 in the revised version.

● Do you include corrections for non-linear Ozone absorption effects?

**Responses:** Thank you very much for this suggestion. In our fitting, wavelength dependency of $O_3$ SCDs are not considered. We added the uncertainty analysis from wavelength dependency of $O_3$ SCDs. The uncertainty it causes on SCD is about 3.49%.
**Changes in manuscript:** L267-269, P12 and Table 3 in the revised version.

● How is the radiance reference sector calculated? Per instrument row? Per day?

**Responses:** Thank you very much for this suggestion. Radiances measured 1 day before the processing day over the Pacific with latitudes ranging from 30°S to 30°N and longitude ranging from 180°W to 140°W are averaged and used as reference in the spectral fit.
**Changes in manuscript:** L179-180, P8 in the revised version.

● Why this particular choice of $O_3$ and BrO cross-sections? Can these choices explain the differences with the operational product?

**Responses:** Thank you very much for this suggestion. The $O_3$ and BrO cross-sections are chose following the study of González Abad et al. (2015). The biases between DSCDs and RMS in operational product and our retrieval are mainly related to the difference of retrieval method, retrieval settings and selection of reference.

To eliminate the impact from retrieval settings, BOAS HCHO DSCDs using same retrieval settings with operational DSCD retrieval are compared with DOAS HCHO DSCDs (Figure. A3). Using same retrieval settings, difference between DOAS HCHO DSCDs and BOAS HCHO DSCDs (27.33%) is significantly reduced and the remaining difference is due to retrieval algorithm. Besides, smaller difference (4.41%) in HCHO SCDs indicates that reference sector correction reduces the effect from retrieval method (Figure. A3 (b)).

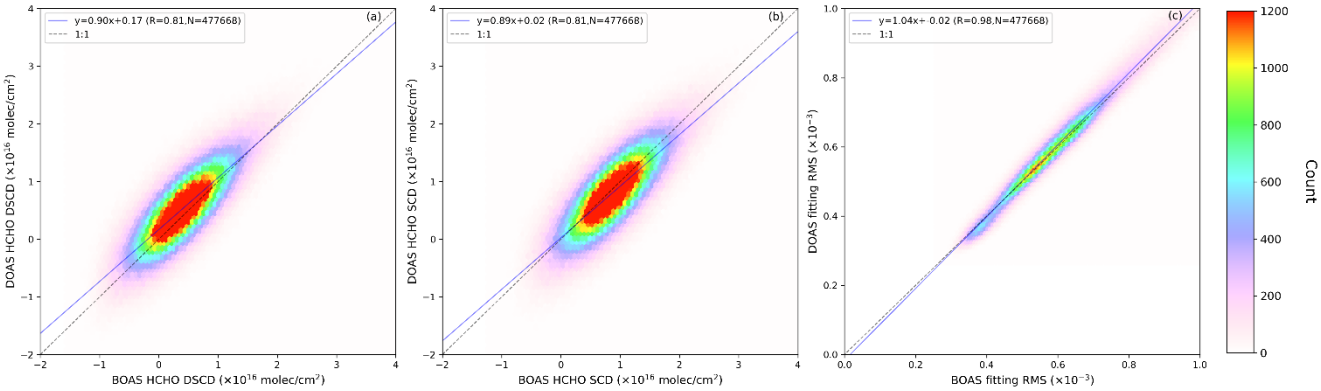


**Figure A3.** (a) Pixel to pixel comparisons of DOAS and BOAS HCHO DSCDs, (b) DOAS and BOAS HCHO SCDs and (c) DOAS and BOAS fitting RMS using same retrieval settings on 06 August 2018 in the region between 73° E and 130° **E**, and 18° N and 54° N.

**Changes in manuscript:** L345-349, P15-16 in the revised version.

L168: the surface albedo is obtained from the S5P operational cloud product. This is a bit surprising. Please specify the wavelength.

**Responses:** Thank you very much for this suggestion. The surface albedo is extracted from the S5P operational HCHO product in which surface albedo is from OMI-based monthly minimum LER at 342 nm for HCHO fitting window. We deleted the sentence and added the information used in AMF calculation in Table 1.

**Changes in manuscript:** Table 1, P12 in the revised version.

L187: specify the meaning of k and m

**Responses:** Thank you very much for this suggestion. In the old version, k and m are the position along track and across track of satellite pixels. The expression in the old version maybe is difficult to understand. We have changed the expression of the Eq. (10) in the revised version.

**Changes in manuscript:** L239, P11 in the revised version.

**Results and discussions**

L196: VT and Vm is the average tropospheric CHO VCD measured by TROPOMI and MAX-DOAS. How are the data averaged in space / time?

**Responses:** Thank you very much for this suggestion. MAX-DOAS measurements are temporally averaged within ±1 h around the TROPOMI overpass time, while TROPOMI pixels within 20 km of the MAX-DOAS site are spatially averaged for comparison. TROPOMI pixels in our retrieval and operational product are both filtered for intensity-weighted cloud fraction smaller than 0.3, root mean square of spectral fit residual smaller than $10^{-3}$, AMF larger than 0.1 and SZA smaller than 70°, quality assurance value (QA value) larger than 0.55 and successful SCD retrieval.

**Changes in manuscript:** L307-311, P14 in the revised version.

Figure 3: Do the maps show SCD, DSCD (as mentioned in Table 2) or corrected SCDs? It would be good to show corrected SCDs (with a color scale including negative values), since an offset is found in the SCDs. It would help to better see differences in the two spatial distributions.

**Responses:** Thank you very much for this suggestion. Figure 3 in the old version shows the maps of DSCDs which are not corrected. Figure 3 in the old version is Figure 4 in the revised version. We added the maps of SCDs which are calculated by applying reference sector correction on DSCDs (Fig. 4 (b) and (d)). The color scale in Fig. 4 is changed to include negative values.

**Changes in manuscript:** L352-355, P16 and Figure 4 in the revised version.

L206: Please compare numbers for the corrected slant columns over Tibet.

**Responses:** Thank you very much for this suggestion. The numbers of valid satellite measurements over Tibet for BOAS and DOAS retrieval are 22244 and 21987, respectively.

**Changes in manuscript:** L325-326, P15 in the revised version.

L218: Please compare the RMS.

**Responses:** Thank you very much for this suggestion. Figure 5 in the revised version adds pixel to pixel comparison of RMS on 06 August 2018 in the region between 73° E and 130° E, and 18° N and 54° N. The result indicate that averaged RMS of the DOAS retrieval ($6.1 \pm 1.56\times10^{-4}$) is slightly higher than that of BOAS retrieval ($5.95 \pm 1.50\times10^{-4}$).

**Changes in manuscript:** L336-337, P15 and Figure 5 in the revised version.

L218-219: This sentence is vague. Please be more specific

**Responses:** Thank you very much for this suggestion. The biases between DSCDs and RMS in operational product and our retrieval is mainly related to the difference of retrieval method, retrieval settings and selection of earthshine radiance reference. The impact of selection of earthshine radiance reference and retrieval method are also investigated in the revised version.

**Changes in manuscript:** L339-349, P15-16 in the revised version.

L223: Please give the numbers in brackets for the Chinese product as well.

**Responses:** Thank you very much for this suggestion. Averaged SCD taken from the operational product on 06 August 2018 over China ($0.85 \pm 0.69\times10^{16}$ molec cm$^{-2}$) is on average 4.49 % lower than our retrieval ($0.89 \pm 0.61\times10^{16}$ molec cm$^{-2}$).

**Changes in manuscript:** L353-355, P16 in the revised version.

L228. It is not clear how using the BOAS HCHO SCDs reduces the overestimation if changing SCD retrieval method only shows a tiny effect of 0.15%? There is a contradiction here.

**Responses:** Thank you very much for this suggestion. We added the error bar in Table 3 and find the conclusion that changing SCD retrieval method only shows a tiny effect of 0.15% is less rigorous. The conclusion is changed into "In summer, using different SCD retrieval methods results a difference of 7.00% ($\pm$ 1.71%, $\pm$ Error) from the TROPOMI operational HCHO VCD. The result shows that using the BOAS HCHO SCDs reduced the underestimation in summer and overestimation in winter of the operational product (Table 5)."

**Changes in manuscript:** L359-362, P16 in the revised version.

L228: The mean random errors relative to BOAS are mentioned. Can you give a definition? And where are those errors presented in the paper?

**Responses:** Thank you very much for this suggestion. Uncertainty analysis is added in Sect. 4 in the revised version. The Random uncertainties can be approximated by the root mean square (RMS) of spectral fitting residual, the degrees of freedom, and the diagonal term of the covariance matrix for HCHO ($C_{j,j}$):

$$\sigma^2_{N_{S,rand}} = RMS^2 \frac{m}{m-n} C_{j,j} C_{j,j} \qquad (A2)$$

Where m is the number of spectral pixels and n is the number of fitted parameters.

**Changes in manuscript:** L255-259, P12 in the revised version.

**AMF calculation**

Table 3: This table is difficult to understand. The presentation of the numbers can be improved. The legend says that NMBs between satellite and MAX-DOAS are provided, but it seems to be more than that (NMB s1, s2). Error bars should be added. It would be more relevant to separated numbers for winter and summer periods.

**Responses:** Thank you very much for this suggestion. The legend of Table 3 is changed into "NMBs between TROPOMI HCHO VCDs with different retrieval settings (NMB $_{S1,S2}$) and NMBs between TROPOMI and MAX-DOAS observations (NMB$_{S1,M}$). TROPOMI HCHO VCDs are calculated with four different settings, (1) operational retrieval setting (2) replacing DOAS SCDs using BOAS SCDs in the operational product, (3) changing the a priori profiles from TM5 to regional WRF-Chem simulations in the operational product and (4) both (2) and (3) changes in the operational product. The error bars are also presented. All values are in %.".

The standard error (SE) of the NMBs is calculated by dividing the standard deviation (SD) by the square root of day numbers. The two times the standard deviation (95% confidence interval (Streiner, 1996)) is regarded as the error of the NMBs in this study. The NMBs larger than the error are considered statistically significant. The error of NMB is calculated following Eq.

(A1). The NMBs in summer and winter are also presented in Table 5.

**Changes in manuscript:** L302-306, P14 and Table 5 in the revised version.

Figure 5:

● Profiles are shown at the more urban CAMS station. It would be interesting to also show a suburban station, in order to detect the gain in spatial resolution.

**Responses:** Thank you very much for this suggestion. Profiles comparison at UCAS site is added in Figure 8 in the revised version. The improvement of WRF-Chem simulations at urban site is more significant than suburban site, which is mainly related to the finer spatial resolution and more up to date emission inventory over China used in the simulations. The bias between simulated and measured HCHO profiles at urban site is larger than that at suburban site, which is mainly due to smaller spatial gradient over suburban areas.

**Changes in manuscript:** L378-381, P17 and Figure 8 in the revised version.

● How many profiles are averaged? What is the spatial resolution?

**Responses:** Thank you very much for this suggestion. In AMF calculations, both WRF-Chem and TM5-MP simulations are interpolated to TROPOMI spatial resolution. Interpolated WRF-Chem and TM5-MP simulations within 20 km of the MAX-DOAS site are spatially averaged to compare with MAX-DOAS profiles. MAX-DOAS profiles are temporally averaged in the period 13:30-14:30 (Local Time) within ±1 h around the TROPOMI overpass time.

**Changes in manuscript:** L366-370, P16 in the revised version.

L249: The operational data are filtered using the QA value. Is the same selection applied to the improved Chinese product? If not, which selection is applied?

**Responses:** Thank you very much for this suggestion. TROPOMI pixels in our retrieval and operational product are both filtered for intensity-weighted cloud fraction smaller than 0.3, root mean square of spectral fit residual (RMS) smaller than $10^{-3}$, AMF larger than 0.1 and SZA smaller than 70°, quality assurance value (QA value) larger than 0.55 and successful SCD retrieval.

**Changes in manuscript:** L308-311, P14 in the revised version.

L255: Validation results are discussed at the 3 sites using correlation, slope and offset. Looking at those 3 parameters, mainly the offset is improved compared to the operational product. Correlations are almost identical. This needs to be discussed more in detail, related to the observed offset in the AMFs.

**Responses:** Thank you very much for this suggestion. The difference in validation results of our retrieval and operational product is caused by not only the AMFs but also the SCD retrieval. The SCD retrieval can effect HCHO VCDs largely by 7.00% (± 1.71%, ± Error) in summer (Table 3 in the revised version). Using the BOAS HCHO SCDs help reduce the underestimation in summer and overestimation in winter of the operational product (Table 5).

L263: Please explain how the MAX-DOAS are used to recompute the AMFs. Do you use the averaging kernels? The same

needs to be done with the operational product.

**Responses:** Thank you very much for this suggestion. We didn't use the averaging kernels in calculation of AMFs using MAX-DOAS measurements as a priori file. We have recalculated HCHO VCD for the operational product by using MAX-DOAS HCHO profiles as a priori profiles. The Pearson correlation coefficient (R) between the recalculated operational product and MAX-DOAS HCHO VCD decreases by 0.02 to 0.79. The slope of the regression line increases by 0.19 to 0.84 with offset reduces by $0.24 \times 10^{16}$ molec $cm^{-2}$ to $0.15 \times 10^{16}$ molec $cm^{-2}$.

**Changes in manuscript:** L406-409, P18 and Figure 10 in the revised version.

L272: The vertical profiles simulated by WRF-Chem are similar to the one measured by MAX-DOAS in ~~summer~~ winter !

**Responses:** Thank you very much for this suggestion. Changed

L273: The underestimation of both retrievals in summer time are similar. 9.96% versus 10.88% is not significant. Please add error bars. Only the differences in winter time are significant.

**Responses:** Thank you very much for this suggestion. We recalculated the NMBs in summer and added the error bars calculated following Eq. A(1). The sentence is changed to "Therefore, our retrieval shows slightly better agreement with the ground based measurements (underestimation of 15.81 ± 2.71 %) compared to the operational product (underestimation of 18.33 ± 3.10 %) during summer."

**Changes in manuscript:** L427-428, P19 in the revised version.

**Section 4.3**

Not much useful information is given in this short paragraph. I suggest extending with a comparison with maps of VCD from the operational product, for the 4 seasons.

**Responses:** Thank you very much for this suggestion. The spatial distribution of the improved and operational HCHO VCDs is compared in Section 5.4 in the revised version. Operational product shows similar spatio-temporal distribution with our retrieval over China while the absolute values are (slight) smaller than our retrieval (Figure 12). In summer, hotspots can be observed over BTH, YRD, PRD, Shandong province, Henan province, Wuhan (Hubei's provincial capital), SCB and cities along Fen nutrient-laden valley in Shaanxi and Shanxi provinces in our retrieval. These hotspot patterns are strongly correlated to the population density and industrial emission pattern indicating a significant anthropogenic contribution. These hotspots are less obvious in the operational product in summer. The distribution of high HCHO VCDs observed in our retrieval over the Xinjiang Uygur Autonomous Region is related to the unique topography and industrial areas. The total industrial VOCs emission over the Xinjiang Uygur Autonomous Region is higher than Shanxi province (Zheng et al., 2017).

**Changes in manuscript:** L473-474 and L477-480, P21 and Figure 12 in the revised version.

**Conclusion**

As for the abstract and the title, the conclusions need to be redirected towards the real content of the paper, which is the use of a regional model to compute the AMFs, and the validation at 3 sites in Beijing.

**Responses:** Thank you very much for this suggestion. The abstract and conclusions are rewrote.

Chance, K. V., and Spurr, R. J.: Ring effect studies: Rayleigh scattering, including molecular parameters for rotational Raman scattering, and the Fraunhofer spectrum, Appl Optics, 36, 5224-5230, https://doi.org/10.1364/AO.36.005224, 1997.

Li, M., Zhang, Q., Kurokawa, J., Woo, J., He, K., Lu, Z., Ohara, T., Song, Y., Streets, D. G., and Carmichael, G. R.: MIX: a mosaic Asian anthropogenic emission inventory under the international collaboration framework of the MICS-Asia and HTAP, Atmos. Chem. Phys., 17, 935-963, 2017.

Liu, F., Zhang, Q., Tong, D., Zheng, B., Li, M., Huo, H., and He, K. B.: High-resolution inventory of technologies, activities, and emissions of coal-fired power plants in China from 1990 to 2010, Atmos. Chem. Phys., 15, 13299-13317, 2015.

Peng, L., Zhang, Q., Yao, Z., Mauzerall, D. L., Kang, S., Du, Z., Zheng, Y., Xue, T., and He, K.: Underreported coal in statistics: A survey-based solid fuel consumption and emission inventory for the rural residential sector in China, Applied Energy, 235, 1169-1182, 2019.

Streiner, D. L.: Maintaining Standards: Differences between the Standard Deviation and Standard Error, and When to Use Each, The Canadian Journal of Psychiatry, 41, 498-502, https://doi.org/10.1177/070674379604100805, 1996.

Zheng, C., Shen, J., Zhang, Y., Huang, W., Zhu, X., Wu, X., Chen, L., Gao, X., and Cen, K.: Quantitative assessment of industrial VOC emissions in China: Historical trend, spatial distribution, uncertainties, and projection, Atmos Environ, 150, 116-125, https://doi.org/10.1016/j.atmosenv.2016.11.023, 2017.

Zheng, B., Huo, H., Zhang, Q., Yao, Z., Wang, X., Yang, X., Liu, H., and He, K. B.: High-resolution mapping of vehicle emissions in China in 2008, Atmos. Chem. Phys., 14, 9787-9805, 2014.

# An improved TROPOMI tropospheric HCHO retrieval over China

Wenjing Su[1*], Cheng Liu[2,3,4,5,6,*], Ka Lok Chan[7], Qihou Hu[2], Haoran Liu[4], Xiangguang Ji[2,8], Yizhi Zhu[2], Ting Liu[1], Chengxin Zhang[1], Yujia Chen[2], Jianguo Liu[2]

[1]School of Earth and Space Sciences, University of Science and Technology of China, Hefei 230026, China

[2]Key Lab of Environmental Optics and Technology, Anhui Institute of Optics and Fine Mechanics, Hefei Institutes of Physical Science, Chinese Academy of Sciences, Hefei 230031, China

[3]Center for Excellence in Regional Atmospheric Environment, Institute of Urban Environment, Chinese Academy of Sciences, Xiamen 361021, China

[4]Department of Precision Machinery and Precision Instrumentation, University of Science and Technology of China, Hefei 230027, China

[5]Key Laboratory of Precision Scientific Instrumentation of Anhui Higher Education Institutes, University of Science and Technology of China, Hefei 230027, China

[6]Anhui Province Key Laboratory of Polar Environment and Global Change, USTC, Hefei 230026, China

[7]Remote Sensing Technology Institute (IMF), German Aerospace Center (DLR), Oberpfaffenhofen, Germany

[8]School of Environmental Science and Optoelectronic Technology, University of Science and Technology of China, Hefei 230026, China

*Corresponding author*: Cheng Liu (chliu81@ustc.edu.cn) and Ka Lok Chan (ka.chan@dlr.de)

**Abstract.** We present an improved TROPOspheric Monitoring Instrument (TROPOMI) retrieval of formaldehyde (HCHO) over China. The new retrieval optimizes the slant column density (SCD) retrieval and air mass factor (AMF) calculation for TROPOMI observations of HCHO over China. HCHO differential SCDs (DSCDs) are retrieved using the basic optical differential spectroscopy (BOAS) technique, while AMFs are improved with a priori HCHO profiles from a higher resolution regional chemistry transport model. Compared to the operational product, the new TROPOMI HCHO retrieval shows better agreement with ground based Multi-AXis Differential Optical Absorption Spectroscopy (MAX-DOAS) measurements in Beijing. The improvements are mainly related to the AMF calculation with more precise a priori profiles in winter. Using more precise a priori profiles in general reduces HCHO VCDs by 52.37 % (± 27.09 %) in winter. Considering aerosol effect in AMF calculation reduces operational product by 11.46% ( ± 1.48%) and our retrieval by 17.61% (± 1.92%) in winter. The improved

and operational HCHO are also used to investigate the spatial-temporal characteristic of HCHO over China. The result shows that both improved and operational HCHO VCDs reach maximum in summer and minimum in winter. High HCHO VCDs mainly located over populated areas, i.e., Sichuan Basin, Central and Eastern China, indicating a significant contribution of anthropogenic emissions. The hotspots are more obvious in the map of the improved HCHO than operational product. The result indicates the improved TROPOMI HCHO is more suitable for the analysis of regional and city scale pollution in China.

## 1 Introduction

Formaldehyde (HCHO) is an important trace gas playing a crucial role in atmospheric chemistry process. Hydroxyl radicals ($HO_x$ = OH+$HO_2$) produced from HCHO photolysis show a strong influence on the oxidative capacity of the atmosphere (Li et al., 2011; Xue et al., 2016), and contribute to the formation of secondary organic aerosol (SOA) (Jang and Kamens, 2001). Atmospheric HCHO can be emitted from both primary and secondary sources. Primary emissions include industrial sources, vehicle emissions (Wei et al., 2008), biogenic emissions from vegetation and biomass burning (Bauwens et al., 2016). The contribution of secondary sources to ambient HCHO sources is in general much higher than the primary emissions, especially in summer (Su et al., 2019). Secondary HCHO is formed through the oxidation of almost all volatile organic compounds (VOCs). Therefore, it is usually regarded as an indicator of VOCs and being used to analyze sensitivity regimes of ozone ($O_3$) formation (Martin et al., 2004; Choi et al., 2012; Jin and Holloway, 2015; Liu et al., 2016). Accurate HCHO measurement is important for the investigation of HCHO and $O_3$ interactions and for the understanding of atmospheric chemistry process.

Satellite observations provide indispensable information on HCHO spatial distribution. Satellite observations of HCHO have been conducted since 1996 with a series of satellite borne instruments (Bovensmann et al., 1999; Martin et al., 2004; De Smedt et al., 2012; Barkley et al., 2013; González Abad et al., 2015; González Abad et al., 2016). TROPOspheric Monitoring Instrument (TROPOMI) was launched on 13 October 2017. Compared to its predecessor satellite instruments, TROPOMI provides HCHO observations with a much higher spatial resolution with daily global coverage. The high resolution satellite measurement enables us to analyze the finer scale spatio-temporal characteristic of HCHO.

In this study, we have improved the TROPOMI HCHO over China by optimizing the slant column density (SCD) retrieval and the air mass factor (AMF) calculation. Different from the operational product (De Smedt et al. 2018), our retrieval uses the

basic optical differential spectroscopy (BOAS) technique for the differential SCD (DSCD) retrieval. In addition, the AMF calculation is improved by using higher resolution a priori profiles from the regional Weather Research and Forecasting model (WRF-Chem). It takes the fine scale pollution into account and the result is expected to be more realistic for the investigation of spatio-temporal variation of HCHO over China. Vigouroux et al. (2020) have validated the operational TROPOMI HCHO product using ground-based solar-absorption Fourier Transform Infrared (FTIR) HCHO measurements. However, validating and improvement of TROPOMI HCHO observations over China are still necessary. Therefore, we have analyzed the quality of the operational HCHO product in details and further improved TROPOMI HCHO observations over China.

The paper is organized as follows. Section 2 describes all data sets used in this study. Section 3 presents the improved TROPOMI HCHO retrieval algorithm over China. Uncertainties analysis in HCHO VCD retrieval is discussed in Section 4. The comparisons to TROPOMI HCHO VCDs and ground based Multi-AXis Differential Optical Absorption Spectroscopy (MAX-DOAS) are shown in Section 5. Finally, the summary and conclusion are drawn in Section 6.

## 2 Data Sets

### 2.1 The TROPOMI instrument

TROPOMI is onboard the Sentinel-5 Precursor (S5P) satellite. The S5P satellite orbits on the near-polar sun-synchronous orbit at an attitude of 824 km with a 17 days repeat cycle and equator-crossing time of 13:30 h local solar time (LST) on the ascending node. A scanning swath of TROPOMI covers a width of 2600 km providing daily global coverage. TROPOMI has four spectrometers for medium wave ultraviolet (UV), long wave ultraviolet combined with visual (UVIS), near infrared (NIR), and short wave infrared (SWIR), covering non-overlapping and non-contiguous wavelengths from 270 to 2385 nm which are divided into eight spectral bands. The Band 3 with wavelength from 320 to 405 nm is used for HCHO retrieval. Radiance in Band 3 is measured by UVIS spectrometer. The detector for UVIS spectrometer is a two-dimensional charge-coupled device (CCDs) with one dimension for wavelengths and the other dimension for across track spatial coverage (450 rows). Earth radiance is collected along the dayside of the earth, while solar irradiance measurements are performed near the North Pole every 15 orbits, approximately once a day. In the UVIS channel, the spectral resolution and spectral sampling is about 0.5 nm

and 0.2 nm, respectively. Individual ground pixels size of radiance measurement is approximately 3.5 km in the across-track and 7 km (5.5 km since August 2019), with integration time of 1.08 s (0.84 s since August 2019). The Level 1B radiance and solar irradiance are available at the Copernicus Open Access Hub (https://scihub.copernicus.eu/, last access: 22 May 2019).

### 2.2 Operational TROPOMI HCHO product

The operational TROPOMI HCHO product is jointly developed at the German Aerospace Center (DLR) and Royal Belgian Institute for Space Aeronomy (BIRA) (available at https://scihub.copernicus.eu/, last access: 22 May 2019). The operational product is used to compare to the improved TROPOMI HCHO data set over China. The operational product retrieves HCHO DSCDs using the DOAS spectral fitting technique in the wavelength range of 328.5-359 nm. The DSCD retrieval settings of the operational product are listed in Table 1. Using earthshine radiance over remote Pacific Ocean as reference significantly reduces the influence from unresolved spectral structures which could significantly improve the spectral retrieval of weak absorber, i.e., HCHO. Using radiance as reference reduces the fit residual as it already account for the $O_3$ absorption and Ring effect. Daily detector row averaged radiance over the equatorial Pacific (latitude from 5°S to 5°N and longitude from 180°W to 140°W) is used as reference spectra. Due to residual HCHO signals in reference, the differential SCD (DSCD) is retrieved in spectra fitting. The conversion of DSCD to VCD uses the AMF approach. A priori HCHO profiles are taken from the global chemistry transport model Tracer Model 5 (TM5-MP) with a spatial resolution of 1° × 1° with 34 vertical layers up to 0.1hpa and spatio-temporally interpolated to the measurement time and location. Information about data sets used in AMF calculation is also listed in Table 1. In order to remove the residual HCHO signal in the reference spectra, zonal reference sector correction is applied following the equation:

$$N_v = (N_s + N_{v,0,CTM} \times M_0 - N_{s,0})/M \quad (1)$$

Where $N_v$ is the vertical column. $N_s$ is the uncorrected DSCDs. $N_{s,0}$ and $M_0$ is DSCD and AMF of retrieved over the reference sector ([90°S, 90°N], [180°W to 120°W]). $N_{v,0,CTM}$ is the simulated HCHO vertical column of the reference sector. The operational algorithm assumes $M_0$ equals to M and the equation (1) can be expressed as:

$$N_v = (N_s - N_{s,0})/M + N_{v,0,CTM} \quad (2)$$

The latitude dependency is approximated by a polynomial. DSCDs are averaged into a 5° latitude bin and subsequently used

to approximate the coefficient of the polynomial. Detail of S5P operational HCHO algorithm can be found in De Smedt et al. (2018).

### 2.3 Operational TROPOMI cloud product

Cloud parameters used in AMF calculation in our retrieval are from the operational TROPOMI cloud product. Cloud fraction is retrieved using the Optical Cloud Recognition Algorithm (OCRA) and cloud top height (pressure) and optical thickness (albedo) are retrieved using Neural Networks (ROCINN) algorithm using the "Clouds-as-Reflecting-Boundaries" (CRB) model, treating clouds as simple Lambertian surfaces (Loyola et al., 2018). The operational TROPOMI cloud product is also available at the Copernicus Open Access Hub (https://scihub.copernicus.eu/, last access: 22 May 2019).

### 2.4 WRF-Chem model

In our retrieval, the chemistry transport model WRF-Chem is used to simulate a priori HCHO profile over China. Compared to TM5-MP, the regional WRF-Chem simulation has higher spatial resolution of $20 \times 20\ km^2$. WRF-Chem simulates air pollutions at 44 vertical layers extending from the ground up to 50 hPa. The initial and boundary conditions of the meteorological field for simulation are taken from the National Centers for Environmental Prediction (NCEP) 6-hour Final Operational Global (FNL) reanalysis data with spatial and temporal resolutions of 1° × 1° and 6-hour. The CBMZ (Carbon-Bond Mechanism version Z) photochemical mechanism combined with the MOSAIC (Model for Simulating Aerosol Interactions and Chemistry) aerosol model was used to simulate the chemical process in the atmosphere. WRF-chem simulations also has more up to date emission inventory over China. The anthropogenic and biogenic emissions are obtained from The Multi-resolution Emission Inventory for China (MEIC) and the Model of Emissions of Gases and Aerosols from Nature (MEGAN) (Guenther et al., 2006; Li et al., 2017), respectively. The MEIC emission inventory has improved the emissions estimation from power plants (Liu et al., 2015), vehicles (Zheng et al., 2014), and residential combustions of non-methane volatile organic compounds (NMVOCs) (Li et al., 2013; Peng et al., 2019). The open burning emission is obtained from the Fire INventory from NCAR (FINN) model (Wiedinmyer et al., 2010). WRF-Chem simulation is carried out from July 2019 to July 2019 with five days spun up prior to the simulation.

### 2.5 MAX-DOAS HCHO measurements

MAX-DOAS HCHO measurements are used to validate TROPOMI HCHO observations in this study. The MAX-DOAS measurements are performed at three sites in Beijing (Fig. 1), including one urban and two suburban sites. One suburban site is located in Nancheng (NC) in the southern side of Beijing, while another suburban site is located at the University of Chinese Academy of Sciences (UCAS) in the northeastern side of Beijing. The urban site is located in the Chinese academy of meteorological sciences (CAMS). The locations of three MAX-DOAS sites are indicated in Fig. S1. The distances of three MAX-DOAS sites from city center of Beijing are 8, 27 and 61 km of CAMS, NC, and UCAS sites. The three MAX-DOAS sites are representative of urban and suburban regions of Beijing. The MAX-DOAS instrument consists of a scanning telescope, a stepping motor controlling the viewing direction of the telescope and a spectrometer with Hamamatsu backthinned charge-coupled device (CCD) detector. The spectrometer measures scattered sunlight in the spectral range of 300 - 505 nm. Details of the MAX-DOAS measurement setup are shown in Table S1. Scattered sunlight spectra measured by MAX-DOAS are recoded and analyzed using DOAS Intelligent System (DOASIS) spectral fitting software (Kraus, 2006). Details of the MAX-DOAS HCHO DCSD retrieval settings are listed in Table S1. HCHO vertical profiles are retrieved using Munich Multiple wavelength MAX-DOAS retrieval algorithm ($M^3$) (Chan et al., 2018). The algorithm is developed based on the optimal estimation method (Rodgers, 2000) and utilizes the radiative transfer model LibRadTran (Emde et al., 2016) as the forward model. In the MAX-DOAS profile retrieval, the lowest 1 km is divided into 10 layers with the thickness of each layer of 100 m, while the thickness of the layers between 1 km and 3 km is set to 200 m. Details of MAX-DOAS HCHO profile retrieval can be found in (Chan et al., 2018; Chan et al., 2019).

## 3 Improved HCHO retrieval algorithm

The retrieval of HCHO vertical column densities (VCDs) from TROPOMI observations can be separated into three major steps. The first step is the retrieval of HCHO DSCDs. The second step is the reference sector correction, converting DSCDs into SCDs. The final step is the conversion of SCD to VCD using AMF. Details of the improved HCHO retrieval algorithm are presented in the following.

### 3.1 HCHO DSCD retrieval

#### 3.1.1 Wavelength calibration

Measured solar irradiances and earthshine radiances are often slightly misaligned with the on ground calibration due to temperature variation of the spectrograph, Doppler shift, non-uniform slit illumination due to presence of clouds or other high reflectance surface. To achieve accurate radiance fitting, it is necessary to calibrate the wavelength mapping before further processing. Irradiance and radiance wavelength are calibrated using a high resolution solar spectrum with accuracy of 0.001 nm (Chance and Kurucz, 2010). The high resolution solar spectrum is convolved with TROPOMI slit function to calculate the solar spectrum with the instrument resolution. This process can be described by Eq. 3:

$$I_r = I_0^h \otimes S(\lambda + \Delta\lambda) \times P_s^m(\lambda) + P_b^m(\lambda) \quad (3)$$

Where $I_r$ is the calculated solar spectrum with the instrument resolution. $I_0^h$ is the high resolution solar spectrum. λ represents the wavelength. $\Delta\lambda$ indicates the wavelength shift parameter. $S$ is TROPOMI slit function. $\otimes$ represents convolution procedure. $P_s^m(\lambda)$ and $P_b^m(\lambda)$ are scaling and baseline polynomial, respectively, which account for the low-frequency structures of the measured spectra. The polynomial is calculated as:

$$\mathrm{P^m}(\lambda) = \sum_{\mathrm{i=0}}^{\mathrm{m}} \mathrm{C_i}(\lambda - \lambda_{\mathrm{avg}})^{\mathrm{i}} \quad (4)$$

Where $\lambda_{avg}$ is the center wavelength of the fitting window. $C_i$ is the coefficient of the fitted polynomial and m is the order of polynomial. The Full-Width at Half-Maximum (FWHM) and asymmetric factor of the instrument slit function are obtained by fitting the $I_r$ to the measured irradiance using the Gauss-Newton Nonlinear Least Squares (NLLS) method assuming the asymmetric Gaussian shape of slit function. The time series of the fitted TROPOMI slit function parameter from August 2018 to July 2019 in Fig. S2 shows that the TROPOMI slit function is stable after lunch. Therefore, the preflight TROPOMI slit function is used in wavelength calibration procedure. The preflight slit function is obtained from the TROPOMI Calibration Key Data (CKD) (available at http://www.tropomi.eu/data-products/isrf-dataset, last access: 22 May 2019) which is derived from TROPOMI calibration measurements performed in March 2015 at CSL in Liege. Comparing the spectral fit residual of

using different versions of preflight slit function in the spectral fitting, we found that using version v3.0.0 results in lowest residual (Fig. S3). The preflight instrument slit function version v3.0.0 is used in our retrieval, while the operational product uses version v1.0.0 preflight slit function. In the operational algorithm, polynomials are not considered in Eq. (3). In our retrieval, the third order polynomials are selected through sensitivity analysis (Fig. S3). The result shows that using the third order polynomials contributes to reducing residual in wavelength calibration. In wavelength calibration procedure, wavelength shift and coefficients of the polynomials are obtained.

### 3.1.2 Radiance fitting

HCHO DCSDs are retrieved using the basic optical differential spectroscopy (BOAS) method (Chance, 1998) which has been applied to OMI and OMPS HCHO retrieval (González Abad et al., 2015; González Abad et al., 2016). The BOAS method is based on the direct radiance fit. HCHO DSCDs are determined by fitting the simulated and measured radiance using the NLLS method. The simulated radiance $I_s(\lambda)$ is calculated following the Eq. 5:

$$I_s(\lambda) = \left[\left(aI_0(\lambda + \Delta\lambda) + \alpha_r X_r(\lambda)\right) \times e^{-\sum_j \alpha_j X_j(\lambda)}\right] \times P_s^m(\lambda) + P_b^m(\lambda) \quad (5)$$

Where $\lambda$ represents the wavelength. a is the scaling factor of $I_0$. $I_0(\lambda + \Delta\lambda)$ denotes the daily average earthshine radiance over the remote Pacific. Radiances measured 1 day before the processing day over the Pacific with latitudes ranging from 30°S to 30°N and longitude ranging from 180°W to 140°W are averaged and used as reference in the spectral fit. $\Delta\lambda$ indicates the wavelength shift parameter. $X_r(\lambda)$ refers to the Raman spectrum (Chance and Spurr, 1997) and $\alpha_r$ is the fitted coefficient to $X_r(\lambda)$. $\alpha_j$ refer to the cross section of trace gas j, respectively. Detail of TROPOMI HCHO DSCD retrieval setting is listed in Table 1. Sensitivity analysis is performed to optimize the absorption cross section used in the spectral fit. The sensitivity analysis results are shown in Fig. S4. As expected, considering all absorption cross sections listed in Table 1 significantly reduces fitting residual. Fig. 2 shows the fitted optical depth and residual for two spectra measured on 6 August 2018 over China (orbit 4211). For the spectrum with higher HCHO DSCD, the HCHO absorption can be clearly distinguished in the fitting (see Fig. 2 (a)). The HCHO absorption structures are less significant in the other spectrum as the HCHO DSCD is reaching the detection limit (see Fig. 2 (b)). The detection limit of HCHO DSCD can be expressed by the ratio of root mean square (RMS) to the peak to peak optical density of HCHO in the fitting window (Schönhardt A, 2008). The RMS of fit

residual for TROPOMI observation typically varies from $5 \times 10^{-4}$ to $1 \times 10^{-3}$, corresponding to detection limits of HCHO DSCD from ~$7 \times 10^{15}$ to ~$1 \times 10^{16}$ molec cm$^{-2}$.

### 3.2 AMF calculation

HCHO SCDs represent the integration of HCHO concentration along the light path. Therefore, it is strongly dependent on the viewing and solar geometries, surface albedo, and the state of the atmosphere (presence of clouds, vertical HCHO distribution, pressure, temperature, etc). The AMF approach is used to convert SCD to VCD. For optically thin species, the height dependent sensitivity (box AMF) is insensitive to the vertical profile of the species. Therefore, tropospheric HCHO AMF (M) is calculated following the approach of Palmer et al. (2001), which can be described as:

$$\mathrm{M} = \frac{\int_{zs}^{zt} \mathrm{w} \times n_a \mathrm{dz}}{\int_{zs}^{zt} n_a dz} \quad (6)$$

where $zs$ and $zt$ are the altitude of surface and the tropopause, respectively. $n_a$ is the partial column of the corresponding layer of the a priori profile, which the a priori profile is taken from the regional WRF-Chem simulation. A priori HCHO profile for TROPOMI AMF calculations are calculated by interpolating WRF-Chem simulation spatio-temporally to the measurement time and location. Box AMF (w) represents the height dependent sensitivity of the TROPOMI measurement. The box AMF depends on wavelength, solar zenith angle (SZA), viewing zenith angle (VZA), relative azimuth angle (RAA), surface albedo, surface pressure, cloud albedo, cloud fraction and cloud pressure. As the wavelength dependency of box AMF in the HCHO fitting windows rather small (less than 5 % for SZA<70°), the box AMF can be calculated at a representative wavelength of 340nm. In order to improve the computational efficiency, the box AMF are pre-calculated using the radiative transfer model VLIDORT (version 2.6) (Spurr, 2008) with a number of surface albedos, surface pressures, solar and viewing geometries and stored in a look up table (LUT). The grid points of these parameters in creating the LUT are same with De Smedt et al (2018). An aerosol free U.S. standard atmosphere is assumed in the radiative transfer calculation of box AMF. Box AMF within the LUT is interpolated into each particular observation condition. Linear interpolation is performed in solar and viewing geometries and surface albedo dimensions and a nearest neighbor interpolation is performed in surface pressure dimension. Box AMF at each particular observation condition is then linearly interpolated to the pressure level of the a priori HCHO

profile.

For partly cloudy pixels, cloud correction is applied using the independent pixel approximation (Martin et al., 2002) in which scattering weights of inhomogeneous scenes are considered as a linear combination of box AMF for cloud-free scenes ($w_{clear}$) and cloudy scene ($w_{cloud}$) following Eq. (7):

$$w(z) = (1 - CF_{iw}) \times w_{clear} + CF_{iw} \times w_{cloud} \quad (7)$$

where $CF_{iw}$ is the intensity-weighted cloud fraction, defined as:

$$CF_{iw} = \frac{C_f \times I_{cloud}}{(1 - C_f) \times I_{clear} + C_f \times I_{cloud}} \quad (8)$$

Where $C_f$ is cloud fraction. $I_{cloud}$ and $I_{clear}$ are the radiance intensities for cloudy scene and cloud-free scene, respectively. Radiance intensities are pre-calculated using VLIDORT and saved in the LUT with the same setting as box AMF LUT. Detail information about data sets in AMF calculation are is listed in Table 1.

### 3.3 Reference sector correction

Since there are residual HCHO signals in the earthshine reference spectra, therefore, an offset correction has to be applied to the retrieved DSCDs. The first step of reference sector correction is retrieving the DSCDs using average earthshine radiance reference, calculating the corresponding AMFs and storing them as a separate database. The HCHO VCD over remote Pacific Ocean is simulated by GEOS-Chem assuming HCHO over this region is mainly from the oxidation of $CH_4$. The simulated HCHO SCD is calculated by multiplying the VCD ($VCD_G$) taken from GEOS-Chem with the corresponding AMF ($M_0$). Assuming HCHO in the reference sector correction is well simulated by GEOS-Chem, the difference between the simulated and retrieved DSCD ($DSCD_0$) is recognized as the SCD bias caused by residual HCHO signal in reference spectrum. TROPOMI measurements over the Pacific (latitude from 90°S to 90°N and longitude from 160°W to 140°W) are first binned according to their latitude to 500 bins with a resolution of 0.36°. The median value of each bin is then used for the calculation of the SCD background correction (González Abad et al., 2015; González Abad et al., 2016). The SCD correction can be expressed as the following:

$$\mathrm{Corr(lat)} = \mathrm{Median}(\mathrm{VCD}_G(\mathrm{lat}) \times M_0 - \mathrm{DSCD}_0) \quad (9)$$

Assuming the SCD correction is constant in the longitude direction, the SCD correction at 500 gridded latitude points are linearly interpolated to the latitude of each pixel over China. The interpolated SCD correction is then applied on the retrieved DSCDs to calculate SCDs. Finally, the HCHO VCDs are calculated as follows:

$$VCD = \frac{DSCD + Corr(lat)}{M} \quad (10)$$

We improved the reference sector correction by considering the variability of $M_0/M$ ratio.

## 4 Uncertainty analysis

Based on equation 10, the uncertainty of VCD can be derived analytically by uncertainty propagation. As VCD retrieval steps in Section 3 are performed independently, their uncertainties are assumed to be uncorrelated. The total uncertainty in HCHO VCD can be expressed following (Boersma et al., 2004; De Smedt et al., 2008):

$$\sigma_{N_V}^2 = (\frac{\partial N_V}{\partial N_S})^2 {\sigma_{N_S}}^2 + (\frac{\partial N_V}{\partial M})^2 {\sigma_M}^2 + (\frac{\partial N_V}{\partial N_{S,0}})^2 {\sigma_{N_{S,0}}}^2 + (\frac{\partial N_V}{\partial N_{V,0,G}})^2 {\sigma_{N_{V,0,G}}}^2 + (\frac{\partial N_V}{\partial M_0})^2 {\sigma_{M_0}}^2 \quad (11)$$

Where $N_S$ is retrieved DSCDs. $M$ and $M_0$ are both AMFs while $M_0$ refers to AMF in reference sector. $N_{S,0}$ and $N_{V,0,G}$ are retrieved DSCDs and simulated HCHO VCDs by GEOS in reference sector. $\sigma_{N_S}$ and $\sigma_M$ are the uncertainties on SCD and AMF. $\sigma_{N_{S,0}}, \sigma_{N_{V,0,G}}, \sigma_{M_0}$ are the uncertainties on SCD, simulated HCHO VCDs and AMF in the reference sector. The Eq. (11) can be transformed into the following equation:

$$\sigma_{N_V}^2 = \frac{1}{M^2}({\sigma_{N_S}}^2 + \frac{N_S - N_{S,0} + N_{V,0,G} \times M_0}{M^2} {\sigma_M}^2 + {\sigma_{N_{S,0}}}^2 + M_0^2 {\sigma_{N_{V,0,G}}}^2 + N_{V,0,G}^2 {\sigma_{M_0}}^2) \quad (12)$$

### 4.1 Uncertainties in SCDs

Uncertainties of SCD retrieval can be separated into random and systematic uncertainties, and they can be expressed as the following equation.

$${\sigma_{N_S}}^2 = \sigma_{N_{S,rand}}^2 + \sigma_{N_{S,sys}}^2 \quad (13)$$

255 random uncertainties are mainly related to instrument noises. Random uncertainties can be approximated by the root mean square (RMS) of spectral fitting residual, the degrees of freedom, and the diagonal term of the covariance matrix for HCHO ($C_{j,j}$):

$$\sigma^2_{N_{S,rand}} = RMS^2 \frac{m}{m-n} C_{j,j} C_{j,j} \quad (14)$$

Where m is the number of spectral pixels and n is the number of fitted parameters. The mean RMS for measurements taken on
260 06 August 2018 over the region of 73° E - 130° E, 18° N - 54° N and the corresponding random uncertainty are 5.52 $\times 10^{-4}$ and $0.49 \times 10^{16}$ molec cm$^{-2}$, respectively. Systematic uncertainties are mainly from absorption cross sections, choice of fitting window, choice of polynomials and TROPOMI slit function used in the spectral fit. We perform sensitivity analysis to evaluate these effects on HCHO SCD retrieval (Table 3). Fitting results using five different fitting windows which are used in previous satellite HCHO retrievals (De Smedt et al., 2008; De Smedt et al., 2012; González Abad et al., 2015) are compared to the our
265 result. The results show the fitting window and polynomials show large impacts on HCHO DSCDs. However, after applying reference sector correction significantly reduced their differences in HCHO SCDs. The effect of using Taylor series of $O_3$ cross section in the spectral retrieval is evaluated through sensitivity analysis (Table 3). After reference sector correction, systematic differences regarding to spectral fitting window, polynomials, slit function and Taylor series of $O_3$ cross section are estimated to be 15.11%, 2.33%, 2.33% and 3.49%, respectively. Put together with the systematic uncertainty (7%) caused by absorption
270 cross sections used in the spectral fit González Abad et al. (2016), we estimated the total systematic uncertainty is about 17.3 %.

### 4.2 Uncertainties in AMF calculations

According to Eq. (6), the uncertainties of AMF calculations can be approximated by uncertainty propagation following the equation below.

$$\sigma_M{}^2 = (\frac{\partial M}{\partial a_s}\sigma_{a_s})^2 + (\frac{\partial M}{\partial c_f}\sigma_{c_f})^2 + +(\frac{\partial M}{\partial c_p}\sigma_{c_p})^2 + (\frac{\partial M}{\partial p_h}\sigma_{p_h})^2 \quad (15)$$

275 Where $\sigma_{a_s}$, $\sigma_{c_f}$, $\sigma_{c_p}$ and $\sigma_{p_h}$ represent the uncertainties of surface albedo ($a_s$), cloud fraction ($c_f$), cloud pressure ($c_p$) and a priori HCHO profile height ($p_h$), respectively. A priori HCHO profile height is defined as 75% HCHO is located below this altitude (De Smedt et al. 2018). The observation geometries is measured with high accuracy, therefore, their uncertainties

toward AMF uncertainties are negligible. We estimated AMF uncertainties related to surface albedo, cloud fraction, cloud pressure and profile height through sensitivity analysis with a fixed set of observation geometry (SZA=30°, VZA=30°, RAA=0°). Through the sensitivity analysis, we estimated the VCD uncertainty caused by surface albedo, cloud top pressure, cloud fraction and profile height are 0-9%, 3-10%, 1-15% and 1-16% for clean case and 0-10%, 3-15%, 1-11% and 7-31% for polluted case, respectively, Details of the error analysis are summarized in table 4. The VCD uncertainty from wavelength dependency of AMF, LUT error, cloud correction and no explicit aerosol correction is about 15-35% (De Smedt et al. 2018). Considering above uncertainties sources, the VCD uncertainties from AMF calculation are about 17-51% and 15-43% in polluted and clean cases.

### 4.3 Uncertainties in reference sector correction

Uncertainty in reference sector correction ($\sigma_{N_{V,0}}$) is caused by HCHO VCD simulation, AMF calculation and SCD retrieval in the reference sector. The uncertainty can be expressed as:

$$\sigma_{N_{V,0}}^2 = \frac{1}{M^2}\left(\sigma_{N_{S,0}}{}^2 + M_0^2\sigma_{N_{V,0,G}}{}^2 + N_{V,0,G}^2\sigma_{M_0}{}^2\right) \quad (16)$$

We take into account the mean standard deviation of simulated HCHO VCD in the reference sector to estimate the uncertainty from model simulation. The uncertainty from VCD simulation is $1.43 \times 10^{16}$ molec cm$^{-2}$. The uncertainties from SCD retrieval and AMF calculations in reference sector are calculated same as Eq. (13) and Eq. (15).

## 5 Results and discussions

### 5.1 Comparison of operational and improved HCHO product

To analyze the improvement of the new TROPOMI HCHO product, we compared the new HCHO data set to the operational product. The contribution of SCD retrieval and AMF calculation are investigated separately. Both the improved and operation data sets are compared to the MAX-DOAS HCHO measurements to quantify the improvements. The normalized mean bias (NMB) between satellite and MAX-DOAS data is used as benchmark in the comparison. NMBs between two data sets can be calculated following:

$$\mathrm{NMB} = \frac{\sum_{i=1}^{i=n}(V_T(i) - V_M(i))}{\sum_{i=1}^{i=n} V_M(i)} \times 100\% \quad (17)$$

Where $V_T(i)$ and $V_M(i)$ is the average tropospheric HCHO VCD measured by TROPOMI and MAX-DOAS on day i, respectively. The standard error (SE) of the NMBs is calculated by dividing the standard deviation (SD) by the square root of day numbers. The two times the standard deviation (95% confidence interval (Streiner, 1996)) is regarded as the error of the NMBs in this study. The NMBs larger than the error are considered statistically significant. The error of NMB is calculated following:

$$\mathrm{Error} = 2 \times \sqrt{\frac{1}{n(n-1)} \frac{\sum_{i=1}^{i=n}\left(V_T(i) - V_M(i) - \overline{V_T(i) - V_M(i)}\right)^2}{\left(\sum_{i=1}^{i=n} V_M(i)/n\right)^2}} \times 100\% \quad (18)$$

MAX-DOAS measurements are temporally averaged within $\pm 1$ h around the TROPOMI overpass time, while TROPOMI pixels within 20 km of the MAX-DOAS site are spatially averaged for comparison. TROPOMI pixels in our retrieval and operational product are both filtered for intensity-weighted cloud fraction smaller than 0.3, root mean square of spectral fit residual (RMS) smaller than $10^{-3}$, AMF larger than 0.1 and SZA smaller than 70°, quality assurance value (QA value) larger than 0.55 and successful SCD retrieval. The histograms showing the distributions of RMS of spectral fit of the operational product and our retrieval on 06 August 2018 over China are shown in Figure. S5. About 15% and 17% of measurements in the operational product and our retrieval show RMS larger than $10^{-3}$.

### 5.1.1 SCD retrieval

In this section, we compare DSCDs and SCDs after applying reference sector correction between operational product and the new retrieval. The improved TROPOMI HCHO is retrieved using the BOAS approach, while the operational product uses the DOAS technique to retrieve the HCHO DSCDs. Both data sets are filtered for RMS smaller than $10^{-3}$. Fig. 4 (a) and (c) shows the TROPOMI HCHO DSCDs retrieved by BOAS and DOAS methods. HCHO DSCDs from both data sets show very similar spatial pattern over China with higher values over industrialized region such as, Beijing-Tianjin-Hebei region (BTH), Yangtze River Delta (YRD), Pearl River Delta (PRD) and Sichuan Basin (SCB). However, the DOAS DSCDs show more scattered outliers while the BOAS data set show a smoother appearance. As the anthropogenic VOC emission in Tibet is small (Wu et

al., 2016; Li et al., 2017) and the oxidation of VOCs is a significant source of HCHO, HCHO in this region is expected to have small spatial variation. The averaged HCHO DSCD of the BOAS retrieval is $0.076\times10^{16}$ molec $cm^{-2}$ with a standard deviation (SD) of $0.51\times10^{16}$ molec $cm^{-2}$ over Tibet (area indicated with blue line), while the DOAS dataset shows higher averaged column of $0.34\times10^{16}$ molec $cm^{-2}$ as well as standard deviation of $0.66\times10^{16}$ molec $cm^{-2}$. The numbers of valid satellite measurements over Tibet for BOAS and DOAS retrieval are 22244 and 21987, respectively. Larger standard deviation implies the data set contains more outliers. The DOAS HCHO DSCDs are rather noisy over Shaanxi province and its surrounding regions, while BOAS DSCDs appear to be much smoother with a significant hotspot over Xi'an (provincial capital of Shaanxi). As the spatial distribution of HCHO is expected to be smooth, less noisy DSCDs indicate that the BOAS technique is less sensitive to measurement noise.

The scatter plot of the BOAS and DOAS retrieval of HCHO DSCDs over China on 06 August 2018 is in Fig. 5 (a). The result shows BOAS and DOAS retrievals agree well with each other with Pearson correlation coefficient (R) of 0.80. The slope and offset of the linear least squares regression line are 0.91 and $0.24\times10^{16}$ molec $cm^{-2}$, respectively. Averaged DSCDs on 06 August 2018 over China retrieved by DOAS and BOAS algorithms are 0.57 ($\pm$ 0.68, $\pm$ SD) $\times10^{16}$ molec $cm^{-2}$ and 0.36 ($\pm$ 0.60)$\times10^{16}$ molec $cm^{-2}$, respectively. Averaged DSCD retrieved by DOAS method is 58.33 % higher ($0.21 \pm 0.41\times10^{16}$ molec $cm^{-2}$, average $\pm$ SD) than the BOAS retrieval. On the other hand, RMS comparisons shown in Fig. 5 (c) indicate that averaged RMS of the DOAS retrieval ($6.1 \pm 1.56\times10^{-4}$) is slightly higher than that of BOAS retrieval ($5.95 \pm 1.50\times10^{-4}$). The biases between DSCDs and RMS in operational product and our retrieval are mainly related to the difference of retrieval method, retrieval settings and selection of reference.

To investigate the impact of selection of earthshine radiance reference, we retrieved HCHO DSCDs using daily detector row averaged radiance over the equatorial Pacific (latitude from 5°S to 5°N and longitude from 180°W to 120°W) as reference using BOAS method. Comparisons of HCHO DSCDs and HCHO SCDs after applying reference sector correction using different earthshine radiance reference are presented in Figure. S6. The retrieved DSCDs using different earthshine radiance reference correlated well (R=0.99, Slope=0.99) and with a difference of 30% ($0.11 \pm 0.08 \times 10^{16}$ molec $cm^{-2}$). The bias is compensated (1.9%) by the reference sector correction (Figure. S6 (b)). To investigate the impact from retrieval method, BOAS HCHO DSCDs using same retrieval settings with operational DSCD retrieval are compared with DOAS HCHO DSCDs

(Figure. S7). Using same retrieval settings, difference between DOAS HCHO DSCDs and BOAS HCHO DSCDs (27.33%) is significantly reduced and the remaining difference is due to retrieval algorithm. Besides, smaller difference (4.41%) in HCHO SCDs indicates that reference sector correction reduces the effect from retrieval method (Figure. S7 (b)).

HCHO SCDs after applying reference sector correction in operational product and in our retrieval also show good agreement with Pearson correlation coefficient (R) of 0.80 (Fig. 5 (b)). The slope and intercept of the linear least squares regression line are 0.92 and $0.03\times10^{16}$ molec $cm^{-2}$. BOAS and DOAS HCHO SCDs also show very similar spatial pattern and the biases between BOAS and DOAS HCHO SCDs reduce after background correction (Fig. 4 (b) and (d)). Averaged SCD taken from the operational product on 06 August 2018 over China ($0.85 \pm 0.69\times10^{16}$ molec $cm^{-2}$) is on average 4.49 % lower than our retrieval ($0.89 \pm 0.61\times10^{16}$ molec $cm^{-2}$).

To evaluate improvement of SCD retrieval, the control variable method is applied on operational product. We use SCDs in our retrieval and AMFs in operational product to calculated the updated HCHO VCD. The NMB of the two data sets are shown in Table 5. The bias between the updated HCHO VCD and operational HCHO VCD is caused by difference in SCD retrieval. The updated and operational product is also compared to the MAX-DOAS observations. In summer, using different SCD retrieval methods results a difference of 7.00% ($\pm$ 1.71%, $\pm$ Error) from the TROPOMI operational HCHO VCD. The result shows that using the BOAS HCHO SCDs reduced the underestimation in summer and overestimation in winter of the operational product (Table 5). Besides, the mean random errors relative to BOAS are about 22 % lower than DOAS at three MAX-DOAS sites. The result indicates the BOAS technique provides a slightly more stable retrieval of HCHO SCDs.

### 5.1.2 AMF calculation

The improved TROPOMI HCHO over China uses a priori profile information from higher resolution regional WRF-Chem simulation, while the operational product uses a priori profile from the global TM5-MP model with 1° × 1° resolution. In AMF calculations, both WRF-Chem and TM5-MP simulations are interpolated to TROPOMI spatial resolution. Interpolated WRF-Chem and TM5-MP simulations within 20 km of the MAX-DOAS site are spatially averaged to compare with MAX-DOAS profiles. MAX-DOAS profiles are temporally averaged in the period 13:30-14:30 (Local Time) within ±1 h around the TROPOMI overpass time. Fig. 6 (a) and (c) show daily averaged a priori HCHO profiles from WRF-Chem and TRM5-MP

simulations and MAX-DOAS measured profiles. Besides higher horizontal resolution, WRF-Chem simulation also has a higher vertical spatial resolution compared to TM5-MP data set. Although the difference in vertical resolution only shows negligible effect on box AMF under clear sky condition (Fig. 6 (b)), lower vertical resolution profiles would cause significant impact for cloudy cases due to the interpolation of coarse grid (Fig. 6 (d)). Fig. 7 and Fig. 8 show comparisons of seasonal averaged a priori HCHO profiles from MAX-DOAS, WRF-Chem and TM5-MP simulations at urban (CAMS) and suburban (UCAS) sites in spring (March, April, May), summer (June, July, August), autumn (September, October, November) and winter (December, January, February). A priori HCHO profiles simulated by WRF-Chem are similar to MAX-DOAS measurements, while TM5-MP a priori profiles show a larger difference from the MAX-DOAS measurements. The improvement of WRF-Chem simulations at urban site is more significant than suburban site, which is mainly related to the finer spatial resolution and more up to date emission inventory over China used in the simulations. The bias between simulated and measured HCHO profiles at urban site is larger than that at suburban site, which is mainly due to smaller spatial gradient over suburban areas. The AMFs calculated with WRF-Chem and TM5-MP HCHO profiles as a priori are shown in Fig. 9. The results show a similar spatial pattern. However, WRF-Chem AMF is mostly higher than the one calculated with TM5-MP HCHO profiles. The big differences of two AMFs are mainly occurred in pixels with large cloud fraction. To evaluate influence of a priori HCHO profile on VCD retrieval, we updated operational product by keeping the SCDs unchanged and use a priori profile from WRF-Chem for the AMF calculation. The AMF is calculated following Sect 3.2 and using same parameters with operational algorithm except for a priori HCHO profile. The NMBs between the updated and operational HCHO and MAX-DOAS HCHO are shown in Table 5. The effect of a priori HCHO profile is much larger than that from SCD retrieval in winter. Using a priori HCHO profile from WRF-Chem reduces the bias between TROPOMI and MAX-DOAS by 11.48 % (± 8.39 %) in summer and 52.37 % (± 27.09 %) in winter. The reduction at urban site in winter is larger than suburban site.

### 5.2 Comparison between HCHO VCDs observed by MAX-DOAS and TROPOMI

To validate TROPOMI tropospheric HCHO VCD, TROPOMI HCHO VCDs are compared to the MAX-DOAS measurements. The left panels in Fig.10 show the comparison of TROPOMI HCHO VCDs from our retrieval and operational product to the MAX-DOAS HCHO VCDs at three MAX-DOAS sites in Beijing. Our retrieval shows better agreement with MAX-DOAS

tropospheric HCHO VCD compared to the operational product. The Pearson correlation coefficients (R) of our retrieval are 0.83, 0.84 and 0.83 at CAMS, UCAS and NC sites, respectively. The corresponding R values of operational product are 0.82, 0.80 and 0.82, which are slightly lower than our retrieval. Besides, the slopes of linear least squares regression lines of our retrieval are 0.77, 0.72 and 0.70 at CAMS, UCAS and NC sites. The corresponding values for the operational retrieval are 0.66, 0.67, and 0.62. In addition, the offsets of linear least squares regression lines of our retrieval are 0.37, 0.20 and 0.37 $\times$ $10^{16}$ molec $cm^{-2}$ at three MAX-DOAS sites, with the corresponding values for operational product of 0.41, 0.31 and 0.47 $\times$ $10^{16}$molec $cm^{-2}$. The agreement between our retrieval and MAX-DOAS observations is in general better than the operational product, suggesting that our retrieval is better than the operational product both in urban and suburban in China. In order to investigate the influence of HCHO a priori profile in the satellite retrieval, we used the MAX-DOAS HCHO profiles as a priori in our TROPOMI AMF calculation following Sect 3.2. The results show an improvement of correlation and absolute agreements. The Pearson correlation coefficient (R) increases by about 0.03. The linear fitting slopes increase by 0.14 and the offsets decrease by 0.09 $\times$ $10^{16}$ molec $cm^{-2}$. We have recalculated HCHO VCD for the operational product by using MAX-DOAS HCHO profiles as a priori profiles. The Pearson correlation coefficient (R) between the recalculated operational product and MAX-DOAS HCHO VCD decreases by 0.02 to 0.79. The slope of the regression line increases by 0.19 to 0.84 with offset reduces by 0.24 $\times$ $10^{16}$ molec $cm^{-2}$ to 0.15 $\times$ $10^{16}$ molec $cm^{-2}$. Although the recalculated TROPOMI operational product shows improved correlation with MAX-DOAS observations, our retrieval using MAX-DOAS measurements as a priori profile still shows a better agreement with MAX-DOAS HCHO VCDs. It also indicates that the BOAS spectral retrieval of SCDs agree better to the ground based observations over China.

The right panels of Fig. 10 show the time series of HCHO VCDs from MAX-DOAS, our retrieval and operational product. HCHO VCDs from our retrieval, operational product and MAX-DOAS show a similar temporal variation pattern, reaching maximum value in summer and minimum value in winter. At CAMS site, HCHO VCDs are underestimated by TROPOMI observations and the underestimation of our retrieval (5.78 $\pm$ 3.49 %) is slightly smaller (29.77 $\pm$ 22.83 %) than that of the operational product (8.23 $\pm$ 3.09 %). At UCAS site, both our retrieval and operational product overestimate HCHO VCDs and the overestimation of our retrieval (5.22 $\pm$ 3.49 %) is smaller (51.44 $\pm$ 33.70 %) than that of the operational product (10.75 $\pm$ 3.09 %). The overestimation of operational product at UCAS site is opposite to previous study that TROPOMI

operational product underestimated HCHO VCDs in Xianghe located at ~ 50 km southeast of Beijing compared to FTIR measurements (Vigouroux et al., 2020). In order to investigate the reason of the overestimation, we separated the data by seasons for comparison at three MAX-DOAS sites (Table 5). In summer, high HCHO columns are due to oxidation of VOCs related to enhanced biogenic emissions. Both our retrieval and operational product underestimate HCHO VCD in summer which is consistent with previous studies (Vigouroux et al., 2020; Chan et al., 2020). As shown in Fig. 7 (b) and Fig. 8 (b), WRF-Chem and TM5-MP model both underestimate HCHO concentration in the lower troposphere in summer and result in an overestimation of AMFs. The vertical HCHO profiles simulated by WRF-Chem model are better match with the one measured by MAX-DOAS in summer compared to TM5-MP. Therefore, our retrieval shows slightly better agreement with the ground based measurements (underestimation of 15.81 ± 2.71 %) compared to the operational product (underestimation of 18.33 ± 3.10 %) during summer. We have also calculated the AMFs using a priori HCHO profile measured by MAX-DOAS for comparison. The underestimation of our retrieval reduces to 1.39 % (± 2.67 %) and the underestimation of operational product reduces to 9.74 % ( ± 2.78 %) by using MAX-DOAS profiles for AMF calculations. In wither, lower HCHO columns ($< 1\times10^{16}$ molec $cm^{-2}$) are mainly related to anthropogenic emissions including vehicle exhaust and industrial emissions. The vertical HCHO profiles simulated by WRF-Chem model are similar to the one measured by MAX-DOAS in winter, while the TM5-MP profiles show larger difference to the MAX-DOAS measurements. Both our retrieval and operational product overestimate HCHO VCDs in winter. The overestimation of our retrieval (11.23 ± 4.61 %) is 63.18 % (± 22.63 %) smaller than operational product (29.08 ± 5.59 %) and the overestimation in urban area (QKY) is smaller than that in suburban areas (UCAS and NC sites). The improvements of our retrieval in winter time are more significant and the improvement at urban site is also more significant than suburban sites in winter, which are mainly related to better anthropogenic emission inventory and the finer spatial resolution over China in WRF-Chem simulations. In order to eliminate effect from a priori HCHO profile, a priori HCHO profiles from MAX-DOAS measurements are used for AMF calculations for comparison. The overestimations at CAMS and NC sites become less significant. The overestimation at UCAS site of our retrieval reduces to 3.94 % (± 6.87 %), while the overestimation of operational product reduces to 10.60 % ( ± 8.71 %). Our result shows an overestimation of TROPOMI HCHO VCDs during winter at UCAS site. Our result is different from the previous FTIR comparison study (Vigouroux et al., 2020) which shows TROPOMI underestimated HCHO columns in winter. On the one hand, the pollution

conditions at three MAX-DOAS sites are different from the FTIR sites used in Vigouroux et al. (2020). On the other hand, HCHO concentrations in the lower troposphere is lower in winter, resulting a relatively larger portion of HCHO above the MAX-DOAS retrieval height of 3km. Therefore, the MAX-DOAS measurements show an underestimation in winter. Our findings are consistence with the previous study that SCIAMACHY HCHO VCDs are in general lower than FTIR measurements while higher than MAX-DOAS observations (Vigouroux et al. 2009). The remaining overestimation is mainly related to a portion of HCHO above 3 km where the MAX-DOAS is not sensitive. In addition, the TROPOMI retrieval assumes aerosol free atmosphere which might also lead to the overestimations.

### 5.3 Aerosol effect on TROPOMI HCHO retrieval

Aerosol extinction profiles are also retrieved by the MAX-DOAS. Aerosol optical properties, such as single-scattering albedo (SSA) and Ångström exponent obtained from the Aerosol Robotic Network (AERONET) station in Beijing (https://aeronet.gsfc.nasa.gov/, last access: 22 May 2019) are used as input parameters for the MAX-DOAS aerosol profile retrieval. As the aerosol profiles from MAX-DOAS are retrieved at 360nm, we further converted the profile to 340nm using Ångström exponent obtained from the AERONET measurements. To estimate aerosol effect on TROPOMI HCHO retrieval, we calculate the AMFs using MAX-DOAS measured aerosol extinction profiles using VLIDORT (version 2.6) (Spurr, 2008). The AMFs are applied on the operational product and our retrieval. The TROPOMI HCHO VCDs with and without considering aerosols are compared to MAX-DOAS HCHO VCDs. The comparison results are shown in Figure 10. The results show that considering aerosol in the AMF calculations does not improve the agreement with ground based measurements. Considering aerosol effect in TROPOMI retrieval reduces HCHO VCDs by 11.46% ( $\pm$ 1.48%) for the operational product and 17.61% ( $\pm$ 1.92%) for our retrieval in winter. The reduction over urban site is more significant than suburban sites, mainly due to higher aerosol load. Operational product using both HCHO and aerosol extinction profiles from MAX-DOAS shows underestimation of 8.36 % ($\pm$ 4.63 %). Our retrieval using MAX-DOAS HCHO and aerosol extinction profiles for AMF calculation underestimates HCHO VCD by 18.53% ( $\pm$ 4.04 %).

### 5.4 Spatial-temporal characteristic of HCHO over China

Fig. 11 shows the spatial distribution of HCHO VCDs over China in spring, summer, autumn and winter. HCHO VCDs reach highest values in summer and lowest values in winter over China. This is due to higher biogenic emissions (Guenther et al., 1995; Li and Xie, 2014; Jiang et al., 2019) and secondary formation in summer (Wang et al., 2016; Su et al., 2019). The average HCHO VCDs over China in autumn 2018, winter 2018, spring 2019 and summer 2019 are 0.93, 0.91, 0.98 and $1.21\times 10^{16}$ molec $cm^{-2}$, respectively (Table S3). High HCHO VCDs are mainly occurred in central and eastern China and SCB. Lower HCHO values are observed in the western China. Operational product shows similar spatio-temporal distribution with our retrieval over China while the absolute values are (slight) smaller than our retrieval (Figure 12). In summer, hotspots can be observed over BTH, YRD, PRD, Shandong province, Henan province, Wuhan (Hubei's provincial capital), SCB and cities along Fen nutrient-laden valley in Shaanxi and Shanxi provinces in our retrieval. These hotspot patterns are strongly correlated to the population density and industrial emission pattern indicating a significant anthropogenic contribution. These hotspots are less obvious in the operational product in summer. The distribution of high HCHO VCDs observed in our retrieval over the Xinjiang Uygur Autonomous Region is related to the unique topography and industrial areas. The total industrial VOCs emission over the Xinjiang Uygur Autonomous Region is higher than Shanxi province (Zheng et al., 2017).

## 6 Conclusions

In this paper, we present an improved TROPOMI HCHO retrieval over China. We mainly improve the retrieval in two aspects, SCD and AMF calculations. The improved HCHO uses the BOAS technique for the retrieval of HCHO DSCDs. Compared to the DOAS retrieval technique used in the operational product, results retrieved with the BOAS technique are less noisy while the spatial pattern of HCHO remains similar. DSCDs retrieval with both BOAS and DOAS correlate well with each other with a correlation coefficient of 0.83 and a linear fitting slope of 0.93. The AMF calculations are improved by using HCHO profiles from the regional chemistry transport model WRF-Chem. The WRF-Chem simulation is featured with higher horizontal and vertical resolution. In addition, the emission inventories used in the model are more up to date. A priori HCHO profiles from WRF-Chem in general agree much better with the MAX-DOAS measurements compared to TM5-MP simulation. The

improvement related to the use of finer resolution a priori profile is more significant at urban site, as it better resolved the spatial gradient over these areas.

We also compared the improved and operational TROPOMI HCHO VCDs to MAX-DOAS observations at three MAX-DOAS sites in Beijing. The improved HCHO shows better correlation with MAX-DOAS HCHO VCDs compared to the operational product. The improvement of our HCHO retrieval is significant in winter time, mainly related to the use of better a priori profile. Using different spectral retrieval technique for the retrieval of HCHO slant columns only shows a less significant effect in winter. The bias between the improved TROPOMI HCHO VCDs and MAX-DOAS observations is 63.18 % (± 22.63 %) smaller than operational product during winter. Moreover, the improvement at urban site in winter is more important than suburban site. These results suggest our retrieval can better capture the fine scale variation of HCHO in both urban and suburban regions. The improved TROPOMI HCHO VCDs and MAX-DOAS show a similar temporal variation pattern with higher values in summer and lower values in winter, while the operational product shows less pronounced seasonal pattern. The improved and operational products both underestimate HCHO VCDs in summer while overestimate HCHO VCDs in winter. Using MAX-DOAS measurements as a priori HCHO profiles in TROPOMI VCD retrieval improves the correlation and reduces the bias between TROPOMI and MAX-DOAS HCHO VCDs. Considering aerosol effect in AMF calculation reduces operational product by 11.46% ( ± 1.48%) and our retrieval by 17.61% ( ± 1.92%) in winter.

The analysis of HCHO spatial distribution shows higher values over SCB, Central and Eastern China and SCB. Lower HCHO VCDs can be observed over western China. In summer, hotspots can be observed over BTH, YRD, PRD, Shandong province, Henan province, Wuhan (Hubei's provincial capital), SCB and cities along Fen nutrient-laden valley in Shaanxi and Shanxi provinces. These spatial patterns indicate significant anthropogenic contributions of atmospheric HCHO. While these hotspots is less obvious indicating that the improved TROPOMI data set provides a better support for the monitoring and controlling the VOCs related pollution.

*Data availability.* The data used in this paper is available on request from the corresponding author (chliu81@ustc.edu.cn).

*Author contributions.* The first two authors contributed equally. CL and KLC designed and supervised the study and CL also help retrieve the satellite data. WS prepared and analyzed satellite data and wrote the manuscript. QH provided useful comments regarding the results. HL and XJ contributed to providing MAX-DOAS HCHO measurements. YZ and TL help ran

the WRF-Chem model. CZ and YC help prepare satellite retrieval. JL supported the project.

*Acknowledgments.* This work was supported by grants from the National Key Research and Development Program of China (No. 2018YFC0213104, 2017YFC0210002 and 2016YFC0203302), Anhui Science and Technology Major Project (18030801111), National Natural Science Foundation of China (No. 41722501, 51778596 and 41977184), the Strategic Priority Research Program of the Chinese Academy of Sciences (No. XDA23020301), the National Key Project for Causes and Control of Heavy Air Pollution (No. DQGG0102 and DQGG0205), the National High-Resolution Earth Observation Project of China (No. 05-Y20A16-9001-15/17-2), Natural Science Foundation of Guangzhou Province (No.2016A030310115) and Civil Aerospace Technology Advance Research Project (No.Y7K00100KJ). The TROPOMI operational Level-1b product and HCHO product are available at https://scihub.copernicus.eu/.

*Competing interests.* The authors declare that they have no conflict of interest.

## References

Barkley, M. P., De Smedt, I., Van Roozendael, M., Kurosu, T. P., Chance, K., Arneth, A., Hagberg, D., Guenther, A., Paulot, F., and Marais, E.: Top‐down isoprene emissions over tropical South America inferred from SCIAMACHY and OMI formaldehyde columns, Journal of Geophysical Research: Atmospheres, 118, 6849-6868, https://doi.org/10.1002/jgrd.50552, 2013.

Bauwens, M., Stavrakou, T., Müller, J.-F., Smedt, I. D., Roozendael, M. V., Werf, G. R., Wiedinmyer, C., Kaiser, J. W., Sindelarova, K., and Guenther, A.: Nine years of global hydrocarbon emissions based on source inversion of OMI formaldehyde observations, Atmos. Chem. Phys., 16, 10133-10158, https://doi.org/10.5194/acp-16-10133-2016, 2016.

Boersma, K. F., Eskes, H., and Brinksma, E. J.: Error analysis for tropospheric NO2 retrieval from space, Journal of Geophysical Research, 109, https://doi.org/10.1029/2003JD003962, 2004.

Bovensmann, H., Burrows, J., Buchwitz, M., Frerick, J., Noël, S., Rozanov, V., Chance, K., and Goede, A.: SCIAMACHY: Mission objectives and measurement modes, J Atmos Sci, 56, 127-150, https://doi.org/10.1175/1520-0469(1999)056<0127:SMOAMM>2.0.CO;2, 1999.

Chan, K., Wiegner, M., Wenig, M., and Pöhler, D.: Observations of tropospheric aerosols and NO2 in Hong Kong over 5 years using ground based MAX-DOAS, Science of the total environment, 619, 1545-1556, https://doi.org/10.1016/j.scitotenv.2017.10.153, 2018.

Chan, K. L., Wang, Z., Ding, A., Heue, K.-P., Shen, Y., Wang, J., Zhang, F., Shi, Y., Hao, N., and Wenig, M.: MAX-DOAS measurements of tropospheric $NO_2$ and HCHO in Nanjing and a comparison to ozone monitoring instrument observations, Atmos. Chem. Phys., 19, 10051-10071, https://doi.org/10.5194/acp-19-10051-2019, 2019.

Chan, K. L., Wiegner, M., Alberti, C., and Wenig, M.: MAX-DOAS measurements of tropospheric NO2 and HCHO in Munich and the comparison to OMI and TROPOMI satellite observations, Atmos. Meas. Tech. Discuss., 2020, 1-31, https://doi.org/10.5194/amt-2020-35, 2020.

Chance, K. V., and Spurr, R. J.: Ring effect studies: Rayleigh scattering, including molecular parameters for rotational Raman scattering, and the Fraunhofer spectrum, Appl Optics, 36, 5224-5230, https://doi.org/10.1364/AO.36.005224, 1997.

Chance, K.: Analysis of BrO measurements from the global ozone monitoring experiment, Geophys Res Lett, 25, 3335-3338, https://doi.org/10.1029/98GL52359, 1998.

Chance, K., and Kurucz, R. L.: An improved high-resolution solar reference spectrum for earth's atmosphere measurements in the ultraviolet, visible, and near infrared, Journal of quantitative spectroscopy and radiative transfer, 111, 1289-1295, https://doi.org/10.1016/j.jqsrt.2010.01.036, 2010.

Chance, K., and Orphal, J.: Revised ultraviolet absorption cross sections of H2CO for the HITRAN database, Journal of Quantitative Spectroscopy and Radiative Transfer, 112, 1509-1510, https://doi.org/10.1016/j.jqsrt.2011.02.002, 2011.

Choi, Y., Kim, H., Tong, D., and Lee, P.: Summertime weekly cycles of observed and modeled NOx and $O_3$ concentrations as a function of satellite-derived ozone production sensitivity and land use types over the Continental United States, Atmos. Chem. Phys., 12, 6291-6307, https://doi.org/10.5194/acp-12-6291-2012, 2012.

De Smedt, I., Muller, J., Stavrakou, T., Eskes, H., and Van Roozendael, M.: Twelve years of global observations of formaldehyde in the troposphere using GOME and SCIAMACHY sensors, Atmos. Chem. Phys., 8, 4947-4963, https://doi.org/10.5194/acp-8-4947-2008, 2008.

De Smedt, I., Van Roozendael, M., Stavrakou, T., Müller, J., Lerot, C., Theys, N., Valks, P., Hao, N., and Van Der A, R.: Improved retrieval of global tropospheric formaldehyde columns from GOME-2/MetOp-A addressing noise reduction and instrumental degradation issues, Atmos. Meas. Tech., 5, 2933-2949, https://doi.org/10.5194/amt-5-2933-2012, 2012.

De Smedt, I., Theys, N., Yu, H., Danckaert, T., Lerot, C., Compernolle, S., Van Roozendael, M., Richter, A., Hilboll, A., and Peters, E.: Algorithm theoretical baseline for formaldehyde retrievals from S5P TROPOMI and from the QA4ECV project, https://doi.org/10.5194/amt-11-2395-2018, 2018.

Fleischmann, O. C., Hartmann, M., Burrows, J. P., and Orphal, J.: New ultraviolet absorption cross-sections of BrO at atmospheric temperatures measured by time-windowing Fourier transform spectroscopy, Journal of Photochemistry and Photobiology A-chemistry, 168, 117-132, https://doi.org/10.1016/j.jphotochem.2004.03.026, 2004.

González Abad, G., Liu, X., Chance, K., Wang, H., Kurosu, T. P., and Suleiman, R.: Updated Smithsonian Astrophysical Observatory Ozone Monitoring Instrument (SAO OMI) formaldehyde retrieval, Atmos. Meas. Tech., 8, 19-32, https://doi.org/10.5194/amt-8-19-2015, 2015.

González Abad, G., Vasilkov, A., Seftor, C., Liu, X., and Chance, K.: Smithsonian Astrophysical Observatory Ozone Mapping and Profiler Suite (SAO OMPS) formaldehyde retrieval, Atmos. Meas. Tech., 9, 2797-2812, https://doi.org/10.5194/amt-9-2797-2016, 2016.

Guenther, A., Hewitt, C. N., Erickson, D., Fall, R., Geron, C., Graedel, T., Harley, P., Klinger, L., Lerdau, M., and McKay, W.: A global model of natural volatile organic compound emissions, Journal of Geophysical Research: Atmospheres, 100, 8873-8892, https://doi.org/10.1029/94JD02950, 1995.

Guenther, A., Karl, T., Harley, P., Wiedinmyer, C., Palmer, P., and Geron, C.: Estimates of global terrestrial isoprene emissions using MEGAN (Model of Emissions of Gases and Aerosols from Nature), Atmos. Chem. Phys., 6, 3181-3210, https://doi.org/10.5194/acp-6-3181-2006, 2006.

Jang, M., and Kamens, R. M.: Characterization of secondary aerosol from the photooxidation of toluene in the presence of NO x and 1-propene, Environ Sci Technol, 35, 3626-3639, https://doi.org/10.1021/es010676+, 2001.

Jiang, Z., Zheng, X., Zhai, H., Wang, Y., Wang, Q., and Yang, Z.: Seasonal and diurnal characteristics of carbonyls in the urban atmosphere of Changsha, a mountainous city in south-central China, Environ Pollut, 253, 259-267, https://doi.org/10.1016/j.envpol.2019.06.127, 2019.

Jin, X., and Holloway, T.: Spatial and temporal variability of ozone sensitivity over China observed from the Ozone Monitoring Instrument, Journal of Geophysical Research: Atmospheres, 120, 7229-7246, https://doi.org/10.1002/2015JD023250, 2015.

Kleipool, Q., Dobber, M., De Haan, J. F., and Levelt, P. F.: Earth surface reflectance climatology from 3 years of OMI data, Journal of Geophysical Research, 113, https://doi.org/10.1029/2008JD010290, 2008.

Kraus, S.: DOASIS: A framework design for DOAS, Ph.D. thesis, University of Heidelberg, Germany, 2006.

Li, H., He, Q., Song, Q., Chen, L., Song, Y., Wang, Y., Lin, K., Xu, Z., and Shao, M.: Diagnosing Tibetan pollutant sources via volatile organic compound observations, Atmos Environ, 166, 244-254, https://doi.org/10.1016/j.atmosenv.2017.07.031, 2017.

Li, J., Wang, Z., and Xiang, W.: Daytime atmospheric oxidation capacity of urban Beijing under polluted conditions during the 2008 Beijing Olympic Games and the impact of aerosols, Sola, 7, 73-76, https://doi.org/10.2151/sola.2011-019, 2011.

Li, L., and Xie, S.: Historical variations of biogenic volatile organic compound emission inventories in China, 1981–2003, Atmos Environ, 95, 185-196, https://doi.org/10.1016/j.atmosenv.2014.06.033, 2014.

Li, M., Zhang, Q., Streets, D. G., He, K. B., Cheng, Y., Emmons, L. K., Huo, H., Kang, S., Lu, Z., and Shao, M.: Mapping Asian anthropogenic emissions of non-methane volatile organic compounds to multiple chemical mechanisms, Atmos. Chem. Phys., 14, 5617-5638, https://doi.org/10.5194/acp-14-5617-2014, 2013.

Li, M., Zhang, Q., Kurokawa, J., Woo, J., He, K., Lu, Z., Ohara, T., Song, Y., Streets, D. G., and Carmichael, G. R.: MIX: a mosaic Asian anthropogenic emission inventory under the international collaboration framework of the MICS-Asia and HTAP, Atmos. Chem. Phys., 17, 935-963, https://doi.org/10.5194/acp-17-935-2017, 2017.

Liu, F., Zhang, Q., Tong, D., Zheng, B., Li, M., Huo, H., and He, K. B.: High-resolution inventory of technologies, activities, and emissions of coal-fired power plants in China from 1990 to 2010, Atmos. Chem. Phys., 15, 13299-13317, https://doi.org/10.5194/acp-15-13299-2015, 2015.

Liu, H., Liu, C., Xie, Z., Li, Y., Huang, X., Wang, S., Xu, J., and Xie, P.: A paradox for air pollution controlling in China revealed by "APEC Blue" and "Parade Blue", Sci Rep, 6, 34408, https://doi.org/10.1038/srep34408, 2016.

Loyola, D. G., Gimeno García, S., Lutz, R., Argyrouli, A., Romahn, F., Spurr, R. J., Pedergnana, M., Doicu, A., Molina García, V., and Schüssler, O.: The operational cloud retrieval algorithms from TROPOMI on board Sentinel-5 Precursor, Atmos. Meas. Tech., 11, https://doi.org/10.5194/amt-11-409-2018, 2018.

Malicet, J., Daumont, D., Charbonnier, J., Parisse, C., Chakir, A., and Brion, J.: Ozone UV spectroscopy. II. Absorption cross-sections and temperature dependence, J Atmos Chem, 21, 263-273, https://doi.org/10.1007/BF00696758, 1995.

Martin, R., Parrish, D., Ryerson, T., Nicks, D., Chance, K., Kurosu, T., Jacob, D. J., Sturges, E., Fried, A., and Wert, B.: Evaluation of GOME satellite measurements of tropospheric $NO_2$ and HCHO using regional data from aircraft campaigns in the southeastern United States, Journal of Geophysical Research: Atmospheres, 109, https://doi.org/10.1029/2004jd004869, 2004.

Martin, R. V., Chance, K., Jacob, D. J., Kurosu, T. P., Spurr, R. J., Bucsela, E., Gleason, J. F., Palmer, P. I., Bey, I., and Fiore, A. M.: An improved retrieval of tropospheric nitrogen dioxide from GOME, Journal of Geophysical Research: Atmospheres, 107, ACH 9-1-ACH 9-21, https://doi.org/10.1029/2001JD001027, 2002.

Meller, R., and Moortgat, G. K.: Temperature dependence of the absorption cross sections of formaldehyde between 223 and 323 K in the wavelength range 225–375 nm, Journal of Geophysical Research, 105, 7089-7101, https://doi.org/10.1029/1999JD901074, 2000.

Palmer, P. I., Jacob, D. J., Chance, K., Martin, R. V., Spurr, R. J., Kurosu, T. P., Bey, I., Yantosca, R., Fiore, A., and Li, Q.: Air mass factor formulation for spectroscopic measurements from satellites: Application to formaldehyde retrievals from the Global Ozone Monitoring Experiment, Journal of Geophysical Research: Atmospheres, 106, 14539-14550, https://doi.org/10.1029/2000JD900772, 2001.

Rodgers, C. D.: Inverse methods for atmospheric sounding: theory and practice, World scientific, 2000.

Peng, L., Zhang, Q., Yao, Z., Mauzerall, D. L., Kang, S., Du, Z., Zheng, Y., Xue, T., and He, K.: Underreported coal in statistics: A survey-based solid fuel consumption and emission inventory for the rural residential sector in China, Applied Energy, 235, 1169-1182, https://doi.org/10.1016/j.apenergy.2018.11.043, 2019.

Schönhardt A, R. A., Wittrock F: Observations of iodine monoxide columns from satellite, Atmos. Chem. Phys., https://doi.org/10.5194/acp-8-637-2008, 2008.

Serdyuchenko, A., Gorshelev, V., Weber, M., Chehade, W., and Burrows, J. P.: High spectral resolution ozone absorption cross-sections – Part 2: Temperature dependence, Atmos. Meas. Tech., 7, 625-636, https://doi.org/10.5194/amt-7-625-2014, 2014.

Spurr, R.: LIDORT and VLIDORT: Linearized pseudo-spherical scalar and vector discrete ordinate radiative transfer models for use in remote sensing retrieval problems, in: Light Scattering Reviews 3: Light Scattering and Reflection, edited by: Kokhanovsky, A. A., Springer Berlin Heidelberg, Berlin, Heidelberg, 229-275, 2008.

Streiner, D. L.: Maintaining Standards: Differences between the Standard Deviation and Standard Error, and When to Use Each, The Canadian Journal of Psychiatry, 41, 498-502, https://doi.org/10.1177/070674379604100805, 1996.

Su, W., Liu, C., Hu, Q., Zhao, S., Sun, Y., Wang, W., Zhu, Y., Liu, J., and Kim, J.: Primary and secondary sources of ambient formaldehyde in the Yangtze River Delta based on Ozone Mapping and Profiler Suite (OMPS) observations, Atmos. Chem. Phys., 19, 6717-6736, https://doi.org/10.5194/acp-19-6717-2019, 2019.

Thalman, R., and Volkamer, R.: Temperature dependent absorption cross-sections of $O_2$–$O_2$ collision pairs between 340 and 630 nm and at atmospherically relevant pressure, Phys Chem Chem Phys, 15, 15371-15381, https://doi.org/versity o, 2013.

Vandaele, A. C., Hermans, C., Simon, P. C., Carleer, M., Colin, R., Fally, S., Merienne, M.-F., Jenouvrier, A., and Coquart, B.: Measurements of the $NO_2$ absorption cross-section from 42000 $cm^{-1}$ to 10000 $cm^{-1}$ (238–1000 nm) at 220 K and 294 K, Journal of Quantitative Spectroscopy and Radiative Transfer, 59, 171-184, https://doi.org/10.1016/S0022-4073(97)00168-4, 1998.

Vigouroux, C., Hendrick, F., Stavrakou, T., Dils, B., Smedt, I. D., Hermans, C., Merlaud, A., Scolas, F., Senten, C., and Vanhaelewyn, G.: Ground-based FTIR and MAX-DOAS observations of formaldehyde at Réunion Island and comparisons with satellite and model data, Atmos. Chem. Phys., 9, 9523-9544, https://doi.org/10.5194/acp-9-9523-2009, 2009.

Vigouroux, C., Langerock, B., Bauer Aquino, C. A., Blumenstock, T., Cheng, Z., De Mazière, M., De Smedt, I., Grutter, M., Hannigan, J. W., Jones, N., Kivi, R., Loyola, D., Lutsch, E., Mahieu, E., Makarova, M., Metzger, J.-M., Morino, I., Murata, I., Nagahama, T., Notholt, J., Ortega, I., Palm, M., Pinardi, G., Röhling, A., Smale, D., Stremme, W., Strong, K., Sussmann,

R., Té, Y., van Roozendael, M., Wang, P., and Winkler, H.: TROPOMI–Sentinel-5 Precursor formaldehyde validation using an extensive network of ground-based Fourier-transform infrared stations, Atmos. Meas. Tech., 13, 3751–3767, https://doi.org/10.5194/amt-13-3751-2020, 2020.

Wang, D., Zhou, B., Fu, Q., Zhao, Q., Zhang, Q., Chen, J., Yang, X., Duan, Y., and Li, J.: Intense secondary aerosol formation due to strong atmospheric photochemical reactions in summer: observations at a rural site in eastern Yangtze River Delta of China, Science of the Total Environment, 571, 1454-1466, https://doi.org/10.1016/j.scitotenv.2016.06.212, 2016.

Wei, W., Wang, S., Chatani, S., Klimont, Z., Cofala, J., and Hao, J.: Emission and speciation of non-methane volatile organic compounds from anthropogenic sources in China, Atmos Environ, 42, 4976-4988, https://doi.org/10.1016/j.atmosenv.2008.02.044, 2008.

Wiedinmyer, C., Akagi, S. K., Yokelson, R. J., Emmons, L. K., Alsaadi, J. A., Orlando, J. J., and Soja, A. J.: The Fire INventory from NCAR (FINN): a high resolution global model to estimate the emissions from open burning, Geosci Model Dev, 4, 625-641, https://doi.org/10.5194/gmd-4-625-2011, 2010.

Wilmouth, D. M., Hanisco, T. F., Donahue, N. M., and Anderson, J. G.: Fourier transform ultraviolet spectroscopy of the A 2Π3/2← X 2Π3/2 transition of BrO, The journal of physical chemistry a, 103, 8935-8945, https://doi.org/10.1021/jp991651o, 1999.

Wu, R., Bo, Y., Li, J., Li, L., Li, Y., and Xie, S.: Method to establish the emission inventory of anthropogenic volatile organic compounds in China and its application in the period 2008–2012, Atmos Environ, 127, 244-254, https://doi.org/10.1016/j.atmosenv.2015.12.015, 2016.

Xue, L., Gu, R., Wang, T., Wang, X., Saunders, S., Blake, D., Louie, P. K., Luk, C. W., Simpson, I., and Xu, Z.: Oxidative capacity and radical chemistry in the polluted atmosphere of Hong Kong and Pearl River Delta region: analysis of a severe photochemical smog episode, Atmos. Chem. Phys., https://doi.org/10.5194/acp-16-9891-2016, 2016.

Zheng, B., Huo, H., Zhang, Q., Yao, Z., Wang, X., Yang, X., Liu, H., and He, K. B.: High-resolution mapping of vehicle emissions in China in 2008, Atmos. Chem. Phys., 14, 9787-9805, https://doi.org/10.5194/acp-14-9787-2014, 2014.

Zheng, C., Shen, J., Zhang, Y., Huang, W., Zhu, X., Wu, X., Chen, L., Gao, X., and Cen, K.: Quantitative assessment of industrial VOC emissions in China: Historical trend, spatial distribution, uncertainties, and projection, Atmos Environ, 150, 116-125, https://doi.org/10.1016/j.atmosenv.2016.11.023, 2017.

Zhou, Y., Brunner, D., Boersma, K. F., Dirksen, R., and Wang, P.: An improved tropospheric NO2 retrieval for OMI observations in the vicinity of mountainous terrain, Atmos. Meas. Tech., 2, 401-416, https://doi.org/10.5194/amt-2-401-2009, 2009.

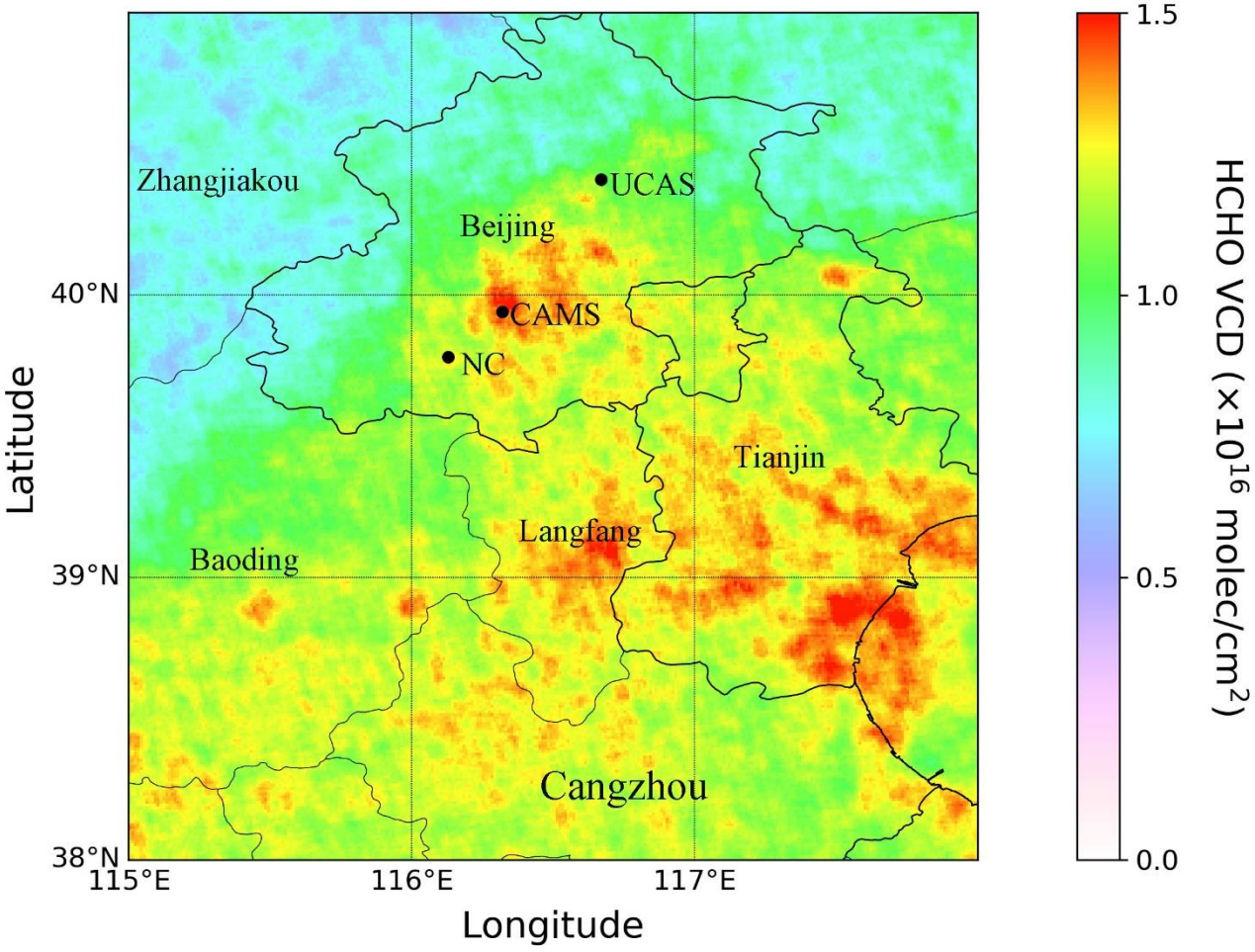


**Figure 1. Annual average of the improved TROPOMI tropospheric HCHO VCD from August 2018 to July 2019 in Beijing and its surrounding region on a 0.01°×0.01° grid. The black dots indicate the locations of MAX-DOAS sites.**

**Table 1. The retrieval settings for TROPOMI HCHO DSCD and information used in AMF calculations in operational product and our retrieval.**

| | Operational product (De Smedt et al. 2018) | Our retrieval |
|---|---|---|
| SCD retrieval | | |
| algorithm | DOAS | BOAS |
| Fitting window | 328.5-359 nm | 328.5-359 nm |
| Radiance reference spectrum | Daily average of radiances of the Pacific orbit between 5°S and 5°N, 180 °W and 120 °W | Daily average of radiances of the Pacific orbit between 30°S and 30°N, 180 °W and 140 °W |
| Polynomial | 5th order | Scaling polynomial: 3rd order<br>Baseline polynomial: 3rd order |
| Instrument slit function | TROPOMI ISRF Calibration Key Data (CKD) v1.0.0 | TROPOMI ISRF Calibration Key Data (CKD) v3.0.0 |
| Solar reference spectrum | (Chance and Kurucz, 2010) | (Chance and Kurucz, 2010) |
| Ring effect | Ring cross section (Chance and Spurr, 1997) | Raman spectrum (Chance and Spurr, 1997) |
| HCHO cross sections | (Meller and Moortgat, 2000), 298K | (Chance and Orphal, 2011) , 300K |
| $O_3$ cross sections | (Serdyuchenko et al., 2014), 223 and 243K | (Malicet et al., 1995) , 228 and 295K, $I_0$ corrected |
| $NO_2$ cross sections | (Vandaele et al., 1998) , 220K | (Vandaele et al., 1998) , 220K |
| BrO cross sections | (Fleischmann et al., 2004), 223K | (Wilmouth et al., 1999) , 228K |
| $O_4$ cross sections | (Thalman and Volkamer, 2013) , 293K | (Thalman and Volkamer, 2013) , 293K |
| AMF calculations | | |
| Altitude-dependent AMFs | VLIDORT, 340 nm, 6-D AMF look-up table | VLIDORT, 340 nm, 6-D AMF look-up table |
| Cloud parameter | S5P operational cloud product (see Sect. 2.2) | Same as left |
| Treatment of partly cloudy scenes | IPA, no correction for $f_{eff}$ <10% | Same as left |
| Surface albedo | OMI-based monthly minimum LER at 342 nm (Kleipool et al., 2008) | Same as left |
| A priori HCHO profile | TM5-MP daily forecast with the spatial | WRF-Chem daily simulations with the spatial |

| | | |
|---|---|---|
| | resolution of 1°×1° (lat×long) | resolution of $20 \times 20$ km$^2$ |
| Aerosols | No explicit correction | Same as left |

695

**Table 2. Information of the MAX-DOAS measurements. Viewing azimuth angle of the north is taken as zero degree. Relative error is calculated by mean of relative errors of MAX-DOAS measurements within ±1 h around the TROPOMI overpass time.**

| Site name | Location | Region | Height above sea level (m) | viewing azimuth angle (°) | elevation angles (°) | Relative error | Available days |
|---|---|---|---|---|---|---|---|
| CAMS | 39.94° N, 116.32° E | urban area | 100 | 130 (southeast) | 1, 2, 3, 4, 5, 6, 8, 10, 15, 30, 90 | 14.32% | 352 |
| UCAS | 40.41° N, 116.67° E | suburb | 120 | 67 (northeast) | 1, 2, 3, 4, 5, 6, 8, 10, 15, 30, 90 | 14.03% | 321 |
| NC | 39.78° N, 116.13° E | suburb | 60 | 48 (northeast) | 1, 2, 3, 4, 5, 6, 8, 10, 15, 30, 90 | 19.00% | 331 |

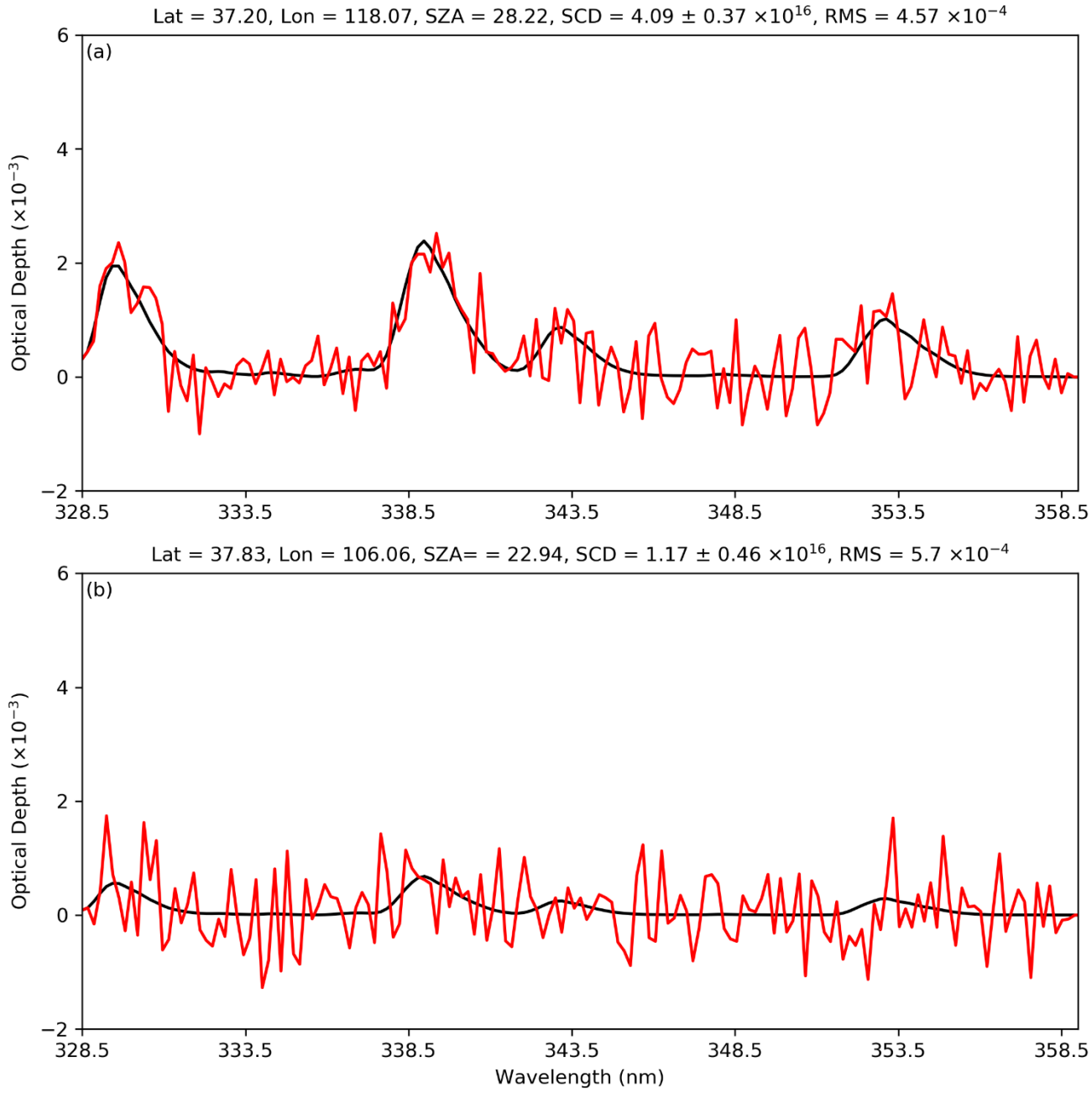


**Figure 2. An example of the spectral retrieval of HCHO DSCD from two TROPOMI spectra measured on 6 August 2018 over China (orbit 4211), for (a) polluted case and (b) clean case. The black lines represent the simulated HCHO optical depth, and the red lines represent the fitted HCHO optical depth plus fitting residuals.**

**Table 3. Parameter effects on daily mean HCHO DSCDs and SCDs, ±1 standard deviation, and mean RMS on 06 August 2018 of the region between 73° E and 130° E, and 18° N and 54° N. Units of DSCDs, SCDs and ±1σ are $\times 10^{16}$ molec $cm^{-2}$. RMS units are $\times 10^{-4}$.**

| Retrieval settings | DSCDs | ± 1σ | RMS | SCDs | ±1 σ |
|---|---|---|---|---|---|
| This study | 0.34 | ± 0.57 | 5.84 | 0.86 | ± 0.58 |
| 328.5-346.0 nm | 0.46 | ± 0.96 | 5.83 | 0.87 | ± 0.96 |
| 328.5-356.5 nm | 0.38 | ± 0.62 | 5.88 | 0.88 | ± 0.63 |
| 337.0-353.0 nm | 0.49 | ± 1.65 | 5.69 | 0.99 | ± 1.65 |
| 337.5-359.0 nm | 0.40 | ± 0.99 | 5.84 | 0.82 | ± 0.99 |
| 334.0-348.0 nm | 0.28 | ± 2.43 | 5.60 | 0.74 | ± 2.43 |
| $4^{th}$ baseline and scaling polynomials | 0.41 | ± 0.65 | 6.00 | 0.88 | ± 0.67 |
| TROPOMI ISRF Calibration Key Data (CKD) v1.0.0 | 0.34 | ± 0.61 | 6.04 | 0.88 | ± 0.61 |
| The first order Taylor series approach for $O_3$ SCDs | 0.33 | ±0.63 | 6.04 | 0.83 | ±0.65 |

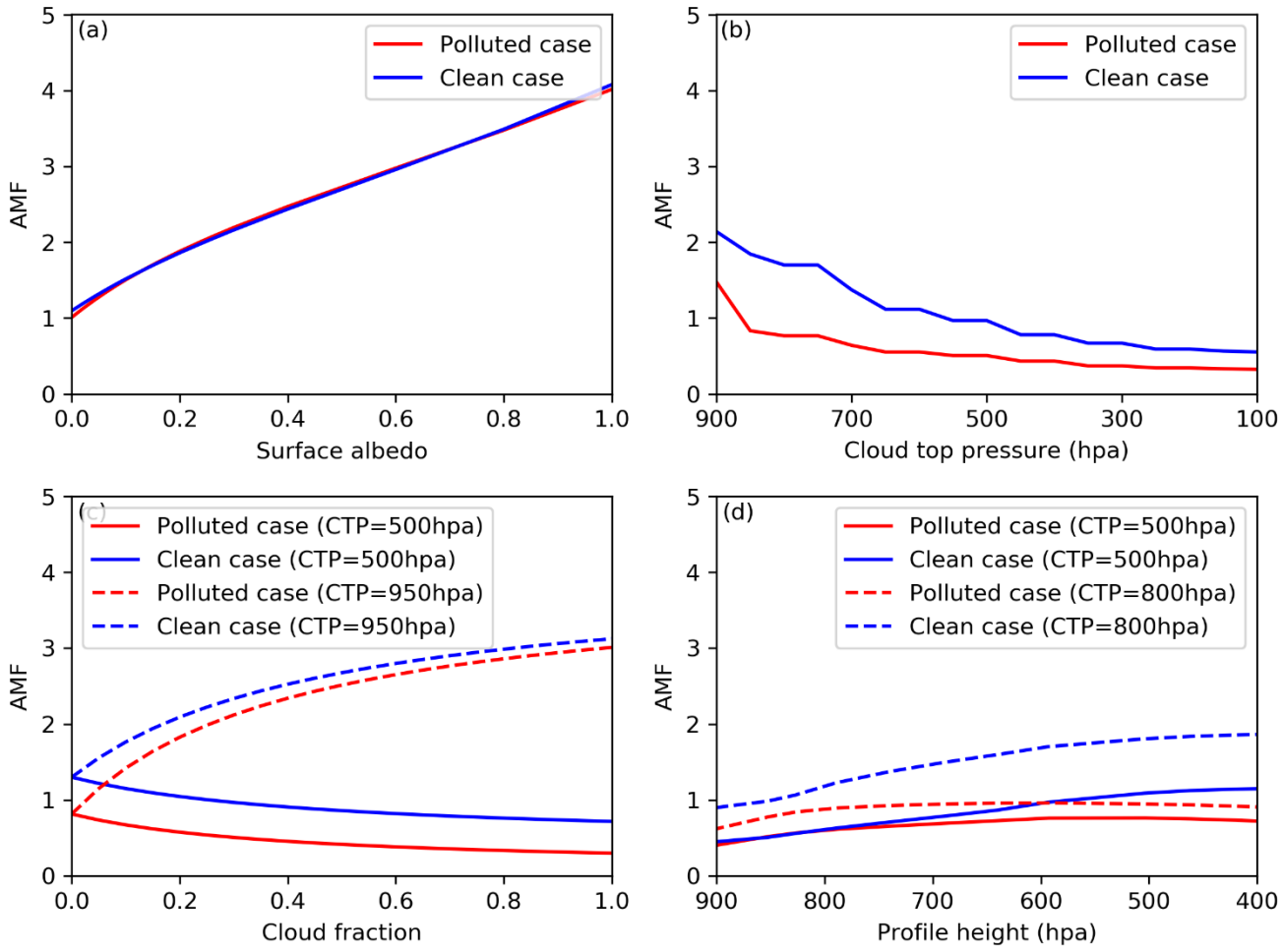


**Figure 3. AMF variations with surface albedo (a), cloud top pressure (b), cloud fraction (c) and profile height (d) over clean and polluted cases. In panel (a), cloud fraction is 0. In panel (b) and (d), cloud fractions are 0.3 and surface albedos are 0.05.**

**Table 4.** Uncertainties of TROPOMI HCHO VCD from the parameters used in AMF calculation. Uncertainties are estimated with a fixed set of observation geometry (SZA=30°, VZA=30°, RAA=0°).

| Uncertainty source | Clean area | Polluted area |
|---|---|---|
| Surface albedo | 0-9% | 0-10% |
| Cloud top pressure | 3-10% | 3-15% |
| Cloud fraction | 1-15% | 1-11% |
| Profile height | 1-16% | 7-31% |

| | | |
|---|---|---|
| AMF LUT and no explicit aerosol correction | 15-35% (De Smedt et al. 2018) | 15-35% (De Smedt et al. 2018) |
| Total | 15-43% | 17-51% |

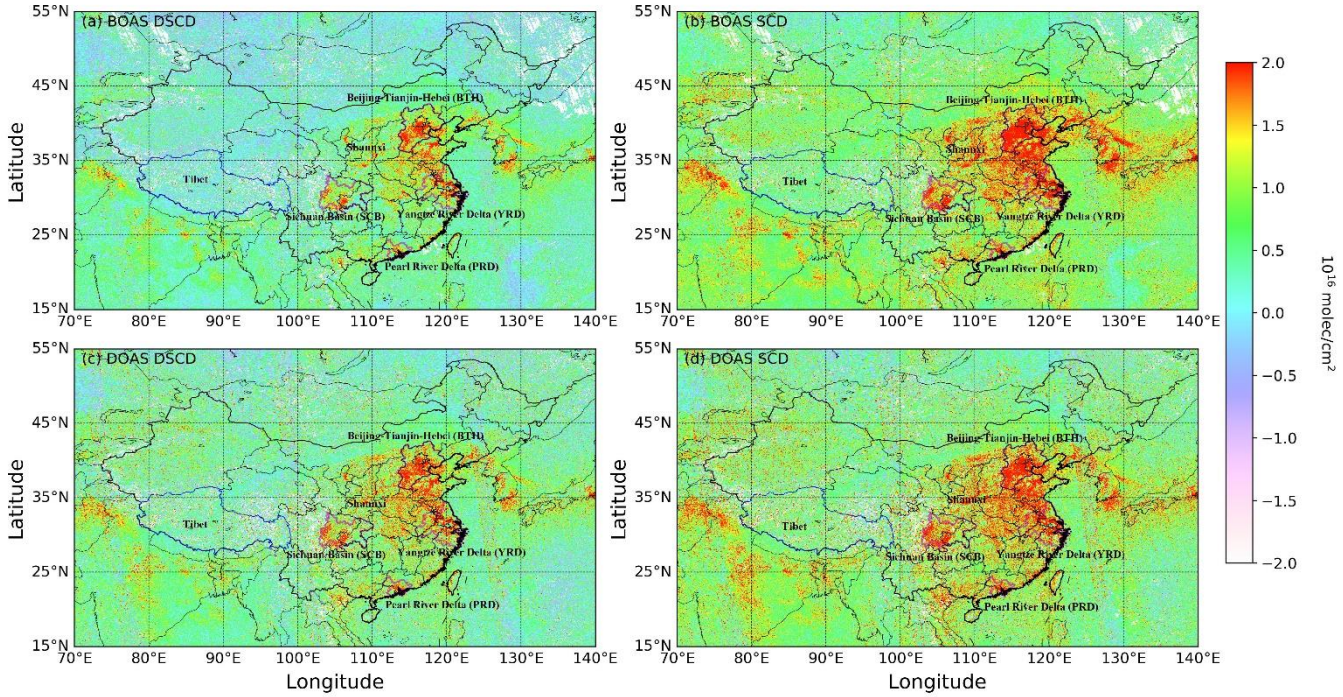


**Figure 4. Spatial distributions of BOAS (a) and DOAS (c) HCHO DSCDs and BOAS (b) and DOAS (d) HCHO SCDs on 06 August 2018 over China from orbit 04210 to orbit 04213. The regional boundaries of BTH, YRD, PRD and SCB are delineated by magenta lines.**

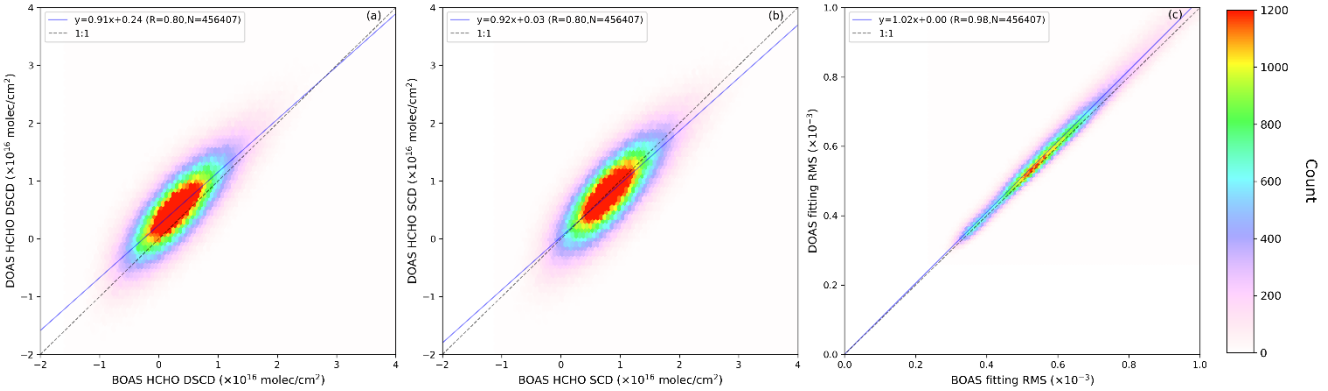


**Figure 5. (a) Pixel to pixel comparisons of DOAS and BOAS HCHO DSCDs, (b) DOAS and BOAS HCHO SCDs and (c) DOAS and BOAS fitting RMS on 06 August 2018 in the region between 73° E and 130° E, and 18° N and 54° N.**

725

**Table 5.** NMBs between TROPOMI HCHO VCDs with different retrieval settings ($NMB_{S1,S2}$) and NMBs between TROPOMI and MAX-DOAS observations ($NMB_{S1,M}$). TROPOMI HCHO VCDs are calculated with four different settings, (1) operational retrieval setting (2) replacing DOAS SCDs using BOAS SCDs in the operational product, (3) changing the a priori profiles from TM5 to regional WRF-Chem simulations in the operational product and (4) both (2) and (3) changes in the operational product. The error bars ( ± 2 SE) are also presented.
730 All values are in %.

| Settings (S1 vs S2) | | CAMS | | UCAS | | NC | |
|---|---|---|---|---|---|---|---|
| | | $NMB_{S1,S2}$ | $NMB_{S1,M}$ | $NMB_{S1,S2}$ | $NMB_{S1,M}$ | $NMB_{S1,S2}$ | $NMB_{S1,M}$ |
| Operational product | Year | - | -8.23±3.09 | - | 10.75±4.82 | - | 3.73±3.77 |
| | Summer | - | -14.92±5.03 | - | -21.96±5.31 | - | -18.12±5.73 |
| | Winter | - | 20.28±8.74 | - | 44.10±11.27 | - | 22.87±8.82 |
| BOAS vs DOAS | Year | 0.20±3.24 | -9.85±4.57 | -0.43±2.95 | 15.33±4.84 | -1.50 ± 2.24 | 2.48±3.59 |
| | Summer | 3.91±1.89 | -11.69±4.94 | 10.00±3.90 | -14.16±5.01 | 7.20 ±2.74 | -12.23±5.33 |
| | Winter | -2.67±4.31 | 18.98±10.15 | -4.15±11.54 | 36.19±18.44 | -3.75 ± 9.56 | 18.12±17.44 |

| | | | | | | | |
|---|---|---|---|---|---|---|---|
| WRF-Chem vs TM5-MP | Year | 7.86±2.84 | -7.10±6.58 | -9.49±3.25 | 6.70±3.19 | -5.61±2.73 | -2.83±3.29 |
| | Summer | 1.12±4.47 | -13.80±7.76 | 5.15±4.81 | -18.66±4.57 | 3.13±4.87 | -15.96±5.19 |
| | Winter | -17.83±8.00 | 10.38±9.36 | -15.19±8.66 | 20.44±11.95 | -14.26±2.70 | 10.37±9.01 |
| BOAS & WRF-Chem vs DOAS &TM5-MP | Year | 2.61±1.87 | -5.78±3.49 | -10.77± 2.11 | 5.22±4.10 | -6.42±1.75 | -3.30±3.29 |
| | Summer | 3.18±3.41 | -12.21±4.81 | 3.65 ± 5.53 | -17.87±4.43 | 0.27±3.60 | -17.34±4.82 |
| | Winter | -13.87±2.93 | 6.38±6.35 | -11.89 ± 3.22 | 19.38±11.44 | -12.56±3.46 | 7.94±4.45 |

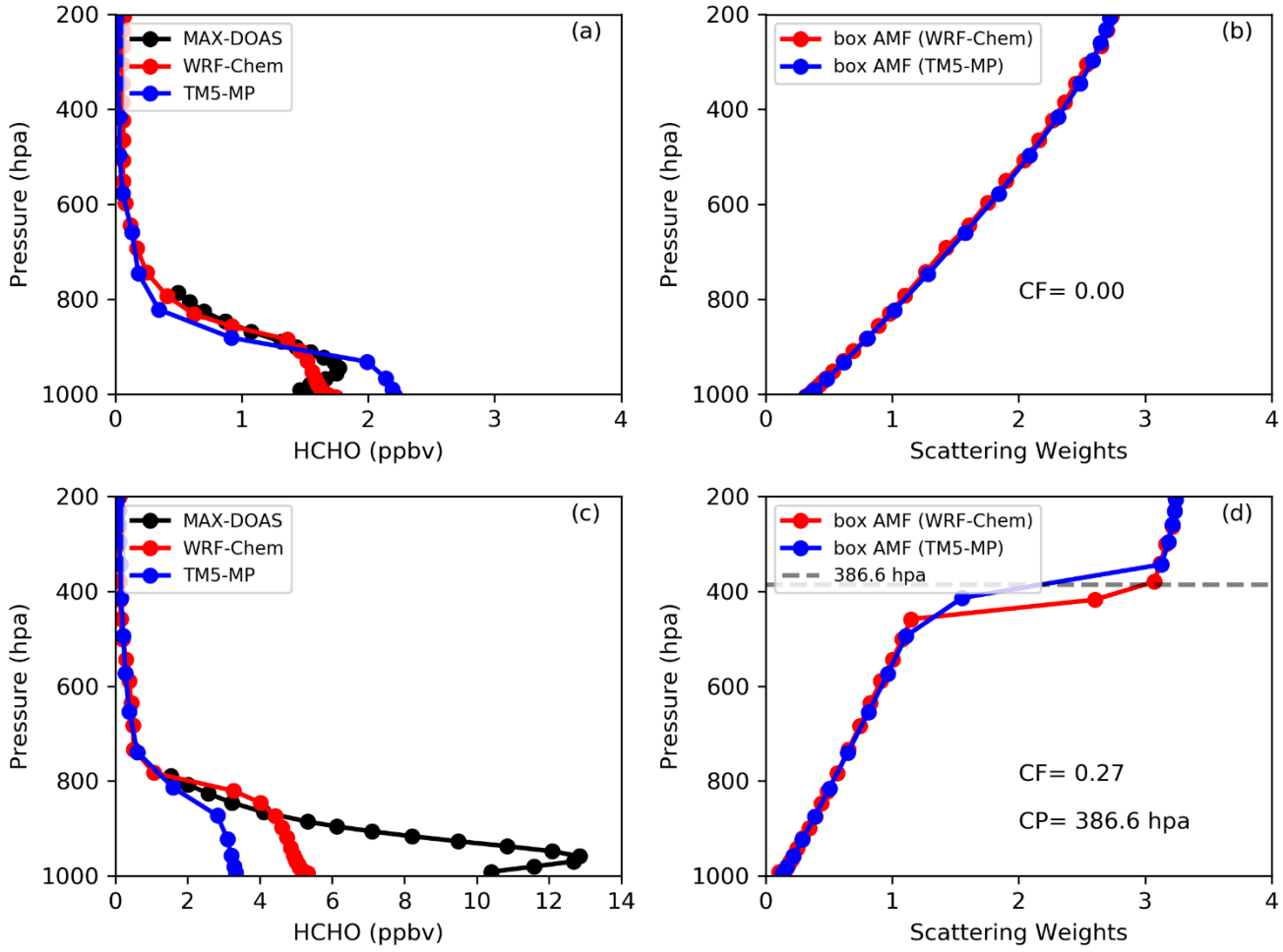


**Figure 6. Daily averaged vertical HCHO profiles obtained from MAX-DOAS, WRF-Chem and TM5-MP model in clean case on 03 March 2019 (a) and in polluted case on 26 June 2019. Comparisons of box AMF using WRF-Chem and TM5-MP simulations in clean case with clear sky on 03 March 2019 (b) and in polluted case with cloudy sky on 26 June 2019 (c). The locations of two pixels are within 20 km of the CAMS site.**

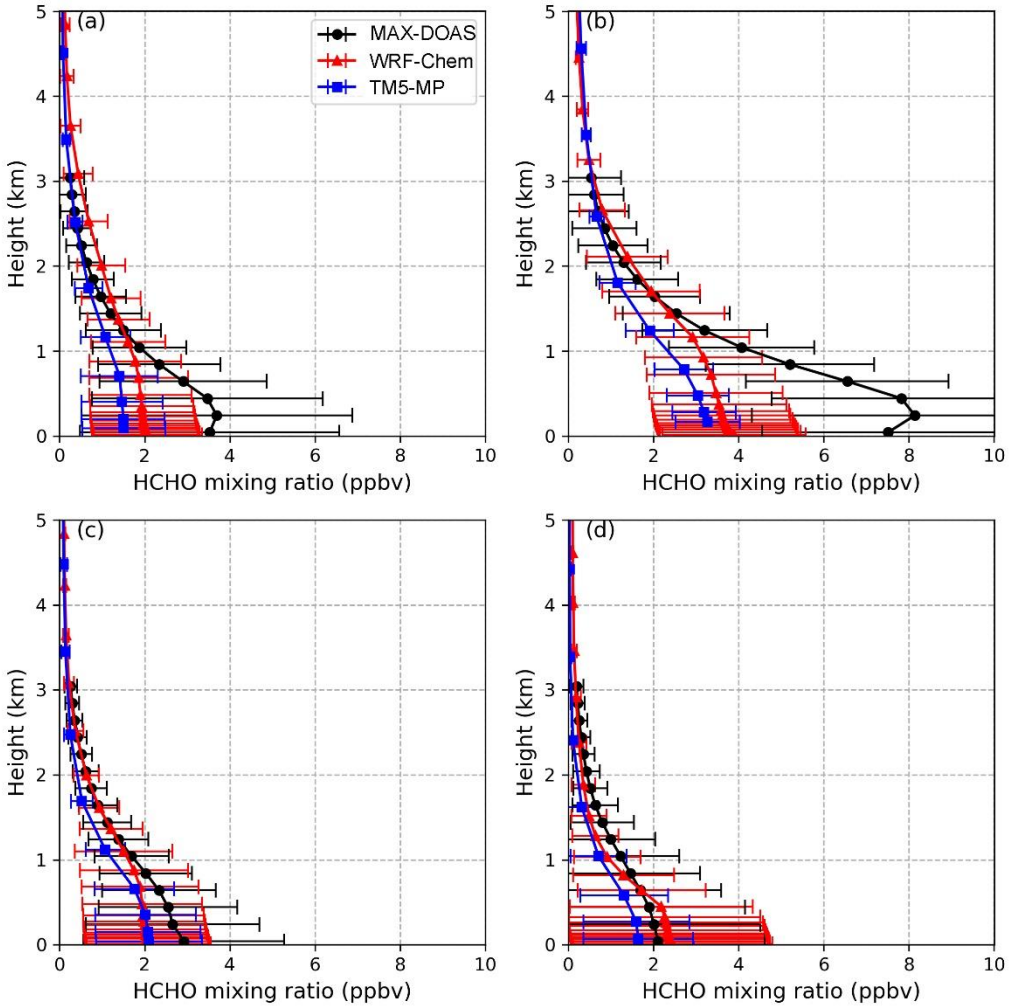


**Figure 7. Seasonal average of vertical HCHO profiles obtained from MAX-DOAS, WRF-Chem and TM5-MP model in spring (a), summer (b), autumn (c) and winter (d) at CAMS site. The error bars represent 1σ standard deviation of variation.**

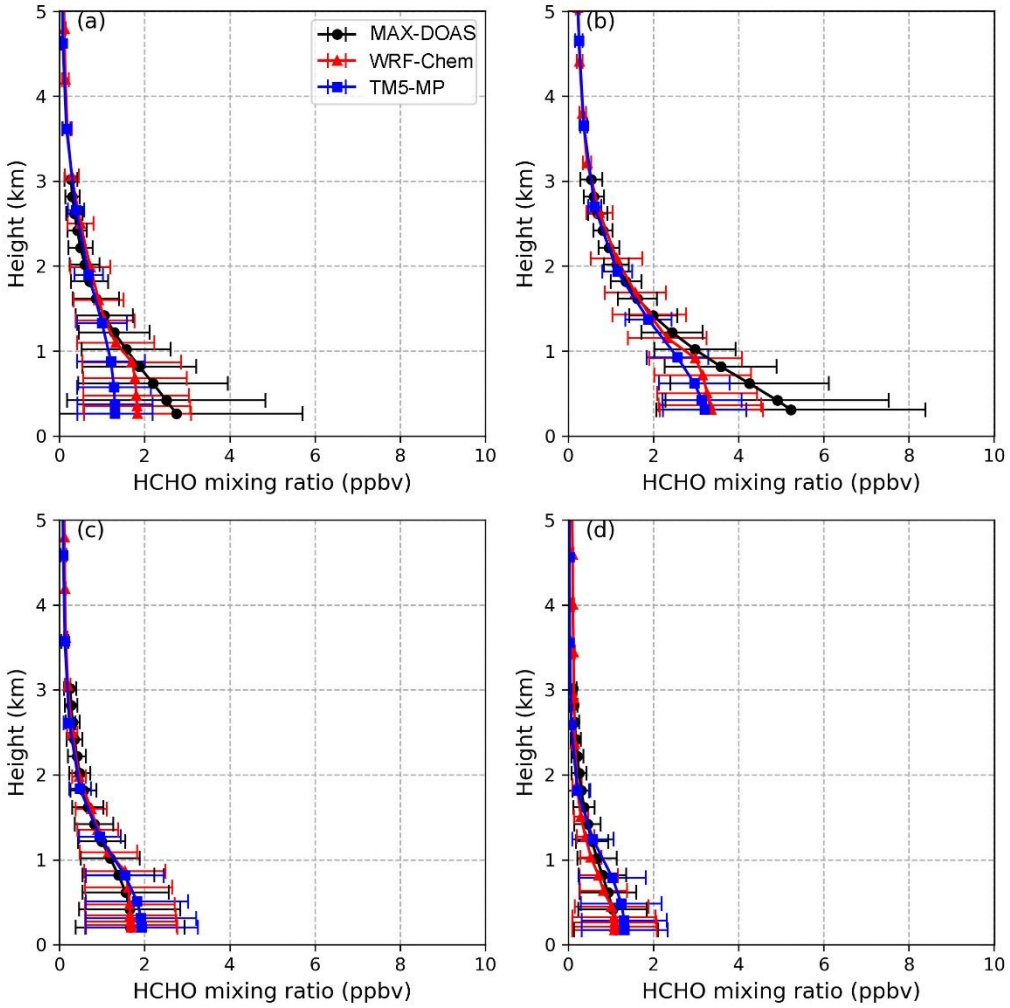


740 **Figure 8. Seasonal average of vertical HCHO profiles obtained from MAX-DOAS, WRF-Chem and TM5-MP model in spring (a), summer (b), autumn (c) and winter (d) at UCAS site. The error bars represent 1σ standard deviation of variation.**

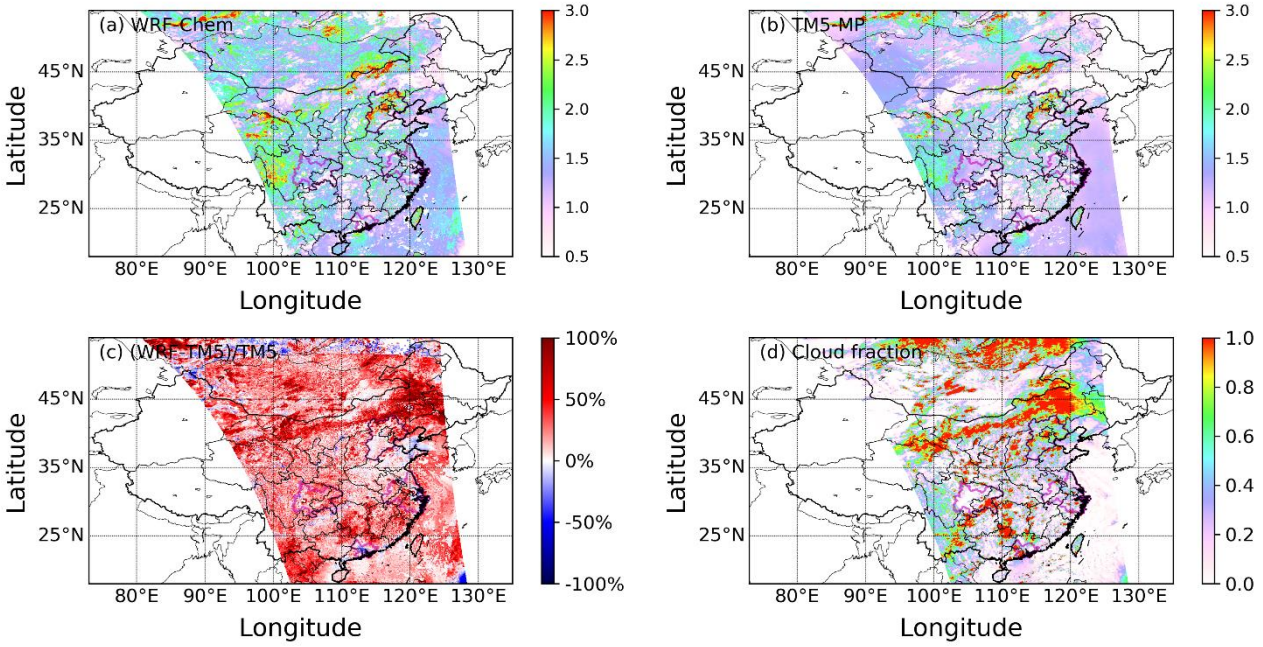


**Figure 9. Spatial distributions of AMFs calculated using WRC-chem (a) and TM5-MP (b) simulations as a priori HCHO profiles of orbit 04211 on 06 August 2018. Spatial distribution of difference of the AMFs (c) and of cloud fraction (d) of orbit 04211 on 06 August 2018.**

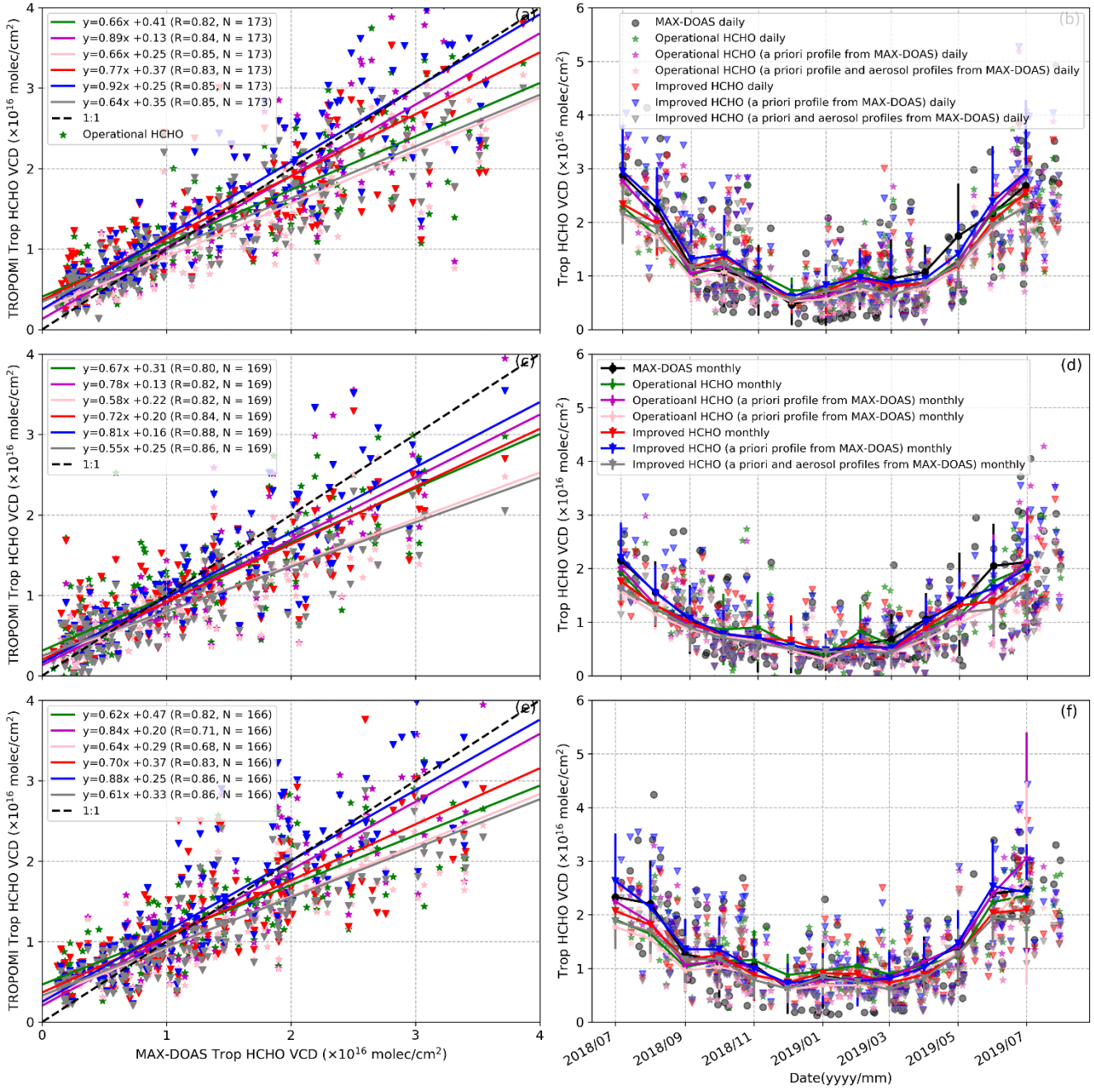


**Figure 10. Comparison of tropospheric HCHO VCDs between TROPOMI and MAX-DOAS measurements from July 2018 to July 2019 at CAMS (a), UCAS (c) and NC (e) sites. Time series of TROPOMI and MAX-DOAS tropospheric HCHO VCDs from July 2018 to July 2019 at CAMS (b), UCAS (d) and NC (f) sites.**

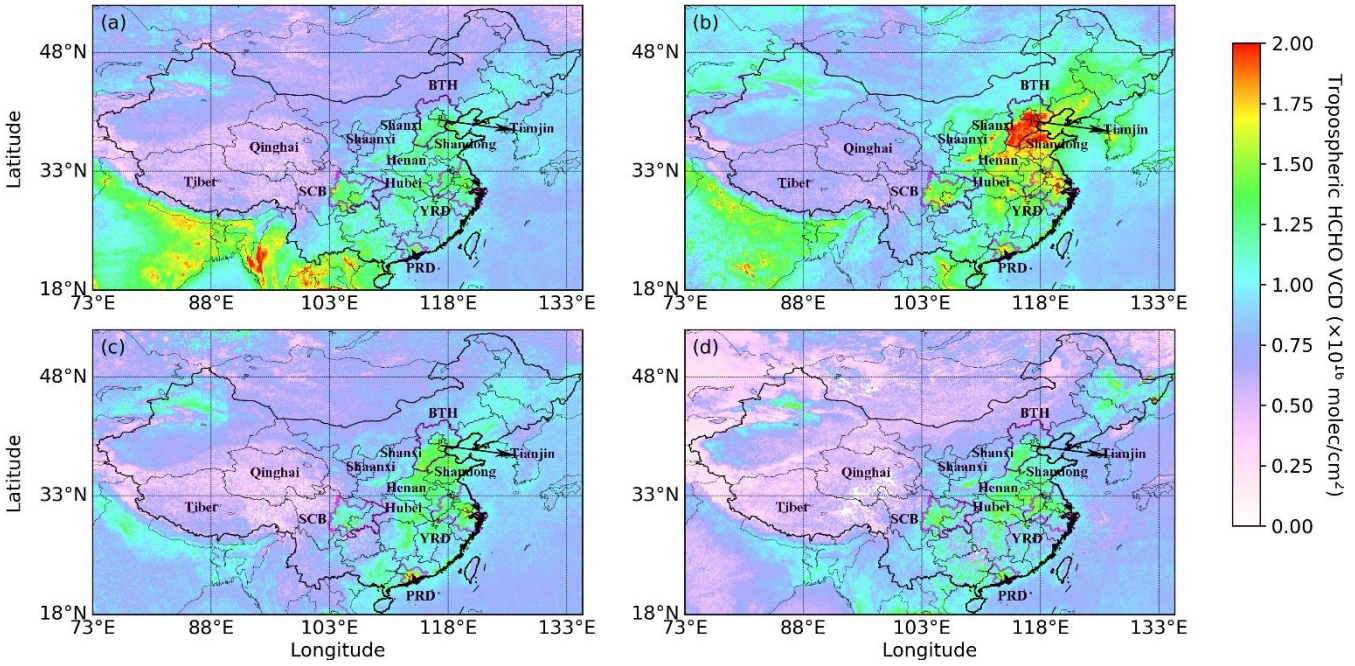


**Figure 11. The spatial distribution of average tropospheric HCHO VCDs over China on a 0.1°×0.1° grid in spring (a), summer (b), winter (c) and winter (d).**

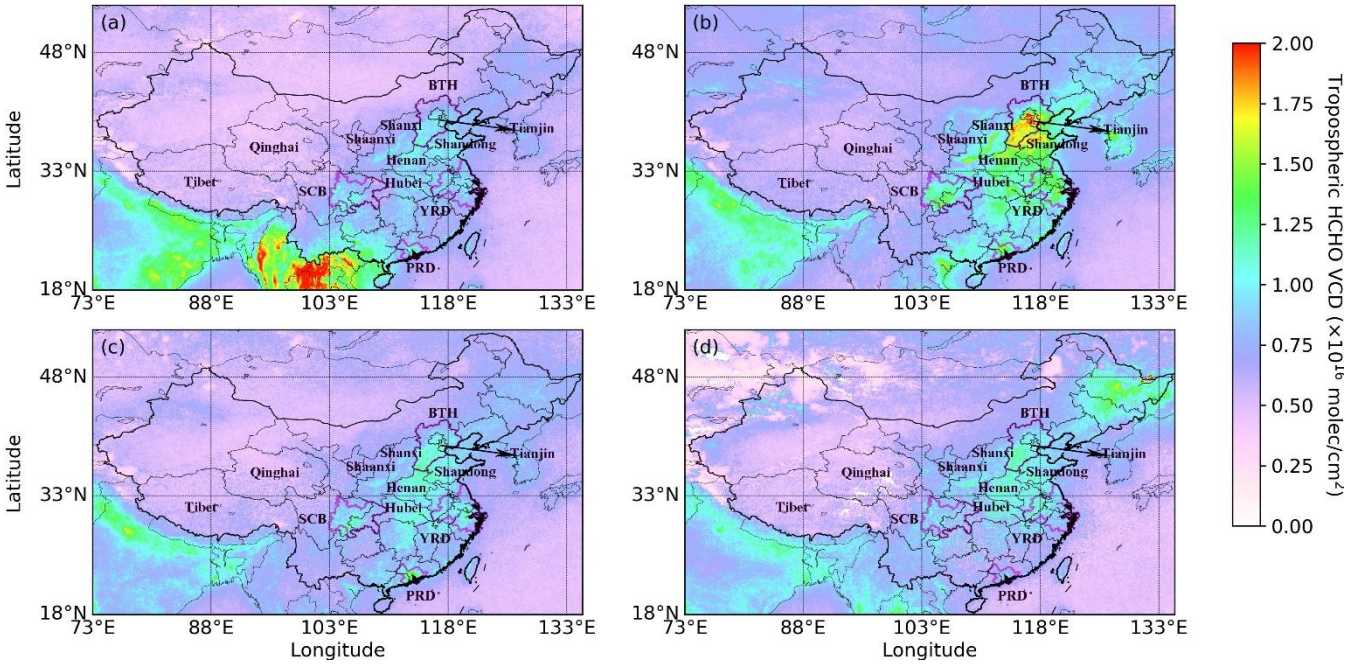


**Figure 12. The spatial distribution of average TROPOMI operational tropospheric HCHO VCDs over China on a 0.1°×0.1° grid in spring (a), summer (b), winter (c) and winter (d).**